THE UNIVERSITY *of* EDINBURGH

Macroscopic Consequences of Demographic Noise in Non-Equilibrium Dynamical Systems

Dominic Russell

Doctor of Philosophy
University of Edinburgh
June 2013

Abstract

For systems that are in equilibrium, fluctuations can be understood through interactions with external heat reservoirs. For this reason these fluctuations are known as thermal noise, and they usually become vanishingly small in the thermodynamic limit. However, many systems comprising interacting constituents studied by physicists in recent years are both far from equilibrium, and sufficiently small so that they must be considered finite. The finite number of constituents gives rise to an inherent demographic noise in the system, a source of fluctuations that is always present in the stochastic dynamics.

This thesis investigates the role of stochastic fluctuations in the macroscopically observable dynamical behaviour of non-equilibrium, finite systems. To facilitate such a study, we construct microscopic models using an individual based modelling approach, allowing the explicit form of the demographic noise to be identified.

In many physical systems and theoretical models, absorbing states are a defining feature. Once a system enters one, it cannot leave. We study the dynamics of a system with two symmetric absorbing states, finding that the amplitude of the multiplicative noise can induce a transition between two universal modes of domain coarsening as the system evolves to one of the absorbing states.

In biological and ecological systems, cycles are a ubiquitously observed phenomenon, but are difficult to predict analytically from stochastic models. We examine a potential mechanism for cycling behaviour due to the flow of probability currents, induced by the athermal nature of the demographic noise, in a single patch population comprising two competing species. We find that such a current by itself cannot generate macroscopic cycles, but when combined with deterministic dynamics which constrain the system to a closed circular manifold, gives rise to global quasicycles in the population densities.

Finally, we examine a spatially extended system comprising many such patch populations, exploring the emergence of synchronisation between the different cycles. By a stability analysis of the global synchronised state, we probe the relationship between the synchronicity of the metapopulation and the magnitude of the coupling between patches due to species migration.

In all cases, we conclude that the nature of the demographic noise can play a pivotal role in the macroscopically observed dynamical behaviour of the system.

Lay Summary

In order to study systems made up of many interacting constituents, a mainstay of materials science and biology, compromise must be made. One cannot hope to solve the governing equations given by either classical Newtonian laws, or quantum theory. Instead, the study of thermodynamics has been developed, which when one considers a system to be infinitely large, gives a description of the characteristic, observable properties and behaviour of such systems in terms of macroscopic, well-defined variables such as the temperature and the pressure.

An alternative formalism, whose origins lie 150 years ago with Boltzmann and Maxwell, has come from the development of statistical mechanics. Beginning with a detailed description of the interactions of a system at the smallest scale, statistical methods can be used to find the behaviour of average properties of the system, akin to thermodynamic variables. However this means information is lost, leading to a randomness entering into the system, commonly referred to as *noise*. The noise manifests itself as fluctuations away from the predicted average behaviour in the thermodynamic limit.

An inherent property of many systems due to their finite number of constituents is *demographic noise*. We investigate the role it can play in the dynamical behaviour of such systems. We consider a system which can be applied to model language development in a community, finding that the strength of the noise can dictate how a consensus is reached in the use of linguistic variables. In biological and ecological systems, cycles in the number of species are a ubiquitously observed phenomenon, but are difficult to predict mathematically from stochastic models. We propose a potential mechanism for cycling behaviour which is controlled by the nature of the noise, exploring model systems where it leads to cycles being observed. Finally, we study a system comprising many such populations, examining the emergence of synchronisation between the cycles of each population through mathematical and computational analysis.

In the study of each of these three very different model systems, we find that the nature of the demographic noise has a direct consequence for their observed global dynamical behaviour.

Declaration

Except where otherwise stated, the research undertaken in this thesis was the unaided work of the author. Where the work was done in collaboration with others, a significant contribution was made by the author. Aspects of the work contained in this thesis have been presented in the following articles:

[1] Russell, D. I. and Blythe, R. A. (2011) Noise-induced dynamical transition in systems with symmetric absorbing states. *Phys. Rev. Lett.*, **106**, 165702.

[2] Russell, D. I. and Blythe, R. A. (2013) Macroscopically observable probability currents in finite populations. *J. Stat. Mech.*, **2013**, P06008.

D.I. Russell
June 2013

Acknowledgements

I would like to record my thanks to all those who have helped me in the course of this work. In particular, the following:

To my supervisor Dr. Richard Blythe for being a brilliant supervisor and friend throughout my Ph.D. studies. Ever patient and always supportive.

To Prof. Martin Evans for encouraging me to pursue a Ph.D. and his ongoing support throughout it.

To the E.P.R.S.C. for financial support.

To my office mates Bengt Tegner and Con Healy whose help manifested itself in myriad forms, computing support and provision of tea, to name a few.

Finally to my parents, for their encouragement and support throughout this and all of my academic studies, and to whom this thesis is dedicated along with my four elder siblings, without whom I am sure my studies would not have led me this far.

"One of your American professors said that to study religion was merely to know the mind of man, but if one truly wanted to know the mind of God, you must study physics."

– Iain Banks, *The Business*

Contents

List of Figures

Chapter 1

Introduction

The advancement of modern science has been accompanied by the progressive specialisation of individual disciplines. This development has enabled the necessary specification required to understand simple characteristic systems [1]. Ideally, these systems are theoretically modelled or experimentally controlled to be isolated from external influences, allowing their fundamental features, processes and mechanisms to be studied. However, while this approach has led to many remarkable discoveries—from the structure of DNA [2] to the Higgs boson [3, 4]—there are few real systems that are truly isolated in nature. Instead, many systems in the physical, biological and social sciences are out of equilibrium as they are in contact with external systems. As a consequence, they can only be analysed through their dynamics due to the interactions of the constituents [5]. Increasingly, scientists drawn from a diverse range of backgrounds are interested in studying these complex systems [6], which have become the subject of intensive research in areas of the natural sciences [7], language dynamics and crowd behaviour [8], economics [9], and finance [10].

At first sight, modelling complex systems made up of many interacting constituents represents a colossal challenge. Assuming that all the interactions are known and can be expressed in a mathematical form, encapsulating them in a model which is amenable to either numerical or analytical study is almost always impossible. Progress can be made by construction of a simplified model which captures the dynamics of the variables of the system which are the interest of study. A popular approach amongst statistical physicists in the modelling of a very diverse range of systems, is to give a probabilistic description, casting

the interactions as stochastic processes [11]. For example, if we are studying a population model, we may be interested in how the abundance of one species or genus evolves over time. The full range of processes that play a part in the birth or death processes of this species may be very complex and intractable to work with mathematically. We can instead posit what we believe to be the relevant processes and express them as rates in a probabilistic description of a birth or death event occurring in a given time period. This makes such events random processes, where the stochasticity enters from the information of other system variables we have discarded [7]. Consequently, fluctuations play a crucial part in our understanding of model complex systems and are empirically relevant due to the limited knowledge of the real system under consideration.

In the thermodynamic limit, where the number of constituents in the system is taken to be infinitely large, relative fluctuations about the average behaviour usually become vanishingly small [12]. However in ecological, biological and sociological systems, while the typical size of systems of interest may span from a few dozen to a few billion, very few are of the order of Avogadro's number, where the thermodynamic regime holds [13]. In a finite system the fluctuations due to the discrete nature of its constituents are an inherent property of the system. This source of stochasticity is referred to as *demographic noise*, and in the words of van Kampen, it cannot be switched off [7]. Its origin is very different from that of an external noise source to the system, such as the environmental changes to a population habitat due to the weather, whose stochastic properties can in principle be known. Instead demographic noise is an intrinsic property of finite, probabilistic systems, inherent in the stochastic processes by which the system evolves. The aim of this thesis is to investigate the consequences that demographic noise can have in non-equilibrium dynamical systems.

For equilibrium systems, fluctuations are conceptually well understood [12]. Taking a statistical mechanical formulation, one can give an exact microscopic description of the system in terms of the relevant constituents and interactions. The lost information can then be interpreted as a heat bath which is coupled to the system, introducing fluctuations to the system in the form of thermal noise. The state of the system is given by the Boltzmann probability distribution defined through the Hamiltonian of the system, and the thermodynamic variables can in principle be derived through minimisation of the free energy [14]. Working

within the relevant ensemble, fluctuation-dissipation theorems can be formulated to describe the response of the system about the mean behaviour due to the fluctuations [15, 12].

Out of equilibrium however, this established framework is of little use as a Hamiltonian cannot be defined for such open systems, and the steady-state probability distribution is rarely known. In the past 20 years there have been successes in developing fluctuation theorems for far-from-equilibrium systems—notably the Crooks relation [16] and the Jarzynski equality [17]—and are the subject of recent reviews by Kurchan [18] and Seifert [19]. Typically in the derivation of work relations of this kind, the system is driven externally through a thermostated Hamiltonian [20], while detailed balance is maintained and the noise is prescribed as thermal. However very often when studying a system defined through its dynamics, the noise is athermal and detailed balance is broken as transitions between configurations in state space are no longer microscopically reversible [21]. In such situations, conceptually very little is understood for fluctuations in non-equilibrium systems [22]. For this reason, we will proceed on a case by case basis in our study of the effects of demographic noise in the macroscopic dynamics of non-equilibrium systems. In this way we may be able to discern what general properties and characteristics give rise to any observed universal features, which in turn may lead to a better understanding of the relevant features in classifying non-equilibrium dynamical behaviour.

In ecology, a traditional approach taken in modelling population dynamics, such as in predator-prey systems and population genetics [23, 24], has been to codify the dynamics of the system in the form of ordinary differential equations. These describe the time evolution of the density of each species—or more generally the type of constituent—which are deterministic coarse-grained variables in the limit of an infinite population size. Models of this type are commonly referred to as population level models (PLM), as they work with the total number of a constituent of a certain type [25]. However for finite systems, they are a limited in their scope to describe the dynamics of the system, as this deterministic approach does not capture its discrete nature.

In this thesis we will follow a more prevalent approach in recent years of constructing *individual based models* (IBMs) of systems we wish to study [25]. The description of the dynamics enters at the level of individual constituents,

with the evolution of the system encapsulated in a master equation [26]. This is a natural approach if one wishes to study demographic stochasticity as it is an inherent property of the model at the outset, making it possible to describe, quantify and even control to some extent the form on the noise. An IBM also has the advantage of being versatile. One can recover the deterministic PLM description of the system in the infinite population limit [27], while the stochastic dynamics can be be studied numerically through computer simulation using Monte Carlo techniques [28, 29]. This makes an IBM an excellent intermediary for developing and evaluating analytical techniques to describe such systems and for studying the effects demographic noise can have in large, yet finite, system where stochastic effects are believed to play an important role. By contrast, if one begins with a PLM, then stochastic differential equations can be formulated by adding Langevin noise terms to the ODEs. This then becomes a numerical study of how fluctuations due to the discrete nature of the system come to perturb the PLM dynamics. To do so one has to somehow deduce the form and nature of the noise, a feature of the system which is neglected in a PLM description. This is a very unsatisfactory approach, as there may be many IBMs defined by different stochastic processes whose average dynamics reduce to the same PLM [25].

Outline of Thesis

We begin our investigation of the macroscopic consequences of demographic noise in non-equilibrium dynamical systems in chapter 2 by reviewing the concepts and methods of stochastic modelling. Here, we introduce the analytical techniques, procedures and practices that we shall employ in the remainder of the thesis where we study three very different model systems. We now present an overview of each of these, highlighting the dynamical behaviour we wish to explore.

Ordering Dynamics in Systems with Absorbing States

An absorbing state is one which if the system enters it, it can never leave. This is most readily understood in the context of population dynamics: if the number of inhabitants of a population falls to zero, then, assuming that only birth and death processes are at work, with no mutation, then it cannot become non-zero again at a later time. While in general phase transitions are conceptually poorly understood in non-equilibrium systems [30, 31], in the past decade, a

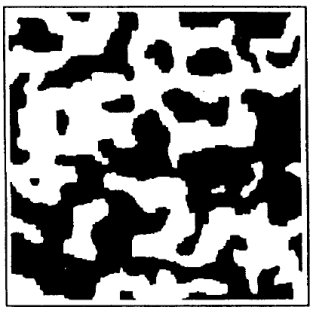

(a) Ising Model

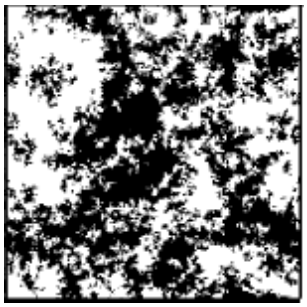

(b) Voter Model

Figure 1.1: The domain ordering dynamics in two dimensions of: (a) the zero temperature Ising model (taken from [39]), and (b) the voter model (from [34]).

framework has emerged to describe the critical behaviour of systems characterised by having two symmetric absorbing states [32, 33, 34] which encapsulates the different observed static order-disorder transitions.

Within this framework, in chapter 3 we investigate what contribution if any the amplitude of the noise can have in a spatially discrete system. In particular we focus on how such out of equilibrium systems evolve to one of the fully ordered, absorbing states. Phase ordering dynamics is an extensive field, as phase separation is a widely observed phenomenon, for example in the grain boundaries of binary alloys [35], coexistence in complex fluids [36] and spinodal decomposition in low temperature polymer solutions [37]. A classic example of domain ordering for a system with two equivalent ordered states is the two-dimensional Ising model, which is illustrated in 1.1(a). Recently, Dornic *et al* [34] revealed a very different coarsening behaviour for a system with two symmetric absorbing states undergoing voter dynamics [38], which is shown in figure 1.1(b). We report the existence of a previously unseen noise-induced dynamical phase transition between these two universal modes of ordering at a non-zero critical value of the amplitude of the demographic noise.

Probability Currents and Quasicycles in Finite Populations

The long term fate of finite populations is often determined by stochastic effects due to the demographic noise, as fluctuations will eventually fix the population by taking the system to an absorbing state of species extinction [40, 41]. For intermediate times, the role that the noise can play in the dynamics of populations

has only recently become better understood. Cycles in biological and ecological systems are a ubiquitous phenomenon that have been studied extensively since the first mathematical models were formulated by Lotka and Volterra over 80 years ago [42, 43, 23]. McKane and Newman [44] have shown how demographic stochasticity can give rise to cycles in finite predator-prey systems. They found that resonances in the power spectra of the fluctuations, combined with a deterministic dynamics given by the Lotka equations naturally gives rise to macroscopic persistent quasicycles in the species abundances. Subsequently this general mechanism has been shown to be versatile, emerging in a broad range of biological and ecological models spanning many orders of magnitude from gene regulation [45] to the spread of epidemics [46].

In chapters 4 and 5 we investigate another potential stochastic mechanism which allows macroscopically observable cycles in two-species finite population dynamical systems, based on the flow of probability currents in the steady state. We deduce what contribution from the deterministic component of the dynamics in concert with the athermal diffusion gives rise to quasicycles in single realisations of the system.

Synchronisation in a Metapopulation

The emergence of synchronisation in the collective dynamics of complex systems is a problem which inspires much research across physical, chemical, biological and social systems [47, 48, 49]. It has recently been shown that demographic noise can play a role in the synchronisation of metapopulations [50, 51], and that desynchronisation between cycles is a key component in the long-term stability of spatially extended predator-prey systems [52, 53]. In chapter 6 we study the onset of synchronisation in a spatially extended multi-patch population model. The single patch populations each undergo noise-induced quasicycles, whose phases become coupled due to migration of species between patches. We investigate how to measure the synchronisation in such systems both analytically and empirically from Monte Carlo simulation, quantifying the relationship with the coupling strength.

In the concluding chapter of this thesis we draw together some common themes from our analysis of these three models, discussing how they could point the way towards a general framework for studying non-equilibrium dynamical systems.

Chapter 2

Concepts and Methods

2.1 Introduction

In this chapter we introduce and review some key concepts and mathematical analysis essential for studying fluctuations. We define standardised language and conventions that will be adhered to in this thesis. While this will be presented in a general context, we will specifically address two variable systems. The generalisation to higher dimensions is straightforward, and does not contain new features, whereas there exist symmetries and constraints in 1D systems that do not feature in higher-dimensional systems and vice-versa, making some analytical procedures unique to one dimension.

Primarily we work from three textbooks which deal with modelling stochastic processes, written by Risken [54], Gardiner [26] and van Kampen [7]. Each cover the same crucial mathematical analysis we introduce here, but with varying motivations, emphases, notation and derivations. Often when looking to these source materials, the link between the mathematical theory and application can be large and difficult to navigate, and translating between the two is not something that is immediately apparent. Here, we will endeavour to present a mathematical framework which brings together the key aspects of the theory of stochastic processes with an eye to making clear how it can be used in practice for a given model.

2.2 Individual Based Models

Historically, the principal approach to modelling ecological systems, like those of predator-prey dynamics or bacterial growth, has been to formulate a *population level model* (PLM) which describes the system's dynamics using ordinary differential equations (ODEs) [23]. The ODEs describe the time evolution of the population densities of each species. These densities are continuous coarse grained variables, which are defined in the deterministic limit of infinite system size. There are many real biological and ecological systems where taking the deterministic limit is not valid and fluctuations play a key role in the behaviour observed in the system. As a PLM by construction neglects demographic noise as a source of fluctuations, it can not predict phenomena stemming from this inherent property of a finite system.

An alternative approach which we adopt in the work presented here is that of *individual based modelling* (IBM), where the dynamics of the system are described in terms of the discrete population numbers n_i, or densities x_i. This is advantageous because fluctuations due to demographic noise enter naturally at the outset of the study of such models, and it is therefore possible to describe, quantify and even control the noise. In this chapter we review the theoretical framework for devising and studying individual based models, deriving and discussing the main analytical tools which we will employ throughout this thesis.

2.2.1 Defining the System

We are interested in studying the evolution of systems of interacting constituents. More specifically, systems whose constituents can be assigned to one of r distinct classes. One example is a binary spin system where spins are classified as being up or down [55]. Another is from evolutionary biology, where genes come in different types known as alleles [24]. Here we will generically refer to a distinct class as a species. The state of the system at a time t is defined by the r-dimensional vector

$$\mathbf{n}(t) = (n_1(t), n_2(t), ..., n_r(t)) \tag{2.1}$$

where $n_i(t)$ is the number of species i at time t. Equivalently, we can describe the system by the vector

$$\mathbf{x}(t) = (x_1(t), x_2(t), ..., x_r(t)) \tag{2.2}$$

where $x_i = n_i/\Omega$ and Ω is an extensive variable which is a measure of the size or volume of the system. For ecological models Ω is known as the carrying capacity and is the maximum population size the environment of a system can sustain indefinitely [23]. Therefore, we regard the variables x_i as population densities of each of the i species. In this chapter we will restrict our descriptions to a system comprising two species, A and B; the number of species A will be denoted by n and the number of species B by m. The state of the system is given by $\mathbf{n} = (n, m)$, or $\mathbf{x} = (x, y)$.

2.3 Jump Processes

In an IBM the state of the system evolves through changes in the number of each type of constituent. The numbers of each species in the systems must be treated as a random variable due to the demographic noise. This means the system will evolve probabilistically in time, and the interactions between the constituents and between the constituents and the environment are stochastic processes [25]. The interactions are referred to as jump processes because the system jumps discontinuously between discretely countable states. Typically these jump processes depend on the state of the system, i.e. the number of each constituent which can partake in the interaction.

We define a jump process in terms of a transition rate $T(n', m'|n, m)$: the probability that a system in a state (n, m) at time t is in a state (n', m') an infinitesimal time τ later is $T(n', m'|n, m)\tau$. Throughout this thesis we regard the time interval τ to be infinitesimal, in this chapter and in subsequent applications of the methods presented here. This allows us to neglect any contributions from higher-order terms $o(\tau)$ when defining a continuous-time limit [26]. The probability density that the system is in the state (n, m) at a time t we denote by $P(n, m)$.

The processes considered in the models studied in this thesis are defined as continuous-time Markov processes [26]. Birth and death processes in a population are the classic example of where this approach is implemented. The Markov property enters naturally as transition rates depend on the state of the system at that time and not on the previous history of the system. The jump processes can be described as inhomogeneous Poisson processes because the rate at which

an event can occur, $T(n', m'|n, m)$, is a function of n and m which are constant between events meaning the rate is constant also [7].

Strictly to define the transition rates we write

$$T(n', m'|n, m) = \lim_{\tau \to 0} \frac{P(n', m'|n, m)}{\tau} \tag{2.3}$$

where $P(n', m'|n, m)$ is the conditional probability. This satisfies the considerations set out by Gardiner [26] which must be made to define a continuous Markov process, via derivation of a differential form of the Chapman-Kolmogorov equation.

One-Step Processes

In this thesis we will be interested in models where the stochastic processes change the species number n_i by increments of 1. In [7], van Kampen describes such processes as *one-step processes*, and gives a general formalism to model them, and extensively details methods of solution. The motivation for doing so is due to their ubiquity in stochastic modelling, for example in the kinetics of chemical reactions and in the birth and death of individuals in population dynamics.

In our definition of a one-step processes we also include processes akin to those such as the predator-prey interaction which allows a birth of one species at the expense of another. For clarity, in a two species model we consider one-step processes to be those with the non-zero transition rates

$$\begin{aligned} T(n', m'|n, m) = T(n', m|n, m)\delta_{n', n\pm1} + T(n, m'|n, m)\delta_{m', m\pm1} \\ + T(n', m'|n, m)\delta_{n', n\pm1}\delta_{m', m\mp1} \end{aligned} \tag{2.4}$$

where δ_{ij} is the Kronecker-Delta symbol.

2.4 Non-Spatial Models: Patch Dynamics

When considering models where the number of constituents is not fixed, extra considerations have to be taken to ensure the population remains finite. For example, if a model of a one species population with birth and death processes given by transition rates $T(n+1|n) = \alpha n$ and $T(n-1|n) = \beta n$ respectively,

if $\alpha > \beta$ the population will become infinitely large. The usual fix for this is to introduce the carrying capacity of the system N. This is the size of population that the system can accommodate indefinitely, and is a natural extensive variable to describe the volume of the system. Now the birth rate is adjusted to inhibit a birth in the event that the population is close to to the carrying capacity: $T(n+1|n) = \alpha n(1 - n/N)$. So the birth rate approaches zero as n approaches N. This form of birth rate is that of the well studied logistic growth [23].

Rather than implementing logistic growth by hand to correct birth rates in a system, it can be incorporated into non-spatial models explicitly by following the formalism presented in [27]. In our model system, each constituent occupies a single site on the patch, and the population is considered *well-mixed* so the distance between sites is coarse-grained out of the system. While the total number of the population $n + m$ is not fixed, we do restrict the number of sites on the patch they inhabit $N = n + m + e$ to be constant, where e are the number of empty sites E. In a sense E is entering as a passive species into this two species population. The kinetics of the interactions are now formulated by consideration of the number of ways the constituents involved can be selected from the patch. So the birth of an A depends not only on the number of A but also on the available spaces on the patch for the new A to inhabit:

$$A + E \xrightarrow{a} A + A \; . \tag{2.5}$$

The corresponding transition rate is

$$T(n+1, m|n, m) = 2a\frac{n}{N}\frac{(N-n-m)}{N-1} \; . \tag{2.6}$$

The factor of 2 is a combinatorial factor accounting for the number of ways of picking an A and an E. The rate constant a could absorb this factor, and also it can be rescaled by one or both of the extensive terms in the denominator. In effect, rescaling the rate constant of the interaction is rescaling time, the significance of which will be explained in due course. One other consideration to be made is how many reactants one draws to decide which reaction occurs. While the birth of an A requires the interaction of an A and an E, the death of an A,

$$A \xrightarrow{d} E, \tag{2.7}$$

with rate

$$T(n-1,m|n,m) = d\frac{n}{N} \tag{2.8}$$

needs only an A for the reaction to occur. While one could have a probability μ_1 to draw one reactant and μ_2 to draw two etc [27], here we will always have it equally likely and these rates can be absorbed into the rate constants.

Copying Dynamics

The conservation of the patch size N can also be achieved through copying dynamics. By this, we mean a death and birth event occur simultaneously so that a newly created constituent assumes the space occupied previously by the constituent which dies. This has the composite effect of one site at a patch copying the state of a site at another patch.

2.4.1 Example Model

To fully elucidate the formalism and methods presented in this chapter, at this stage we present a model that will be analysed in its full physical context in chapter 4. The model is of a non-spatial population comprising two competing species A and B with carrying capacity N. Each species undergoes the same processes with analogous rates. (To write down the reactions and transition rates for species B given those for species A, one simply relabels $A \leftrightarrow B$, $n \leftrightarrow m$ etc.)

Individuals of both species reproduce with rate a according to (2.5) while each can die due to: (i) natural death with rate d, as in (2.7); (ii) predation from the other species with rate p,

$$A + B \xrightarrow{p} A + E\,; \tag{2.9}$$

and (iii) cannibalism from another of its species with rate c,

$$A + A \xrightarrow{c} A + E\,. \tag{2.10}$$

These four processes give us the transition rates for the model

$$\begin{aligned} T(n+1,m|n,m) &= 2a\frac{n(N-n-m)}{N} \\ T(n,m+1|n,m) &= 2a\frac{m(N-n-m)}{N} \\ T(n-1,m|n,m) &= dn + c\frac{n(n-1)}{N} + 2p\frac{nm}{N} \\ T(n,m-1|n,m) &= dm + c\frac{m(m-1)}{N} + 2p\frac{nm}{N}\ . \end{aligned} \tag{2.11}$$

where the rate constant d has been rescaled by N and a, p, c by $N-1$.

Finally, we note that not all models require the consideration of logistic growth to ensure populations remain finite. Typically this is achieved by having more exotic interactions, which require a higher number of reactants or equivalently higher-order polynomials for birth and death rates. In this thesis we shall employ both methods.

2.5 Spatial Models: Migration Between Patches

When constructing a dynamical model it is important to consider whether the system in question is best characterised as being spatially discrete. For example, in many ecological models the role of spatial heterogeneity can play a crucial part in the existence and observed behaviour of a population [51, 56]. To incorporate space into a patch model formalism, we regard the population as a composite system comprising several patches. These patches can be placed on the sites of a lattice, alternatively the nodes of a network, whose topology must be defined. Constituents in the system are then able to migrate between different patches. The local dynamics of each patch are in principle the same, but this does not have to be the case. For example, one may be interested in studying the effect of having a population in a spatially heterogeneous environment. If the birth rate of a species is greater in one region, due for example to a greater abundance of food, then this can be modelled by having patch dependent birth rates [57]. As with single patch dynamics, the size of the composite population can be kept finite. For example, in a two patch system the transition rate for an A at site 1

to move to site 2 is

$$T(n_1 - 1, m_1, n_2 + 1, m_2 | n_1, m_1, n_2, m_2) \propto n_1(N - n_2 - m_2) \ . \tag{2.12}$$

2.5.1 Lattice Populations

We can also study spatially extended systems by modelling the system as a lattice of sites, each site of which hosts a well-mixed population i.e. a non-spatial patch. The topology of the lattice can be defined through the adjacency matrix a_{ij} which has elements 1 if the site i and site j are connected, and otherwise are 0. By connected we mean that interactions may take place between constituents at adjacent patches. In doing so we implicitly introduce a length scale over which the dynamics act. One can assign distances to adjacent patches and thereby to these connections. For example, one can employ the two-dimensional (2D) square lattice where each patch is in contact at a fixed distance δ from its 4 nearest neighbours. Care must be taken in comparing such discrete space systems to continuum field-theoretic results [31]. This will be addressed in the relevant chapters.

2.6 The Master Equation

For a system being described in terms of continuous-time Markov processes we can express the evolution of the system by a linear first-order differential equation in terms of the transition rates T [7]:

$$\frac{dP(\mathbf{n})}{dt} = \sum_{\mathbf{n}'} [T(\mathbf{n}|\mathbf{n}')P(\mathbf{n}') - T(\mathbf{n}'|\mathbf{n})P(\mathbf{n})]. \tag{2.13}$$

We interpret this as a gain-loss equation: the first term is the probability flowing into the state $\mathbf{n}$ from all states $\mathbf{n}'$ for which there is a non-zero transition rate; conversely the second term is the total probability leaving the state $\mathbf{n}$.

Writing the master equation for a stochastic model is akin to writing $F = ma$ in Newtonian physics, or the Hamiltonian in quantum mechanics. In an IBM, the master equation (2.13) give a complete description of the system, describing how it will evolve over time. The particular dynamics of the stochastic processes which the constituents undergo are encoded in the transition rates T. In practice,

the starting point of an IBM is to write down which stochastic processes which the species undergo, define the transitions with which they which occur, and then present the dynamics in a master equation.

This is the simple part: in practice it is very nearly always impossible to solve the master equation [7]. However, as we will show, one can calculate moments of the distribution $P(n, m, t)$ from it which allows the deterministic behaviour to be studied by analysis of the the mean-field equations. More significantly, it is also possible to approximate the master equation by means of a second-order partial differential equation known as a Fokker-Planck equation [54], allowing an analytical description of the fluctuations about the deterministic behaviour predicted by the mean-field equations.

For our toy model defined by the transition rates (2.11) the 2D master equation is

$$\begin{aligned}\frac{dP(n,m)}{dt} = &\quad T(n,m|n-1,m)P(n-1,m) - T(n+1,m|n,m)P(n,m) \\ &+ \quad T(n,m|n+1,m)P(n+1,m) - T(n-1,m|n,m)P(n,m) \\ &+ \quad T(n,m|n,m-1)P(n,m-1) - T(n,m+1|n,m)P(n,m) \\ &+ \quad T(n,m|n,m+1)P(n,m+1) - T(n,m-1|n,m)P(n,m).\end{aligned} \tag{2.14}$$

2.6.1 Mean-Field Equations

In an IBM the first thing one does after writing down the master equation is to find the deterministic behaviour of the system. To do we must find the rate equations for the evolution of the first moments of the distribution $P(n, m)$. The moments are defined as

$$\langle n^p m^q \rangle = \sum_{n=0}^{N-1} \sum_{m=0}^{N-1} n^p m^q P(n,m) \ , \qquad p, q \in \mathbb{N}. \tag{2.15}$$

In practice, it is often straightforward to write down the correct mean-field equations from inspection of the rates, but here we will illustrate with the concrete example of the toy model how to derive them from the master equation.

Formally, the mean-field behaviour is recovered in taking the infinite system size limit, $N \to \infty$ [27]. To derive the rate equation for n we multiply the master

equation (2.14) by n and sum over all n and m. Taking the first two lines of (2.14) and using (2.15) we have

$$\frac{d\langle n\rangle}{dt} = \sum_{m=0}^{\infty}\left(\sum_{n=0}^{\infty} nT(n,m|n-1,m)P(n-1,m) - \sum_{n=0}^{\infty} nT(n+1,m|n,m)P(n,m) + \sum_{n=0}^{\infty} nT(n,m|n+1,m)P(n+1,m) - \sum_{n=0}^{\infty} nT(n-1,m|n,m)P(n,m)\right).$$

We wish to change summation variable to bring the first term to the same form of the second term, and similarly for the third and fourth terms. Noting that the lower limit can begin at 1 due to the first term in the sum contributing zero, we make the substitution $n = n-1$ in the first term and $n = n+1$ in the third term, which after cancellation with the third and fourth terms gives

$$\frac{d\langle n\rangle}{dt} = \sum_{n,m=0}^{\infty}\Big(T(n+1,m|n,m)P(n,m) - T(n-1,m|n,m)P(n,m)\Big). \quad (2.16)$$

We still have to consider the contribution from the third and fourth lines of (2.14):

$$\sum_{m=0}^{\infty}\sum_{n=0}^{\infty} n\Big(T(n,m|n,m-1)P(n,m-1) - T(n,m+1|n,m)P(n,m) + T(n,m|n,m+1)P(n,m+1) - T(n,m-1|n,m)P(n,m)\Big).$$

We can relabel the sum in the first term by $m = m-1$, and use the boundary condition for the probability distribution that $P(n,-1) = 0$ to begin the summation from $m = 0$. This means the first and second terms will cancel. We can also relabel the sum in the third term by $m = m+1$:

$$\sum_{n=0}^{\infty} n\left(\sum_{m=1}^{\infty} T(n,m-1|n,m)P(n,m) - \sum_{m=0}^{\infty} T(n,m-1|n,m)P(n,m)\right).$$

From inspection of the rates (2.11) we see the rate $T(n,m-1|n,m)$ is zero for $m = 0$. Therefore these two terms also cancel and so there is no contribution to the rate equation for $\langle n\rangle$.

We now explicitly put in the rates for our toy model (2.11) into (2.16):

$$\frac{d\langle n\rangle}{dt} = \sum_{n,m=0}^{\infty} \left(2a\frac{n(N-n-m)}{N} - dn - 2p\frac{nm}{N} - c\frac{n(n-1)}{N} \right) P(n,m) \ . \quad (2.17)$$

Now applying the definition of the average (2.15) and dividing through by N we have

$$\frac{d}{dt}\frac{\langle n\rangle}{N} = 2a\frac{\langle n\rangle(N-\langle n\rangle-\langle m\rangle)}{N^2} - d\frac{\langle n\rangle}{N} - 2p\frac{\langle nm\rangle}{N^2} - c\frac{\langle n^2\rangle-\langle n\rangle}{N^2} \quad (2.18)$$

In the deterministic limit $N \to \infty$ we can make the mean-field assumption to neglect fluctuations, meaning the variances and covariances are zero [26]. This means for the hierarchy of moments, we have the separation ansatz:

$$\langle n^p m^q\rangle = \langle n\rangle^p \langle m\rangle^q. \quad (2.19)$$

Applying this and defining the average population densities

$$\rho = \langle n\rangle/N \quad (2.20)$$

$$\sigma = \langle m\rangle/N \quad (2.21)$$

we can write (2.17) as the mean-field rate equation for the evolution of population density of species A,

$$\frac{d\rho}{dt} = 2a\rho(1-\rho-\sigma) - d\rho - 2p\rho\sigma - c\rho^2. \quad (2.22)$$

Unsurprisingly, given the neutrality and symmetry in the processes defined in the toy model, following the same procedure for species B yields the rate equation

$$\frac{d\sigma}{dt} = 2a\sigma(1-\rho-\sigma) - d\sigma - 2p\rho\sigma - c\sigma^2. \quad (2.23)$$

Once one has obtained the mean-field equations of the system they should be solved, where possible. Often, the best that can be done is to solve the linearised system. Stability analysis can then be performed to determine the phase portrait of the deterministic behaviour that is permitted by the system. Our principal interest is to study the role fluctuations due to the demographic noise can have in

producing dynamical behaviour not predicted by this deterministic framework.

2.7 The Fokker-Planck Equation

To understand the nature of fluctuations about the deterministic behaviour a popular approach is to approximate the master equation by a Fokker-Planck equation (FPE). There are several ways to derive an FPE. Here we will present the two methods employed in this thesis: (i) truncation of the Kramers-Moyal expansion of the master equation, following the spirit of the derivation given by Gardiner [26]; (ii) the linear noise approximation of van Kampen [7], where we give a systematic derivation of his system size expansion of the master equation. We will show that to leading order in the inverse system size of the population that the two descriptions are equivalent. From an application perspective however, one is often preferable to the other and so we use both in this thesis.

2.7.1 The Kramers-Moyal Expansion

A Fokker-Planck equation can be obtained for continuous variables only [54]. Taking a small parameter $\epsilon \ll 1$ we define the coarse-grained continuous variables x and y as population densities: $x = \epsilon n, y = \epsilon m$. We will define $\epsilon = 1/\Omega$ where Ω is an extensive variable describing the size or volume of the system, which for our purposes we take to be the carrying capacity.

Our starting point is the two-species master equation

$$\frac{dP(x,y)}{dt} = \sum_{x'}\sum_{y'}\left[T(x,y|x',y')P(x',y') - T(x',y'|x,y)P(x,y)\right] \tag{2.24}$$

giving the evolution of the probability density $P(x,y)$. We can express the transition rates in (2.24) in terms of the jumps in the state space in a small time interval $[t, t+\tau]$. Following the formalism of Gardiner [26] we write

$$r = x - x', s = y - y' \quad \text{in the first sum,} \tag{2.25}$$

$$r = x' - x, s = y' - y \quad \text{in the second sum} \tag{2.26}$$

and express the transition rates in terms of the jumps functionally as

$$T(x', y'|x, y) = w(x, y; x' - x, y' - y) \; . \tag{2.27}$$

This allows us to write (2.24) as

$$\frac{dP(x,y)}{dt} = \sum_{r,s} \Big[w(x, y; -r, -s)P(x - r, y - s) - w(x, y; r, s)P(x, y) \Big] \tag{2.28}$$

where the sum runs over all possible non-zero transitions. As we are restricted to one-step processes we enumerate the sum over $r, s \in [-\epsilon, 0, \epsilon]$. We now Taylor expand the first term about (x, y):

$$\frac{dP(x,y)}{dt} = \sum_{r,s} \Bigg[\sum_{k=0}^{\infty} \sum_{l=0}^{\infty} (-1)^{k+l} \frac{r^k s^l}{k!\; l!} \frac{\partial^k}{\partial x^k} \frac{\partial^l}{\partial y^l} \Big(w(x, y; -r, -s)P(x, y) \Big) - w(x, y; r, s)P(x, y) \Bigg]. \tag{2.29}$$

The first term in the expansion will cancel with the second term in (2.29) as expanding out the sums over r and s will give identical terms in each. The remaining terms we express as

$$\frac{dP(x,y)}{dt} = \sum_{\substack{k,l=0 \\ k+l \neq 0}}^{\infty} (-1)^{k+l} \frac{\partial^k}{\partial x^k} \frac{\partial^l}{\partial y^l} \Big(\alpha_{k,l}(x, y)P(x, y) \Big) \tag{2.30}$$

where we define the jump moments $\alpha_{k,l}(x, y)$ as

$$\alpha_{k,l}(x, y) = \frac{1}{k!\; l!} \sum_{r,s} r^k s^l w(x, y; r, s) \tag{2.31}$$

$$= \frac{1}{k!\; l!} \sum_{x',y'} (x - x')^k (y - y')^l T(x', y'|x, y) \tag{2.32}$$

$$= \lim_{\tau \to 0} \frac{1}{k!\; l!} \sum_{x',y'} (x' - x)^k (y' - y)^l \frac{P(x', y'|x, y)}{\tau} \tag{2.33}$$

$$= \lim_{\tau \to 0} \frac{1}{k!\; l!} \frac{\langle (\delta x)^k (\delta y)^l \rangle_{\mathbf{x}(t)=\mathbf{x}}}{\tau}. \tag{2.34}$$

In the second line we have substituted back to x' and y' using (2.26). We can

absorb a minus sign by relabelling of the sum from $r \to -r, s \to -s$ so we are free to write $r = x' - x$, $s = y' - y$. In the third line the definition (2.3) is used to define the probability of a transition occurring in the continuous-time interval $[t, t + \tau]$. In the final line we introduce the variables

$$\delta x = x' - x \tag{2.35}$$

$$\delta y = y' - y \tag{2.36}$$

and define the average as

$$\langle x \rangle_{\mathbf{x}(t)=\mathbf{x}} = \sum_{x',y'} = xP(x', y'|x, y) \tag{2.37}$$

where the subscript specifies at time t the system was definitely in the state $\mathbf{x}$ and we are averaging over all possible final states $\mathbf{x}'$ at a later time $t + \tau$.

Toy model

In practice we assume that these jump moments are known, as we can calculate the averages straightforwardly from the given transition rates of the model. We will do so here for our toy model. We take the random variables $x = n/N$, $y = m/N$ to be continuous if the carrying capacity N is suitably large. We express the required moments as

$$\langle (\delta x)^k (\delta y)^l \rangle_{\mathbf{x}(t)=\mathbf{x}} = \sum_{x',y'} (x' - x)^k (y' - y)^l P(x', y'|x, y) \tag{2.38}$$

where $P(x', y'|x, y)$ is the probability that x and/or y change by $\epsilon = 1/N$ in a time τ. For the toy model the non-zero moments are

$$\begin{aligned} \langle (\delta x)^k \rangle_{\mathbf{x}(t)=\mathbf{x}} &= \frac{1}{N^k} \Big(P(x + \epsilon, y|x, y) \pm P(x - \epsilon, y|x, y) \Big) \\ \langle (\delta y)^k \rangle_{\mathbf{x}(t)=\mathbf{x}} &= \frac{1}{N^k} \Big(P(x, y + \epsilon|x, y) \pm P(x, y - \epsilon|x, y) \Big) \end{aligned} \tag{2.39}$$

where the $\pm$ sign is negative for odd k and positive for even k.

We know that the probabilities of the densities evolving to (x', y') from (x, y) in a time interval τ is the same as the probability of the population numbers

evolving to (n', m') from (n, m). So for the example of the birth of an A given by the transition rate (2.6) we have

$$\begin{aligned} P(x+\epsilon, y|x, y) &\equiv P(n+1, m|n, m) \\ &= 2an\frac{(N-n-m)}{N}\tau \\ &= 2ax(1-x-y)\tau \end{aligned} \tag{2.40}$$

after rescaling the rate constant a by N. Expressing $P(x-\epsilon, y|x, y)$ in an analogous fashion, the moments are now given by

$$\begin{aligned} \langle(\delta x)^k\rangle_{\mathbf{x}(t)=\mathbf{x}} &= \frac{\tau}{N^k}\Big(2ax(1-x-y) \pm [dx + 2pxy + c(x^2 - N^{-1}x)]\Big) \\ \langle(\delta y)^k\rangle_{\mathbf{x}(t)=\mathbf{x}} &= \frac{\tau}{N^k}\Big(2ay(1-x-y) \pm [dy + 2pxy + c(y^2 - N^{-1}y)]\Big)\,. \end{aligned} \tag{2.41}$$

Truncating the Expansion

The infinite series for the time evolution of the probability density $P(x, y)$ (2.30) is the Kramers-Moyal expansion of the master equation (2.24). To obtain a Fokker-Planck equation we truncate the expansion at the second term, yielding

$$\begin{aligned} \frac{dP(x,y)}{dt} =& -\frac{\partial}{\partial x}\alpha_{1,0}(x,y)P - \frac{\partial}{\partial y}\alpha_{0,1}(x,y)P \\ &+ \frac{\partial^2}{\partial x^2}\alpha_{2,0}(x,y)P + \frac{\partial^2}{\partial x \partial y}\alpha_{1,1}(x,y)P + \frac{\partial^2}{\partial y^2}\alpha_{0,2}(x,y)P. \end{aligned} \tag{2.42}$$

More generally this is often written schematically as

$$\frac{dP(\mathbf{x})}{dt} = \sum_i -\frac{\partial}{\partial x_i}[A_i(\mathbf{x}, t)P] + \sum_{i,j}\frac{\partial^2}{\partial x_i \partial x_j}[D_{ij}(\mathbf{x}, t)P] \tag{2.43}$$

with the drift vector A_i and the diffusion matrix D_{ij} defined as

$$A = \begin{pmatrix} \alpha_{1,0}(x,y) \\ \alpha_{0,1}(x,y) \end{pmatrix}, \qquad D = \begin{pmatrix} \alpha_{2,0}(x,y) & \alpha_{1,1}(x,y)/2 \\ \alpha_{1,1}(x,y)/2 & \alpha_{0,2}(x,y) \end{pmatrix}. \tag{2.44}$$

In order for the truncation to be valid we assume that only the first and second order jump moments are non-zero. That is

$$\alpha_{k,l}(x,y) = 0, \quad k+l > 2. \tag{2.45}$$

Pawula's theorem states that the expansion can be terminated after the first or the second term, or all terms must be included [58, 54]. The jump moments can be expressed in terms of the moments as in (2.34),

$$\alpha_{k,l} = \lim_{\tau\to 0} \frac{1}{k!\ l!} \frac{\langle (\delta x)^k (\delta y)^l \rangle_{\mathbf{x}(t)=\mathbf{x}}}{\tau}. \tag{2.46}$$

We see from the explicit form of the moments given in (2.41) that in general it will always be possible to rescale τ with N before taking the continuous-time limit $\tau \to 0$. If we can do this in such a way so that only the first and second moments are the dominant terms in the Kramers-Moyal expansion in comparison to the higher-order terms, we can legitimately truncate the expansion at the second term. This is necessarily a step in the derivation that must be done on a case by case basis, dependent on the particular processes which define the model.

For the toy model, from the expressions for the moments (2.41) we see for example that

$$\langle (\delta x)^k \rangle_{\mathbf{x}(t)=\mathbf{x}} \sim \tau \left[\frac{1}{N^k} + \mathcal{O}\left(\frac{1}{N^{k+1}} \right) \right] . \tag{2.47}$$

Now to take the $\tau \to 0$ limit to define the jump moments in (2.46) we scale time as $\tau = \tau/N$. Clearly as we are interested in finite systems, we are not actually taking the limit but approximating it with a large but finite N. We see that as the first jump moments have no N dependence they remain. For the higher-order terms we also retain the second order jump moments as they dominate over the rest in the Kramers-Moyal expansion, which fall away in increasing powers of N^{-1} in comparison.

In doing so we can now describe the dynamics of the model using a Fokker-

Planck equation (2.42) as an approximation of the master equation with

$$\alpha_{1,0}(x,y) = 2ax(1-x-y) - dx - 2pxy - cx^2 \tag{2.48}$$

$$\alpha_{0,1}(x,y) = 2ay(1-x-y) - dy - 2pxy - cy^2 \tag{2.49}$$

$$\alpha_{2,0}(x,y) = \frac{1}{N}\Big(2ax(1-x-y) + dx + 2pxy + cx^2\Big) \tag{2.50}$$

$$\alpha_{0,2}(x,y) = \frac{1}{N}\Big(2ay(1-x-y) + dy + 2pxy + cy^2\Big) \tag{2.51}$$

$$\alpha_{1,1}(x,y) = 0. \tag{2.52}$$

2.8 The van Kampen System Size Expansion

Obtaining an FPE from the Kramers-Moyal expansion was criticised by van Kampen due to the arbitrary nature of introducing a small parameter which could be used to truncate the expansion at the second term. Instead, he offered a systematic way [7] in which to expand the master equation, a formulation of which we present here.

The Step Operator $\hat{\mathcal{E}}$

As we are concerned with systems involving one-step processes it is useful to introduce the step operator $\hat{\mathcal{E}}$ which, for example, when it acts upon a function $f(n,m)$ yields

$$\hat{\mathcal{E}}_n^{\pm 1} f(n,m) = f(n \pm 1, m)\ . \tag{2.53}$$

Using this operator allows us to rewrite the master equation

$$\frac{dP(n,m)}{dt} = \sum_{n',m'} [T(n,m|n',m')P(n',m') - T(n'm'|n,m)P(n,m)] \tag{2.54}$$

in a more compact form. We define analogous jumps to those in (2.26)

$$\begin{aligned} &R = n - n', S = m - m' \quad \text{in the first sum} \\ &R = n' - n, S = m' - m \quad \text{in the second sum,} \end{aligned} \tag{2.55}$$

where now $R, S \in [-1, 0, 1]$, and can write the master equation as

$$\frac{dP(n,m)}{dt} = \sum_{R,S}[T(n,m|n-R,m-s)P(n-R,m-S) - T(n+R,m+S|n,m)P(n,m)]. \tag{2.56}$$

We can rewrite this using the step operator $\hat{\mathcal{E}}$ as:

$$\frac{dP(n,m)}{dt} = \sum_{R,S}(\hat{\mathcal{E}}_n^{-R} - 1)(\hat{\mathcal{E}}_m^{-S} - 1)T(n+R, m+S|n,m)P(n,m)\ . \tag{2.57}$$

For example, the toy model master equation (2.14) can be written using the step operator as

$$\begin{aligned}\frac{dP(n,m)}{dt} &= (\hat{\mathcal{E}}_n^{-1} - 1)T(n+1,m|n,m)P(n,m) \\ &+(\hat{\mathcal{E}}_n^{1} - 1)T(n-1,m|n,m)P(n,m) \\ &+(\hat{\mathcal{E}}_m^{-1} - 1)T(n,m+1|n,m)P(n,m) \\ &+(\hat{\mathcal{E}}_m^{1} - 1)T(n,m-1|n,m)P(n,m)\ .\end{aligned} \tag{2.58}$$

2.8.1 Scaling Assumption

The principal assumption of van Kampen is how to express the transition rates $T(n', m'|n, m)$ in terms of the dependence on the system size Ω. While keeping the size of the jumps $R, S \propto \Omega^0$ as defined by (2.55), van Kampen argued it is best to describe the dependence of the system's state by the intensive variables $x = n/\Omega$ and y/Ω. To encapsulate this van Kampen proposed the scaling ansatz [7, 26]

$$T(n', m'|n, m) = W(n, m; R, S) = \Omega w(x, y; R, S). \tag{2.59}$$

Taking the example of the birth rate in our toy model, we can express it as

$$T(n+1,m|n,m) = 2an\frac{(N-n-m)}{N} = 2aNx(1-x-y) \equiv \Omega w(x,y|1,0) \tag{2.60}$$

where $\Omega \equiv N$ and $w(x, y; 1, 0) = 2ax(1-x-y)$. It is always possible when defining a stochastic process following the prescription given in section 2.4 to scale the rate constants $\{a\}$ to bring the transition rates into the form of the scaling ansatz (2.59). For the birth process in the toy model the rate constant a was scaled by

$a = a/(N-1)$ to get the transition rate (2.6). In effect we are rescaling time to leave the transition rates independent of Ω.

2.8.2 Ansatz

The second assumption van Kampen made was to describe the random variables x and y in terms of a well-defined mean value, and a stochastic component to characterise fluctuations about these mean values. Using the observation that in the large system size limit $n \equiv \Omega x$, $m \equiv \Omega y$ and that fluctuations about the mean typically fall off like $\Omega^{-1/2}$, we write the change of variable ansatz [7]

$$\begin{aligned} n &= \Omega\rho(t) + \sqrt{\Omega}\,\xi \\ m &= \Omega\sigma(t) + \sqrt{\Omega}\,\eta \end{aligned} \tag{2.61}$$

to new stochastic variables ξ and η. The two deterministic functions $\rho(t)$ and $\sigma(t)$ are well defined functions which in fact turn out to be the mean-field population densities, whose equations of motion are derived in the systematic expansion of the master equation.

2.8.3 The Expansion

We now wish to apply this ansatz to (2.57). Defining a new probability distribution $P(n,m) = \Pi(\xi,\eta)$, the time derivative transforms as

$$\frac{\partial P}{\partial t} = \frac{\partial \Pi}{\partial t} - \sqrt{\Omega}\,\dot{\rho}\frac{\partial \Pi}{\partial \xi} - \sqrt{\Omega}\,\dot{\sigma}\frac{\partial \Pi}{\partial \eta} \tag{2.62}$$

where the chain rule has been applied using (2.61) while holding n and m constant. The operator $\hat{\mathcal{E}}$ we can express as a power series:

$$\hat{\mathcal{E}}_n^{-R} f(n) = f(n-R) = \sum_{k=0}^{\infty} (-1)^k \frac{R^k}{k!} \Omega^{-k/2} \frac{\partial^k}{\partial \xi^k} f(n) \tag{2.63}$$

where we have Taylor expanded $f(n-R)$ and changed variable via (2.61). As this holds for an arbitrary function f we have the result

$$\hat{\mathcal{E}}_n^{-R} = \sum_{k=0}^{\infty} (-1)^k \frac{R^k}{k!} \Omega^{-k/2} \frac{\partial^k}{\partial \xi^k}. \tag{2.64}$$

Putting all these ingredients together (2.57) becomes

$$\frac{\partial \Pi}{\partial t} - \sqrt{\Omega}\,\dot{\rho}\frac{\partial \Pi}{\partial \xi} - \sqrt{\Omega}\,\dot{\sigma}\frac{\partial \Pi}{\partial \eta} \tag{2.65}$$
$$= \sum_{\substack{k,l=0 \\ k+l\neq 0}}^{\infty} (-1)^{k+l}\Omega^{(2-k-l)/2}\frac{\partial^k}{\partial \xi^k}\frac{\partial^l}{\partial \eta^l}\left[\frac{1}{k!\;l!}\sum_{R,S} R^k S^l w(x,y;R,S)\right]\Pi(\xi,\eta)$$

The term in the square brackets we recognise as being related to the jump moments defined in (2.31). We write it as

$$\tilde{\alpha}_{k,l}(x,y) = \frac{1}{k!\;l!}\sum_{R,S} R^k S^l w(x,y;R,S) \tag{2.66}$$
$$= \frac{1}{k!\;l!}\sum_{n',m'} (n'-n)^k (m-m')^l w(x,y;R,S)\;. \tag{2.67}$$

We carry out a further Taylor expansion in powers of $\Omega^{-1/2}$ of these jump moments about $x=\rho$, $y=\sigma$ using the ansatz (2.61):

$$\tilde{\alpha}_{k,l}(x,y) = \sum_{p,q=0}^{\infty} \frac{\Omega^{-(p+q)/2}}{p!\;q!}\tilde{\alpha}_{k,l}^{(p)(q)}(\rho,\sigma)\xi^p\eta^q \tag{2.68}$$

where

$$\tilde{\alpha}_{k,l}^{(p)(q)}(\rho,\sigma) = \frac{\partial^p}{\partial \xi^p}\frac{\partial^q}{\partial \eta^q}\tilde{\alpha}(x,y)\bigg|_{x=\rho,y=\sigma}. \tag{2.69}$$

This gives us our final expression for the system size expansion:

$$\frac{\partial \Pi}{\partial t} - \sqrt{\Omega}\,\dot{\rho}\frac{\partial \Pi}{\partial \xi} - \sqrt{\Omega}\,\dot{\sigma}\frac{\partial \Pi}{\partial \eta} \tag{2.70}$$
$$= \sum_{\substack{k,l=0 \\ k+l\neq 0}}^{\infty}\sum_{p,q=0}^{\infty} \Omega^{(2-k-l-p-q)/2}\tilde{\alpha}_{k,l}^{(p)(q)}(\rho,\sigma)\frac{\partial^k}{\partial \xi^k}\frac{\partial^l}{\partial \eta^l}\left(\xi^p\eta^q\Pi\right).$$

As in the Kramers-Moyal expansion, we assume the jump moments can be obtained from the stochastic dynamics of the model. Here we find them by explicitly by doing the expansion. We write the master equation for our toy model (2.58) using the van Kampen ansatz (2.61) and the expansion of the step

operator (2.64):

$$\frac{\partial \Pi}{\partial t} - \sqrt{\Omega}\,\dot{\rho}\frac{\partial \Pi}{\partial \xi} - \sqrt{\Omega}\,\dot{\sigma}\frac{\partial \Pi}{\partial \eta} = \tag{2.71}$$

$$\left(-\frac{1}{\sqrt{N}}\frac{\partial}{\partial \xi} + \frac{1}{2N}\frac{\partial^2}{\partial \xi^2} + \dots\right) N2a\left[\rho + \frac{\xi}{\sqrt{N}}\right]\left[1 - \rho - \sigma - \frac{1}{\sqrt{N}}(\xi + \eta)\right]\Pi$$

$$+\left(\frac{1}{\sqrt{N}}\frac{\partial}{\partial \xi} + \frac{1}{2N}\frac{\partial^2}{\partial \xi^2} + \dots\right) N\left[\rho + \frac{\xi}{\sqrt{N}}\right]\left[d + 2p(\sigma + \frac{\eta}{\sqrt{N}}) + c(\rho + \frac{\xi}{\sqrt{N}})\right]\Pi$$

$$+\left(-\frac{1}{\sqrt{N}}\frac{\partial}{\partial \eta} + \frac{1}{2N}\frac{\partial^2}{\partial \eta^2} + \dots\right) N2a\left[\sigma + \frac{\rho}{\sqrt{N}}\right]\left[1 - \rho - \sigma - \frac{1}{\sqrt{N}}(\xi + \eta)\right]\Pi$$

$$+\left(\frac{1}{\sqrt{N}}\frac{\partial}{\partial \eta} + \frac{1}{2N}\frac{\partial^2}{\partial \eta^2} + \dots\right) N\left[\sigma + \frac{\eta}{\sqrt{N}}\right]\left[d + 2p(\rho + \frac{\xi}{\sqrt{N}}) + c(\sigma + \frac{\eta}{\sqrt{N}})\right]\Pi$$

To make progress we now equate the terms on the left and right hand side of the same order of Ω. We have dropped the N^{-1} term in the cannibalistic process with rate c as it will not feature in the order we expand to.

Mean-field Equations

To leading order $\mathcal{O}(\Omega^{1/2})$ we have from the $k = 1, l = 0$ and $k = 0, l = 1$ ($p = q = 0$) terms in (2.70):

$$\dot{\rho}\partial_\xi \Pi + \dot{\sigma}\partial_\eta \Pi = \tilde{\alpha}_{1,0}^{(0)(0)}(\rho, \sigma)\partial_\xi \Pi + \tilde{\alpha}_{0,1}^{(0)(0)}(\rho, \sigma)\partial_\eta \Pi \tag{2.72}$$

which yields the rate equations

$$\begin{aligned} \dot{\rho} &= \tilde{\alpha}_{1,0}^{(0)(0)}(\rho, \sigma) \\ \dot{\sigma} &= \tilde{\alpha}_{0,1}^{(0)(0)}(\rho, \sigma). \end{aligned} \tag{2.73}$$

These are the same deterministic equations found by following the method in section 2.6.1. We can write the deterministic equation for ρ as

$$\begin{aligned}\dot{\rho} = \tilde{\alpha}^{(0)(0)}_{1,0}(\rho,\sigma) &= \sum_{R,S} Rw(\rho,\sigma;R,S) \\ &= w(\rho,\sigma;1,0) - w(\rho,\sigma;-1,0) \\ &\equiv 2a\rho(1-\rho-\sigma) - d\rho - 2p\rho\sigma - c\rho^2 \end{aligned} \tag{2.74}$$

where we have used the jump moment definition (2.66), and the scaling ansatz (2.59). This is the same rate equation derived previously (2.22). It can also be obtained straightforwardly using the explicit van Kampen expansion for the toy model (2.71).

Fokker-Planck Equation

To find the FPE for the probability density of the fluctuations $\Pi(\xi,\eta)$ we equate terms of $\mathcal{O}(\Omega^0)$ in (2.70):

$$\begin{aligned}\frac{\partial \Pi}{\partial t} =& -\tilde{\alpha}^{(1)(0)}_{1,0}\frac{\partial}{\partial \xi}\Big(\xi\Pi\Big) - \tilde{\alpha}^{(0)(1)}_{0,1}\frac{\partial}{\partial \xi}\Big(\eta\Pi\Big) \\ &- \tilde{\alpha}^{(1)(0)}_{1,0}\frac{\partial}{\partial \eta}\Big(\xi\Pi\Big) - \tilde{\alpha}^{(0)(1)}_{0,1}\frac{\partial}{\partial \eta}\Big(\eta\Pi\Big) \\ &+ \tilde{\alpha}^{(0)(0)}_{2,0}\frac{\partial^2}{\partial \xi^2}\Pi + \tilde{\alpha}^{(0)(0)}_{1,1}\frac{\partial^2}{\partial \xi \partial \eta}\Pi + \tilde{\alpha}^{(0)(0)}_{0,2}\frac{\partial^2}{\partial \eta^2}\Pi. \end{aligned} \tag{2.75}$$

Defining the vector $\boldsymbol{\xi} = (\xi,\eta)$, we can express this in matrix notation as

$$\frac{\partial \Pi}{\partial t} = \frac{\partial}{\partial \xi_i}\gamma_{ij}\xi_j\Pi + \frac{\partial}{\partial \xi_i}D_{ij}\frac{\partial}{\partial \xi_j}\Pi \tag{2.76}$$

where the drift matrix γ and the diffusion matrix D are

$$\gamma = -\begin{pmatrix} \tilde{\alpha}^{(1)(0)}_{1,0}(\rho,\sigma) & \tilde{\alpha}^{(0)(1)}_{1,0}(\rho,\sigma) \\ \tilde{\alpha}^{(1)(0)}_{0,1}(\rho,\sigma) & \tilde{\alpha}^{(0)(1)}_{0,1}(\rho,\sigma) \end{pmatrix} \tag{2.77}$$

$$D = \begin{pmatrix} \tilde{\alpha}^{(0)(0)}_{2,0}(\rho,\sigma) & \tilde{\alpha}^{(0)(0)}_{1,1}(\rho,\sigma) \\ \tilde{\alpha}^{(0)(0)}_{1,1}(\rho,\sigma) & \tilde{\alpha}^{(0)(0)}_{0,2}(\rho,\sigma) \end{pmatrix}. \tag{2.78}$$

The FPE (2.76) is described as being linear as the drift terms only contain linear

terms of ξ and η, while the diffusion terms are independent of them. Obtaining a linear FPE at this order of Ω is a generic feature of the van Kampen system size expansion, and is referred to as the *linear noise approximation* [7]. In this thesis we will work within this approximation, which is suitable for a large but finite population. If one was working at an order of $\Omega \sim 10$ it is often necessary to go beyond this [59, 60].

Comparing the drift matrix γ with the mean-field equations (2.73) we recognise $-\gamma$ as the matrix of the linear stability analysis of the deterministic behaviour. In practice, the jump moments $\tilde{\alpha}$ which appear in the FPE (2.76) are found straightforwardly from doing the expansion by hand, such as with the toy model expansion (2.71).

2.8.4 Comparison of the Kramers-Moyal and van Kampen Expansions

It is clear that these two derivations are similar, and because in practice the van Kampen scaling form (2.59) can always be obtained they are often synonymous. The real difference is that the van Kampen expansion stems from acknowledging the physical situation we are interested in describing, that the fluctuations due to the noise can be regarded as some correction to the deterministic behaviour. The Kramers-Moyal expansion is a far more general treatment for a set of stochastic processes governed by a master equation.

To show that to the lowest order in $\Omega^{-1/2}$ the two expansions are equivalent, we give a simplified argument of that presented by Gardiner [26]. We write the jump moments (2.31) in the Kramers-Moyal expansion (2.30) as

$$\alpha_{k,l}(x,y) = \sum_{R,S} \frac{(n'-n)^k (m-m')^l}{\Omega^{k+l}} w(x,y;R,S) = \frac{1}{\Omega^{k+l}} \tilde{\alpha}(x,y) \tag{2.79}$$

where we have used the definition (2.66), and the transition rate $w(x,y;r,s) \equiv w(x,y;R,S) \sim \Omega^0$ describe the same transition probability and so are equivalent, each depending functionally only on x and y, not r and s. The Kramers-Moyal

FPE is then

$$\frac{dP(x,y)}{dt} = -\frac{1}{\Omega}\frac{\partial}{\partial x}\tilde{\alpha}_{1,0}(x,y)P - \frac{1}{\Omega}\frac{\partial}{\partial y}\tilde{\alpha}_{0,1}(x,y)P + \frac{1}{\Omega^2}\frac{\partial^2}{\partial x^2}\tilde{\alpha}_{2,0}(x,y)P + \frac{1}{\Omega^2}\frac{\partial^2}{\partial x \partial y}\tilde{\alpha}_{1,1}(x,y)P + \frac{1}{\Omega^2}\frac{\partial^2}{\partial y^2}\tilde{\alpha}_{0,2}(x,y)P. \tag{2.80}$$

We can multiply this expression by Ω and rescale time by $t = t/\Omega$. Applying the van Kampen transformation using the ansatz (2.61) and Taylor expanding each of the jump moment terms about $x = \rho$, $y = \sigma$ yields

$$\begin{aligned}
&\frac{\partial \Pi}{\partial t} - \sqrt{\Omega}\,\dot{\rho}\frac{\partial \Pi}{\partial \xi} - \sqrt{\Omega}\,\dot{\sigma}\frac{\partial \Pi}{\partial \eta} = \\
&\sqrt{\Omega}\frac{\partial}{\partial \xi}\sum_{p,q=0}^{\infty}\frac{\tilde{\alpha}_{1,0}^{(p)(q)}(\rho,\sigma)}{p!\;q!\;\Omega^{(p+q)/2}}\,\xi^p\eta^q\Pi + \sqrt{\Omega}\frac{\partial}{\partial \eta}\sum_{p,q=0}^{\infty}\frac{\tilde{\alpha}_{0,1}^{(p)(q)}(\rho,\sigma)}{p!\;q!\;\Omega^{(p+q)/2}}\,\xi^p\eta^q\Pi \\
&+ \frac{\partial^2}{\partial \xi^2}\sum_{p,q=0}^{\infty}\frac{\tilde{\alpha}_{2,0}^{(p)(q)}(\rho,\sigma)}{p!\;q!\;\Omega^{(p+q)/2}}\,\xi^p\eta^q\Pi + \frac{\partial^2}{\partial \eta^2}\sum_{p,q=0}^{\infty}\frac{\tilde{\alpha}_{0,2}^{(p)(q)}(\rho,\sigma)}{p!\;q!\;\Omega^{(p+q)/2}}\,\xi^p\eta^q\Pi \\
&+ \frac{\partial^2}{\partial \xi \partial \eta}\sum_{p,q=0}^{\infty}\frac{\tilde{\alpha}_{1,1}^{(p)(q)}(\rho,\sigma)}{p!\;q!\;\Omega^{(p+q)/2}}\,\xi^p\eta^q\Pi\,.
\end{aligned} \tag{2.81}$$

Again, the highest order terms yield the usual rate equations (2.73) which we assume are satisfied for $x = \rho$, $y = \sigma$, i.e. they cancel. What remains to the next lowest order in Ω^0 is the same FPE obtained from the van Kampen system size expansion (2.75). While the two expansions of the master equation agree to this lowest order, they diverge when higher-order terms are kept. Gardiner further elaborates on the significance of this result [26]. If one is only interested in the small noise approximation, i.e. this lowest order agreement, then the Kramers-Moyal FPE can be used to approximate the van Kampen FPE. In this thesis this is the order we shall work to and so both techniques will be used throughout. Often it is the case that to work with the Kramers-Moyal expansion is easier as we given a set of stochastic processes defined by transition rates calculating the moments in (2.34) is straightforward. The van Kampen FPE is useful when explicitly considering the fluctuations about a fixed point, and the linear structure of the FPE means we can solve it and explicitly write down the form of the probability density $\Pi(\xi, \eta)$.

2.9 The Langevin Equation

An alternative formulation to the Fokker-Planck equation in describing stochastic dynamics is to write a system of stochastic differential equations known as Langevin equations (LE). These are of the form

$$\dot{x_i} = f_i(\mathbf{x}) + \eta_i(t) \tag{2.82}$$

where the random variables $\eta_i(t)$ are defined by the statistics of their mean $\langle \eta_i(t) \rangle$ and the covariance matrix $\langle \eta_i(t)\eta_j(t') \rangle = C_{ij}(\mathbf{x}, t, t')$.

An LE is split into a deterministic part and a stochastic part. If one's knowledge of the system is only the equations of motion governing the mean-field behaviour, then care has to be taken in interpreting and dealing with the noise term η. This approach is the one taken in a population level model. If one then wishes to analyse the evolution of the system governed by these stochastic differential equations, they have to be numerically integrated and so somehow the statistics of the noise must be obtained or estimated. Two integration schemes are used, which primarily differ in deciding how to advance the time increment of the noise terms η. The Itô prescription updates at the start of the timestep whereas Stratonovitch updates at some weighted intermediate time between timesteps [26]. The expressions for the drift and diffusion terms in the LE can be written using a different calculus depending on which scheme is used.

The choice of which scheme to use is widely referred to as the Itô-Stratonovitch dilemma, which must be addressed when constructing a PLM from adding noise terms to a set of differential equations to describe the system. However, a great benefit in taking an IBM approach is that there is no ambiguity and the dilemma is avoided. As the transition rates governing the dynamics of the systems we study depend on the state of the system it seems a natural choice to update the noise at the beginning of the timestep where the state of the system is known, so following the Itô prescription. In the example of modelling radioactive decay, van Kampen [7] shows that using the Itô calculus succeeds in recovering the correct mean-field behaviour whereas Stratonovitch fails. The Itô prescription is more suited to dealing with intrinsic noise, a property of the system due to the discrete nature of the constituents and the finite number of them. This can be treated mathematically as idealised white noise which is delta-correlated in time. The

Stratonovitch prescription is more appropriate for dealing with "real" noise like that coming from an external source into the system with finite correlation time and finite amplitudes [26, 7].

2.9.1 Equivalence with the Fokker-Planck Equation

Under the Itô prescription, the equivalent LEs to the FPE (2.43) are

$$\begin{aligned} \dot{x} &= \alpha_{1,0}(x,y) + \eta_x(t) \\ \dot{y} &= \alpha_{0,1}(x,y) + \eta_y(t) \end{aligned} \tag{2.83}$$

where η are Gaussian random variables with statistics

$$\langle \eta_i(t) \rangle = 0 \tag{2.84}$$

$$\langle \eta_i(t)\eta_j(t') \rangle = 2D_{ij}\delta(t-t') \; . \tag{2.85}$$

It is often preferable to work in a Fokker-Planck formalism as there is no such ambiguity with regard to the noise. As the IBM approach begins with a master equation and transition rates, once the moments have been obtained, the jump moments follow and we can write down the FPE and then alternatively the LE under the Itô prescription if we so choose using (2.83).

For 1D problems we can write the LE

$$\dot{\phi} = f(\phi) + g(\phi)\eta(t) \tag{2.86}$$

where η is Gaussian white noise with zero mean and unit variance. This is equivalent, following the Itô prescription, to the 1D FPE [54]

$$\frac{\partial P(\phi,t)}{\partial t} = -\frac{\partial}{\partial \phi}\left(f(\phi)P \right) + \frac{\partial^2}{\partial \phi^2}\left(\frac{g^2(\phi)}{2} P \right) \; . \tag{2.87}$$

2.10 Multiplicative and Additive Noise

When using a Langevin formalism, the noise can be classified according to the form of the multiplicative term $g(x)$. If g is independent of x, then the noise is said to be additive—if not, then it is multiplicative. The physical ramifications of this

will be discussed in the proper context of the relevant chapters. Here, we derive a general result that will be used several times in this thesis. It is, namely, that it is always possible to perform a variable transformation for a 1D system of the form (2.86), from one with multiplicative noise to one with additive noise. Here we expand and elaborate on details of the transformation given by Risken [54]. Starting with the an FPE of the form (2.87) which has the multiplicative noise term $g(\phi)$, writing the second term as

$$\partial_\phi^2(g^2 P) = \partial_\phi((\partial_\phi g)gP) + \partial_\phi(g\partial_\phi(gP))\,, \tag{2.88}$$

we have

$$\partial_t P = -\partial_\phi\left(\frac{f}{g} - \frac{1}{2}\partial_\phi g\right) gP + \frac{1}{2}\partial_\phi(g\partial_\phi(gP))\ . \tag{2.89}$$

Now we define a new probability distribution in a new variable θ:

$$Q(\theta, t) = \frac{g(\phi)}{\sqrt{2D}}\ P(\phi, t)\ . \tag{2.90}$$

This transformation must obey the normalisation condition

$$Q(\theta, t)d\theta = P(\phi, t)d\phi\ . \tag{2.91}$$

Integrating this and using the definition of $Q(\theta, t)$ gives us the required variable transformation:

$$\theta = \sqrt{2D}\int_0^\phi \frac{\mathrm{d}\phi'}{g(\phi')}\ . \tag{2.92}$$

The partial derivative transforms as

$$\frac{\partial}{\partial\phi} = \frac{\partial\theta}{\partial\phi}\frac{\partial}{\partial\theta} = \frac{\sqrt{2D}}{g}\ \partial_\theta$$

$$\therefore \quad g\partial_\phi = \sqrt{2D}\ \partial_\theta\ . \tag{2.93}$$

Multiplying (2.89) by $g/\sqrt{2D}$ we get

$$\partial_t Q(\theta, t) = -\partial_\theta\left(\frac{f}{g} - \frac{1}{2}\partial_\phi g\right)\sqrt{2D}\ Q + \frac{1}{2}\partial_\theta(\sqrt{2D}\ \partial_\theta\sqrt{2D}\ Q)\,, \tag{2.94}$$

or upon tidying up

$$\partial_t Q(\theta, t) = -\partial_\theta \left(F(\theta) Q \right) + D \partial_\theta^2 Q \tag{2.95}$$

$$F(\theta) = \sqrt{2D} \left(\frac{f(\phi)}{g(\phi)} - \frac{1}{2} \partial_\phi g(\phi) \right) \Big|_{\phi=\phi(\theta)}, \tag{2.96}$$

with the corresponding Langevin equation

$$\dot{\theta} = F(\theta) + \sqrt{2D}\, \eta_\theta \tag{2.97}$$

where η_θ is Gaussian white noise with zero mean and unit variance and D is the diffusion constant, giving an additive noise term as required.

2.11 Monte Carlo Simulation

To test the mathematical analysis of a stochastic model we compare it with computer simulation of the full stochastic dynamics which define the model. To simulate stochastic dynamics, several different but equivalent algorithms have been developed. Here we discuss the two methods used in this thesis, both of which can be described as kinetic Monte Carlo methods [28]. In a Monte Carlo procedure, if we know the probability p of an event occurring, in a timestep we can accept or reject an update to the system due to that event by comparison to a random number r. If $r < p$ then we accept the update to the system, if not we reject it. In the Metropolis algorithm [28] for Monte Carlo simulations of equilibrium systems, the probabilities p are known by the Boltzmann factors defined by the Hamiltonian of the system. The most well known and much studied instance of this is the simulation of the Ising spin model. For systems out of equilibrium however, the system cannot be described in terms of a free energy and so the dynamics as defined by the transition rates form the acceptance criterion for whether an update is accepted or rejected.

2.11.1 The Gillespie Algorithm

The most well-known formulation of the kinetic Monte Carlo method for simulating continuous-time stochastic processes is that commonly referred to as

the Gillespie algorithm [61, 29]. Here we outline how the algorithm works and how to implement it. The rate at which an event from process i occurs we denote ω_i. Although each ω_i is implicitly time dependent, as they depend on the state of the system defined by the number of each species in it, these are effectively constant when considering at what time the next event occurs after time t, given the state of the system. To run the simulation defined by these rates we need to know what time the next event occurs at, and which event has occurred.

Time of First Event

We know that for a Poissonian process which has a constant rate ω_i that the probability density P_i that an event of that process occurs at time t is [54]

$$P_i(t) = \omega_i e^{-\omega_i t} \, . \tag{2.98}$$

In the case of a model with several stochastic processes, we need to find the probability that the next event from any of these processes occurs at time t. To do so we first find the probability density $P_i^1(t_i)$ that process i occurs before the others at a time t_i. This is

$$P_i^1(t_i) = \prod_{j \neq i} P(t_i < t_j) = \prod_{j \neq i} P(t_j > t_i) \, . \tag{2.99}$$

Using (2.98) this becomes

$$P_i^1(t_i) = \prod_{j \neq i} \int_{t_i}^{\infty} \mathrm{d}t \; \omega_j e^{-\omega_j t} = \prod_{j \neq i} e^{-\omega_j t_i} = e^{-\omega t_i} e^{\omega_i t_i} \tag{2.100}$$

where $\omega = \sum_i \omega_i$ is the total rate of an event occurring in the system. The probability density $P(i,t)$ that process i was the first to occur at time t is then

$$P(i,t) = P_i^1(t) P_i(t) = e^{-\omega t_i} e^{\omega_i t_i} \omega_i e^{-\omega_i t} = \omega_i e^{-\omega t}. \tag{2.101}$$

Finally, we can now write down the probability density $P(t)$ that the first event from any of the processes occurs at time t:

$$P(t) = \sum_i P(i,t) = \sum_i \omega_i e^{-\omega t} = \omega e^{-\omega t} \, . \tag{2.102}$$

So to obtain the time interval until the next event in the system, we draw a time τ from the distribution $P(t)$.

Finding Which Process Occurred

Given that the event occurs at a time τ after t, the process which occurred at that time is given by the distribution of events $P(i)$:

$$P(i) = \frac{P(i,\tau)}{\sum_j P(j,\tau)} = \frac{\omega_i e^{-\omega\tau}}{\sum_j \omega_j e^{-\omega\tau}} = \frac{\omega_i}{\omega} \,. \tag{2.103}$$

We now have a way of obtaining the two ingredients required for the algorithm. For each iteration we draw a random number from (2.102) to update the simulation time, and a random number from (2.103) to select which event occurred. The state of the system is updated accordingly. By averaging over many realisations, measurements can be made of statistics of the system. For example in the toy model of a population with two competing species we are interested in the mean population numbers $\langle n(t)\rangle$ and $\langle m(t)\rangle$.

2.11.2 Random Sequential Updating

For large systems, using the Gillespie algorithm can become very inefficient. Instead, we can implement a discrete time update [28], where instead of calculating the first reaction to occur as in Gillespie, we choose at random a set of constituents to have an interaction and accept or reject it using a Monte Carlo update. Running for long times and/or averaging over many realisations this allows us to calculate averaged values of interest.

When dealing with a spatially extended system this approach is preferable, as using the Gillespie algorithm involves computing very many probabilities for individual processes, which will be expensive in time, or if one stores them in a list and subsequently updates the list, then it is computationally expensive. It is valid in this context to use random sequential updating if each patch has approximately the same number of constituents, meaning the total rate of an event happening occurring at a patch is the same for each patch. This will be true when the carrying capacity of each patch is equal. If on the other hand the carrying capacity was infinite, or each patch could have a different carrying

capacity, then random sequential updating would not correctly sample the weights assigned to each of the processes. If one patch has the majority of the entire number of constituents in the system, then more updates should occur there than at a sparsely occupied patch. For such a case more care must be taken, and implementing the full Gillespie algorithm is required to get the sampling correct.

2.12 Conclusion

Here we have presented some detailed derivation and overview of the main analytical and numerical methods that will be employed throughout this thesis. We have found by experience that taking these methods from abstract theory to practical application in a stochastic model takes time to understand and appreciate.

Chapter 3

Ordering Dynamics in Systems with Symmetric Absorbing States

In this chapter we review recent work done in building a framework for describing systems characterised by the presence of two symmetric absorbing states, which is encapsulated in a phenomenological Langevin equation proposed by Al Hammal *et al* [32]. We show that there exists a previously unobserved noise-driven transition in the ordering dynamics of systems described by such a Langevin equation, from one driven by surface tension to one driven by interfacial noise alone. This work is done through study of a microscopic lattice spin model with stochastic dynamics. Analytically, we find evidence for the transition by mapping the Langevin equation for the model onto a thermal diffusion process. Numerically, we confirm the transition through studying the evolution of the system from a highly ordered initial condition, that of a circular droplet, from Monte Carlo simulation of the stochastic dynamics.

3.1 Introduction

An *absorbing state* is one that, once a system enters it, is never left. This is most readily understood in the context of population dynamics: if the number of inhabitants of a population falls to zero, then, assuming that only birth and death processes are at work, with no mutation, then it cannot become non-zero again at a later time. Systems characterised by having one or more absorbing state feature readily in many different physical and model systems, from ecology [23] to linguistics [62], in the dynamics of catalytic reactions [63] and of calcium channels in living cells [64].

In condensed matter physics, model systems with *absorbing states* have featured prominently in the quest for a fundamental understanding of far-from-equilibrium phase transitions and critical phenomena [30, 65]. One notable success of the study of non-equilibrium systems has been the classification of systems with a single absorbing state. Much analysis from microscopic models and a field-theoretic approach have culminated in the emergence of the directed percolation (DP) universality class, broadly defined to encompass all systems with a single absorbing state [31].

However for systems with multiple absorbing states, for example the zero-temperature Ising model of magnetism [55, 39] or models of multi-species competition in population ecology [23], there is not such a fundamental understanding or framework in place and only in the past few years has progress been made. In choosing to study systems of this kind, we were particularly interested in viewing the role played by the noise in such systems. Primarily, the noise has a crucial role to play in the manifestation of absorbing states. This is achieved through it having a multiplicative form, as described in section 2.10, ensuring that deterministically determined absorbing states, such as global magnetisation in the zero-temperature Ising model, or extinction in a population remain absorbing, and cannot be exited due to a fluctuation.

The importance of the multiplicative form of the noise for a system with multiple absorbing states eventual fate has been established [32, 66, 67, 68], but little consideration has as yet been given to the possible effects it could have on the *dynamics* of these systems. We begin this chapter with an overview of the different typically observed ordering dynamics in systems with two symmetric absorbing states, in particular focussing on the phase ordering kinetics which govern the

way such systems evolve to one of the fully ordered absorbing states. We then review the static behaviour of these systems, discussing the different order-to-disorder transitions that have been reported. The observed phenomenology has been encapsulated by Al Hammal *et al* in a governing Langevin equation [32] for systems with two symmetric absorbing states.

Our study begins with the devising of a microscopic model which allows an explicit study solely of the effects that the noise can have on the ordering dynamics of systems with two symmetric absorbing states. Through study of the form of potentials obtained by mapping the system to a thermal diffusion process, and Monte Carlo simulations of the model's stochastic dynamics, we confirm the existence of a previously unseen noise-induced transition between two universal modes of domain coarsening. For a non-zero value of the noise strength, the ordering dynamics change from curvature-driven coarsening (like that associated with the Ising model [39]) due to interfacial surface tension, to that of the voter model [34] where no surface tension is present, and ordering occurs due solely to the interfacial noise.

3.1.1 Domain Coarsening

In the study of non-equilibrium systems, a key tool in classifying the dynamics is to look at the way in which phase ordering occurs. There are two modes of coarsening that are of importance in this work: that due to surface tension and that due to interfacial noise.

Coarsening Due to Surface Tension

Domain coarsening like that of the ferromagnetic Ising spin model [55] is a feature of a diverse range of systems such as binary alloys [35] and colloidal suspensions [36]. The Ising model has two fully ordered states, where the magnetisation, more generally a non-conserved order parameter, is $\phi = \pm 1$, though they are only absorbing states strictly at $T = 0$ when no thermal, or bulk, noise is present.

A typical Landau free energy functional [39] to describe such systems is

$$F[\phi] = \int \mathrm{d}\mathbf{x} \, \left(\frac{1}{2}(\nabla\phi)^2 + \frac{a}{2}\phi^2 + \frac{b}{4}\phi^4 \right) . \tag{3.1}$$

The second and third terms are a potential where $b > 0$ keeps ϕ finite and the

sign of a dictates whether the system is in a ferromagnetic ordering phase or in a disordered phase, with a spontaneous symmetry breaking at $a = 0$. The first term contributes an energy cost due a surface tension at an interface between domains of opposite spin. Taking the functional derivative gives the Ginzburg-Landau equation [39]

$$\frac{\partial \phi}{\partial t} = \nabla^2 \phi - a\phi - b\phi^3 \ . \tag{3.2}$$

Adding a Gaussian white noise term to this gives model A in the classification scheme of kinetic Ising models by Hohenberg and Halperin [69].

It is the interfacial surface tension between domain of opposite spin that drives the phase ordering towards global magnetisation in the ferromagnetic, ordering phase. Allen and Cahn [35] derived the general result relating the motion of the domain walls given by their velocity v to their characteristic curvature K due to surface tension,

$$v \propto K \ . \tag{3.3}$$

Out of equilibrium, the dynamical behaviour of a system described by model A is characterised by ordered domains of length L. For a two dimensional (2D) system, which is the focus of our work here, by dimensional arguments Bray shows how this typical size of a domain L evolves with time [39]. The velocity of the interfaces between domains $v \sim dL/dt$ while their curvature $K \sim 1/L$. Applying these to the Allen-Cahn equation (3.3) yields the algebraic expression for domain growth $L \sim t^{1/2}$. This *algebraic* coarsening is general to any dimension, with a universal exponent z, dependent only on certain qualitative features such as conservation laws or symmetries, not on microscopic details of the particular model [8]. This ordering mechanism due to surface tension is referred to in the literature as curvature-driven and is a well established phenomenon.

Coarsening Due to Interfacial Noise

A widely studied model in non-equilibrium statistical mechanics is the voter model, first presented by Clifford and Sudbury [38]. This is partly due to its simplicity: a constituent of a system is chosen at random and then copies the state of one of its neighbours. More importantly, however, is that it has the rather rare distinction of being an exactly analytically solvable model [8, 70]. Much of the success in this regard comes from the equivalence of the voter model to as

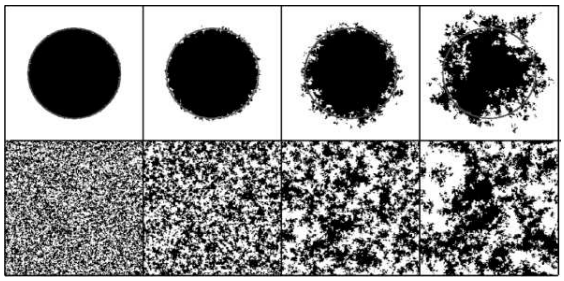

Figure 3.1: The voter model for a droplet (top) and random initial condition (bottom). Time increases left to right. From Dornic *et al* [34].

system of coalescing annihilating random walkers on a lattice [71], first realised by Holley and Liggett [72] who coined the name voter model. Dimensionality plays a crucial role and therefore it does so in the voter model's dynamical behaviour as well. The upper-critical dimension of the voter model is $d = 2$ [34], and the work we present here, along with much work in the literature, is done on a system whose dynamics acts on a 2D regular square lattice. Here, an interface, or domain wall, exists between a pair of neighbouring opposite spins, and a useful dynamical measure of the ordering of the system is the density of interfaces $\rho(t)$.

A direct consequence of the marginality of the voter model in 2D is that a system will order completely but take a very long time to do so. By solving exactly the voter model in arbitrary d dimensions by the study of a model of dimer-dimer kinetics [73], Frachebourg and Krapivsky found the exact asymptotic long-time behaviour of the density of interfaces. In $d = 2$ dimensions the density of interfaces decaying *logarithmically*, $\rho^{-1} \sim \ln(t)$ [70]. The density of interfaces is inversely related to the domain size L. Therefore for curvature-driven coarsening, from the previous discussion we have in 2D the density of interfaces decaying algebraically, $\rho \sim L^{-1} \sim t^{-1/2}$ [39].

A graphical insight into the apparent different ordering behaviour between the voter and Ising-type models was presented by Dornic *et al* through simulating voter dynamics for a 2D lattice initially phase separated into a circular droplet. In the presence of surface tension we expect the droplet to shrink and disappear over time. As can be seen from Fig. 3.1 this does not happen in the case of the voter model, instead the spins from the droplet diffuse into the rest of the lattice. This coarsening is best described as occurring in the absence of surface tension. It had been thought that this feature was due in some way to some of the

remarkable properties of the voter model, such as its integrability, conservation of magnetisation (m-conservation) or the presence of Z_2 symmetry. (Symmetry in this context refers to the equivalence of the dynamical roles of the two absorbing states, which is enforced in the microscopic dynamics.) Dornic *et al* addressed this assumption directly in [34]. They reported that in fact the integrability plays no role in determining the coarsening behaviour. Instead they showed that m-conservation was a sufficient condition for voter-like behaviour without Z_2 symmetry, and vice-versa. This led to the proposition of the existence of a whole class of models which could exhibit voter-like coarsening.

3.1.2 The Generalised Voter Class

By considering a family of kinetic Ising models, Dornic *et al* recast the different behaviour observed in terms of the presence of interfacial noise and bulk noise as done by Drouffe and Godrèche [74]. There is no bulk noise present in systems with one or more absorbing states, otherwise they would not be absorbing. The authors found that in the absence of bulk noise there existed a family of kinetic rules which exhibited voter-like behaviour. In the parameter space of bulk noise and interfacial noise they showed that the the family of voter-like rules formed a line of second order, Ising-like phase transitions, between the ordered and disordered phases.

They claimed that this showed the voter model transition was a more general phenomenon, leading them to propose the existence of a *generalised voter* (GV) universality class, best characterised as: "an order-disorder transition driven by the interfacial noise between two absorbing states possessing equivalent dynamical roles, this symmetry being enforced either by the Z_2 symmetry of the local rules or by the global conservation of the magnetisation" [34].

The concept of m-conserving dynamical rules producing voter-like behaviour is clear to us; a feature of the voter model is that on average the magnetisation is conserved. However, while [34] alludes to non m-conserving, Z_2-symmetric rules doing likewise, it is not clear what constitutes such rules, with no concrete definitions or examples being provided. We feel this requires further elucidation, but does not directly affect the work presented here. In investigating the role of the noise in systems of this kind, we will not be changing any of the universal qualitative features of the systems, be it the m-conservation or Z_2 symmetry,

but rather their relative magnitude. We find this alone is sufficient to induce a transition between the different universal ordering mechanisms.

3.1.3 Langevin Equation for Systems with Z_2 Absorbing States

The proposal of the new GV class was what prompted the work by Al Hammal *et al* to find a general description for systems with Z_2-symmetric absorbing states [32]. As well as the GV transition predicted by Dornic *et al* there was also evidence from Droz *et al* of systems where the disorder to order transition was classified as an Ising-like, spontaneous symmetry breaking transition followed by a DP transition to the effective single absorbing state selected by the symmetry breaking [33]. Prior to both of these studies, Hwang *et al* also observed different universal critical phenomena in systems with two absorbing states when the Z_2 symmetry was broken [75].

Al Hammal *et al* proposed a phenomenological Langevin equation which the authors showed encapsulated all observed critical behaviour in systems with two (Z_2) symmetric absorbing states:

$$\partial_t \phi = (a\phi - b\phi^3)(1-\phi^2) + D\nabla^2\phi + \sigma\sqrt{1-\phi^2}\,\eta \tag{3.4}$$

where $\phi \in [-1,1]$ is an appropriate coarse-grained variable, usually the magnetisation [32], and η is a Gaussian white noise with zero mean and unit variance. The first term is a deterministic force derived from the potential

$$V(\phi) = -\frac{a}{2}\phi^2 + \frac{a+b}{4}\phi^4 - \frac{b}{6}\phi^6 \tag{3.5}$$

shown in figure 3.2, with the minimum number of terms required to give an Ising-like spontaneous symmetry breaking. The Laplacian term serves as the diffusion while the final term is the multiplicative noise. The factor of $\sqrt{1-\phi^2}$ ensures that locally ordered states are absorbing: if $\phi = \pm 1$ then no noise can act at that point to perturb the system away from the ordered, absorbing state.

From analysis of the static potential (3.5), by controlling its shape through the parameters a and b the authors of [32] were successfully able to reproduce the different known critical behaviour for systems with Z_2-symmetric absorbing

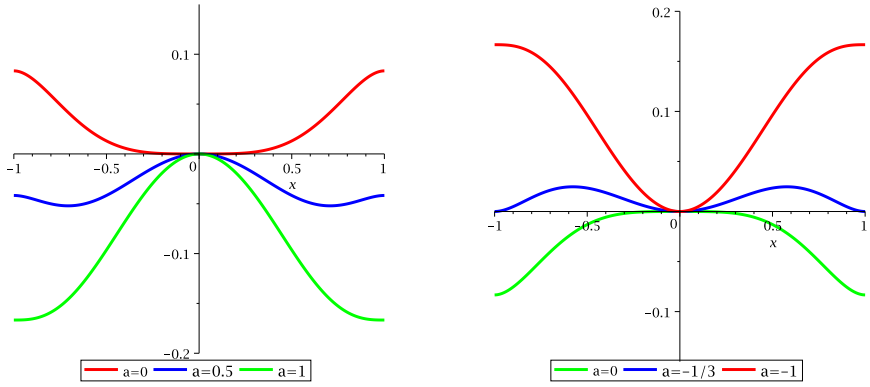

(a) $b = 1$ (b) $b = -1$

Figure 3.2: The static potential for different values of a and b which dictate the order-disorder transitions. The left panel shows an Ising-like symmetry breaking when a becomes positive, the minima of which coincide with the absorbing states at $\phi = \pm 1$ when $a = b$. In the right hand panel, we see the symmetry breaking occurs simultaneously with the system entering the absorbing states $\phi = \pm 1$ at the critical value $a = 0$.

states. They found that: (i) for $b > 0$, the system undergoes an Ising symmetry breaking transition at $a = 0$, followed by a DP transition to the effective single absorbing state of the system selected by the symmetry breaking, as reported by Droz *et al*; (ii) for $b < 0$, the Ising symmetry breaking and the DP transition to the absorbing state occur *simultaneously*—this is commonly considered to be the defining feature of the GV transition. This mean-field picture was verified to be qualitatively correct by direct numerical analysis using an integration scheme devised by Dornic *et al* in [68]. The authors found for the GV transition, at the critical point logarithmic decay of the density of interfaces is observed.

In the generic Langevin equation (3.4) there is a noise strength parameter σ, but its possible role in any critical behaviour was not examined, merely set as an appropriate system parameter. A renormalisation group treatment of a field-theoretic analysis by D'all Asta and Galla [76] suggests that noise is an irrelevant parameter as it is in the equilibrium theory of phase ordering kinetics [39]. However, for spatially discrete models such as the one we will present, it is unclear from this analysis as to whether the multiplicative noise can play a role in the macroscopically observed ordering of such systems.

Microscopic Models

Several microscopic models have been proposed from which have been derived Langevin equations belonging to the Al Hammal description (3.4). Vazquez and Lopez devised a multiple spin lattice model with a flipping probability for a spin is derived under constraint that it complies with the system having symmetric absorbing states [77]. Dall' Asta and Galla constructed a modified voter model in which spins can take on intermediate values between the absorbing, ordered limits [76]. The authors also looked to explain why the introduction of just one intermediate state was enough to break the voter-like coarsening and instead restore an effective surface tension, leading to algebraic coarsening. A similar phenomenon was described in a paper by Castellano and D'All Asta [78]. In the noise reduced voter model (NRVM), memory effects are added to the voter model by placing counters at each site. A spin will then only flip after a specified number of attempts to do so under standard voter model rules, regulated by the counter.

These models each have the capacity for changing the shape of the static potential (3.5). However no model yet exists to our knowledge in which one can control independently the qualitative deterministic behaviour, through the form of the potential, and the amplitude of the noise. In order to investigate the role the multiplicative noise can play, a microscopic model must provide such a mechanism.

3.1.4 Application: Language Development

We conclude this preliminary section with a review of some previous, related work. A concrete example and motivation in studying systems with two absorbing states comes from the field of language learning and development. In previous work [79] we studied a model of language change. In a population who use a language with some linguistic variability (such variability exists at all levels of language, from enunciation of vowel sounds, to the choice of grammar) over time it has been observed, such as in the case of New Zealand English [80], that regularisation can occur, and, roughly speaking, the population come to a consensus - everyone does the same thing. We focused on modelling the competition between two linguistic variants meaning there are two possible consensus states, making it, in effect, a system with Z_2-symmetric absorbing

states.

Our work involved constructing a modified version of an existing model called the utterance selection model (USM) [81]. The USM is a frequency selection model in which speakers use a linguistic variant according to the frequency of past use and exposure to that variant. In the original USM the frequency dependence is a simple linear rule. In the modified model, which we call the utterance selection and regularisation model, we introduced a non-linear bias to this linear rule, meaning that a speaker will overestimate the frequency of the most used variant, and underestimate the minority variant. This concept of a bias in frequency dependent learning was motivated from neurological experiments reported in [82]. A subject views an experiment in which different outcomes occur with a set frequency. In this case, an outcome is one of three lights flashing on and off. When one of the lights is set to flash a majority of the time, subjects would overestimate the frequency with which the majority outcome had occurred. For adults this phenomenon became less prevalent over longer runs of the experiment but persisted with children.

We found that the deterministic qualitative behaviour in a two speaker system was determined by only one parameter r, the relative strength of the diffusion parameter to the amplitude of the potential in the Langevin equation derived for the model (which we now recognise as belonging to the Al Hammal description). Remarkably, if r is large enough there exists two pairs of stable fixed points that the system can evolve to at which the speakers have not reached a consensus. Even though this was found for such a small system size in the deterministic limit, nevertheless the rich dynamical behaviour was unexpected. A pertinent question arising from this study is whether such behaviour persist in the full stochastic system when noise is present. We look to shed light on this by studying effects of the noise in systems with multiple absorbing states.

3.2 Microscopic Spin Model

In order to conduct a study of the effect of the multiplicative noise in systems with Z_2 symmetric absorbing states can have on the phase ordering, we devise a microscopic model whose dynamics are described mesoscopically by a Langevin equation of the kind (3.4). It is essential that we are able to control the amplitude

of the noise without altering the qualitative deterministic behaviour governed by the shape of the static potential (3.5).

3.2.1 Definition

The model is a spatially discrete microscopic, multiple-spin model and is defined as follows:

- The model comprises a 2D square lattice with lattice spacing δ and periodic boundary conditions, meaning each site has $z = 4$ nearest neighbours. At each site is a non-spatial patch, itself comprising a conserved number of sites N, each occupied by a binary spin, which we refer to as being up or down. The number of up-spins at site i we denote by $n_{u,i}$ or n_i, and the number of down-spins $n_{d,i}$ is determined by the constraint $n_{u,i} + n_{d,i} = N$.

  The state of the system is defined by the number of up-spins at each site via the vector $\mathbf{n} = (n_1, \ldots, n_{L^2})$ where L^2 is the total number of patches. Equivalently we can use the vector $\mathbf{x} = \mathbf{n}/N$ where x_i/N is the fraction of up-spins at site i. These can be thought of as local magnetisations at each site.

- In an update of length τ, a spin at a site i is randomly selected.

  - With probability $q = h/N$ it copies a spin selected at random from a neighbouring site j, by which we mean the probability of copying an up-spin is simply x_j, the fraction of up-spins at site j. This move serves as the diffusion process in the system.
  - With probability $q = 1 - h/N$ it copies a spin sitting at its own site with probability $p = x_i + (k/N)f(x_i)$, $k > 0$. The function $f(x) = x(1-x)(2x-1)$, displayed in figure 3.3(b), acts as a perturbation to a linear update rule. This move can be viewed as a biased local sampling and leads to a deterministic force which pushes sites towards the absorbing barriers at $x_i = \{0, 1\}$.

These dynamics are illustrated in figure 3.3(a). In relation to our previous model of language development [79, 81], this model can be applied as follows. Each site represents a speaker, and each spin represents a previously-heard utterance

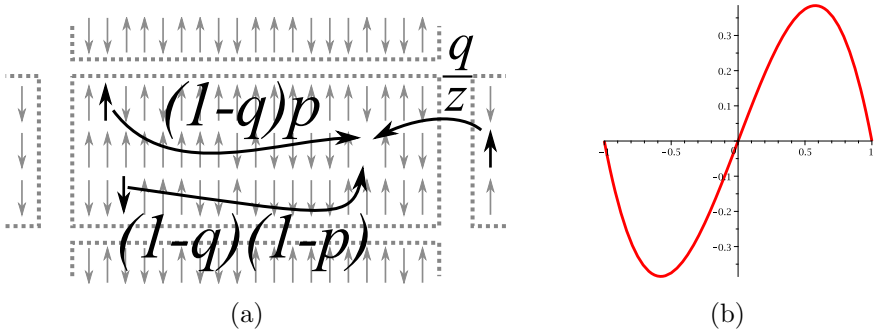

(a) (b)

Figure 3.3: (a) Dynamics of the microscopic model. Each lattice site (shown as a region bounded by a dashed line) contains N spins. In each update, a randomly-chosen spin is replaced with a copy taken from one of the $z = 4$ nearest-neighbour sites, each with probability q/z; an up-spin from the same site with probability $(1 - q)p$ or a down-spin from the same site with probability $(1 - q)(1 - p)$. (b) The function $f(x)$ serving as nonlinear bias in the on-site copying probability of the microscopic spin model.

stored in memory. The two spin states relate to two different ways of saying the same thing (e.g., phonetic realisations of a vowel). The local bias, in which the majority spin state is favoured, then models an experimentally-observed tendency for language users to overproduce the most frequent variant [82]. The key point is that the number of spins per site, N, sets both the noise strength (see below) *and* the lifetime of an utterance in memory. An appropriate choice for this lifetime was a central consideration in an analysis of the New Zealand English dialect [83].

This model can also be employed as a Moran-like [23] population dynamical model for finite-size populations. The binary spins at each patch can be regarded as two competing species. The process of a spin at site i copying a spin at site j can be cast as a migration of a constituent of patch j to patch i at the expense of a constituent at site i. The biased copying rate for an on-site copy translates to non-linear birth rates of the majority species. This gives rise to a deterministic frequency-based selection bias [84], akin to that found for competing phenotypes in evolutionary genetics whose fitness is dependent on the number of phenotypes [24]. Physically, the resulting non-linear terms appearing in the birth and death rates are a result of higher-order processes such as predation, which is a two-body reaction depending on the number of each species.

3.3 Master Equation

The transition rates $T(x_i'|x_i)$ for a patch to go from a state x_i to a state x_i' by a shift $\epsilon = 1/N$ in an update of length τ are given by

$$T(x_i + \epsilon|x_i) = (1 - x_i)\left[\frac{h}{Nz}\sum_j x_j + \left(1 - \frac{h}{N}\right)\left(x_i + \frac{k}{N}f(x_i)\right)\right] \tag{3.6}$$

$$T(x_i - \epsilon|x_i) = x_i\left[\frac{h}{Nz}\sum_j (1 - x_j) + \left(1 - \frac{h}{N}\right)\left(1 - x_i + \frac{k}{N}f(1 - x_i)\right)\right] \tag{3.7}$$

$$T(x_i|x_i) = 1 - T(x_i + \epsilon, x_i) - T(x_i - \epsilon, x_i) \tag{3.8}$$

where the j summation is over the four nearest neighbours on the square lattice. The master equation, which gives a complete description of the stochastic dynamics of the system, is

$$\frac{dP(\{x\}, t)}{dt} = \sum_{i=1}^{L^2}\Big(T(x_i|x_i - \epsilon)P(x_i - \epsilon, \{x\}) + T(x_i|x_i + \epsilon)P(x_i + \epsilon, \{x\}) - [T(x_i - \epsilon|x_i) + T(x_i + \epsilon|x_i)]P(\{x\})\Big) \tag{3.9}$$

where the states in configuration space $(\{x\})$ and $(x_i \pm \epsilon, \{x\})$ differ only in the value of the component x_i.

3.4 Fokker-Planck Equation

We wish to derive a Fokker-Planck equation (FPE) to describe the evolution of the probability of the systems local magnetisation $P(\{x\}, t)$. To do so we will truncate the Kramers-Moyal expansion of the master equation (3.9) as detailed in section 2.7.1. This requires us to calculate the jump moments

$$\alpha_l^{(i)} = \lim_{\tau \to 0} \frac{\langle (\delta x_i)^l \rangle}{\tau} \, . \tag{3.10}$$

For a FPE we require the first and second jump moments to be non-zero when the limit is taken. All of these jump moments will vanish in the in the limit $N \to \infty$ as some power of $1/N$. The first and second moments of the local magnetisation

are

$$\langle \delta x_i \rangle = \frac{1}{N^2}\left[\frac{h}{z}\sum_j (x_j - x_i) + k x_i(1-x_i)(2x_i-1)\left(1-\frac{h}{N}\right)\right]\tau \tag{3.11}$$

$$\langle (\delta x_i)^2 \rangle = \frac{1}{N^2}\Big[2x_i(1-x_i) + \mathcal{O}(N^{-1})\Big]\tau \tag{3.12}$$

with higher-order moments being of the order $\mathcal{O}(N^{-3})$. To obtain a continuous-time limit we rescale the length of an update as $\tau = \tau/N^2$. We see that in taking limit of $\tau \to 0$ in (3.10), or equivalently $N \to \infty$, that only the first and second moments are finite. This then allows us to truncate the Kramers Moyal expansion at the second term giving us the FPE

$$\partial_t P(\{x\}, t) = -\sum_i \frac{\partial}{\partial x_i}\Big[\mathcal{A}_i(\{x\})P\Big] + \frac{1}{2}\sum_i \frac{\partial^2}{\partial x_i^2}\Big[\mathcal{B}_i(\{x\})P\Big]. \tag{3.13}$$

where

$$\mathcal{A}_i(\{x\}) = \frac{h}{z}\sum_j (x_j - x_i) + k x_i(1-x_i)(2x_i-1) \tag{3.14}$$

$$\mathcal{B}_i(\{x\}) = 2x_i(1-x_i)\ . \tag{3.15}$$

This FPE now gives a full description of the stochastic dynamics of the system in this continuous-time limit. Taking $N \to \infty$ also provides for a coarse-grained continuous local magnetisation x_i at each site. In practice, when simulating this model we hope to set N large enough to match the analytical work. We settle on the value of $N = 100$ as a balance between approximating the continuous-time limit and facilitating feasible run times of Monte Carlo simulations.

3.5 A Spatially Discrete Langevin Equation

As discussed in section 2.9.1, the FPE can written equivalently as a set of Langevin equations under the Itô prescription. We have

$$\partial_t x_i = k x_i(1-x_i)(2x_i-1) + h\sum_j (x_j - x_i) + \sqrt{x_i(1-x_i)}\,\eta_i\ . \tag{3.16}$$

where each η_i is delta-correlated white noise with zero mean and unit variance. Now performing the change of variable

$$\phi_i = 2x_i - 1 \tag{3.17}$$

to give us magnetisation variables with a domain $\phi_i \in [-1, 1]$, we arrive at a spatially discrete version of the Langevin equation of Al Hammal *et al* (3.4),

$$\partial_t \phi_i = \frac{k}{2}\phi_i(1 - \phi_i^2) + h\sum_j(\phi_j - \phi_i) + \sqrt{1 - \phi_i^2}\,\eta_i \ . \tag{3.18}$$

The second term we recognise as the the discrete form of the Laplacian operator on a lattice, which serves as the diffusion term. This is a subtle but crucial difference between our Langevin equation and that of Al Hammal *et al*. By constructing a lattice model with a local, on-site update and a diffusive, inter-site update we have implicitly introduced a length scale over which the dynamics act. To explicitly compare our spatially discrete Langevin equation (3.18) with the continuous Al Hammal theory we perform a discretisation procedure on the deterministic part of (3.4):

$$\frac{\partial \phi}{\partial t} = D\nabla^2\phi + (a\phi - b\phi^3)(1 - \phi^2) \ . \tag{3.19}$$

Starting from the standard spatial discretisation

$$\phi(\mathbf{r} + \delta\mathbf{e}, t) = \phi(\mathbf{r}, t) + \delta\frac{\partial\phi(\mathbf{r}, t)}{\partial\alpha} + \frac{\delta^2}{2}\frac{\partial^2\phi(\mathbf{r}, t)}{\partial\alpha^2} \tag{3.20}$$

where $\mathbf{e}$ is a unit basis vector of the lattice, we write

$$\frac{\partial^2\phi}{\partial\alpha^2} = \frac{1}{\delta^2}\Big([\phi(\mathbf{r} + \delta\mathbf{e}, t) - \phi(\mathbf{r}, t)] + [\phi(\mathbf{r} - \delta\mathbf{e}, t) - \phi(\mathbf{r}, t)]\Big) \ , \tag{3.21}$$

and the discrete Laplacian as

$$\nabla^2\phi = \sum_\alpha \frac{\partial^2\phi}{\partial\alpha^2} = \frac{1}{\delta^2}\sum_{\{k\}}\big(\phi(\mathbf{r} + \mathbf{k}, t) - \phi(\mathbf{r}, t)\big) \ , \tag{3.22}$$

where $\{\mathbf{k}\}$ are the unit vectors pointing to the 4 nearest neighbours of the site at

r. We can now write (3.19) as

$$\frac{\partial \phi}{\partial t} = \frac{D}{\delta^2} \sum_{\{\mathbf{k}\}} [\phi(\mathbf{r}+\mathbf{k},t) - \phi(\mathbf{r},t)] + (a\phi - b\phi^3)(1-\phi^2). \tag{3.23}$$

Comparing this with our spatially discrete Langevin equation (3.18) we see that $D = h\delta^2$, $k = 2a$ and $b = 0$. By having $a > 0$ and $b = 0$, the static potential (3.5) of the system is that of the GV-ferromagnetic phase, meaning that the system will evolve to one of the two fully ordered absorbing states $\phi_i = \pm 1, \forall i$ [85].

3.6 Controlling the Noise Strength

There is not an explicit noise strength parameter σ in (3.18); compared to the Al Hammal equation (3.4) we have $\sigma = 1$. However, we can construct one and control it indirectly through h and k. Defining $r = h/k$, we write (3.18) as

$$\partial_t \phi_i = h\left(r\phi_i(1-\phi_i^2) + \sum_j (\phi_j - \phi_i) \right) + \sqrt{1-\phi_i^2}\, \eta_i \, . \tag{3.24}$$

We regard this Langevin equation now as being in two parts: a deterministic term and a stochastic noise term. Written in this way it is clear that if h is varied while holding r constant, the strength of the noise term, relative to the deterministic term, can be varied without changing the shape of the static potential. In effect, the diffusion parameter h is now the inverse noise strength.

Before we can conduct an investigation of the effect of the noise strength has on the ordering dynamics of the system, we must decide what value to assign to the static potential parameter r. In previous work [79], when studying the deterministic behaviour of a two patch version of this model, we found that there existed a threshold for $r = h/k$ above which the system would not fully order, and instead the steady state became frozen at some coexistence, non-consensus state where both up and down spins survived. To find if this holds true for arbitrarily large systems, we numerically integrate the system of ODEs which are given by (3.24) without the noise terms. By implementing the fourth order Runge-Kutta method [86], the iteration continued until the system reached a fixed point. Averaging over many runs, we calculate the probability P_c that the system reached a fully ordered state P_c of consensus from a random initial

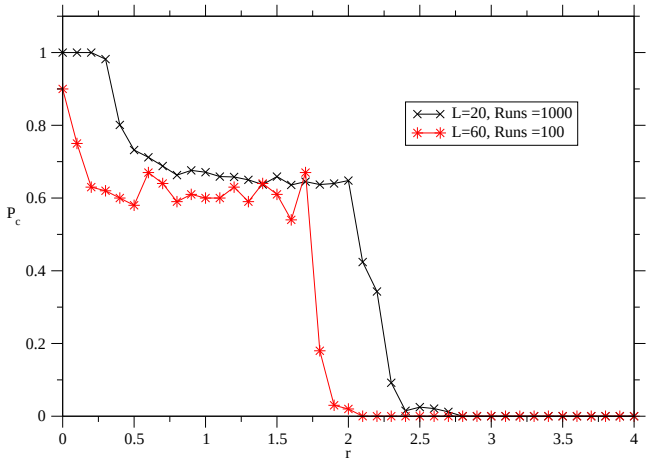

Figure 3.4: Comparison of system sizes for the consensus probability P_c for different values of the r parameter.

condition, for a range of values of r.

As can be seen in Fig. 3.4 there is different qualitative behaviour for different domains of r. For suitably large r the system will not reach consensus. We interpret this as indicative of the existence of many stable or metastable fixed points, whose number increase incrementally with r. In the Allen-Cahn theory of phase ordering, the interfaces between domains become more stable as r increases [35, 39]. This allows us to identify a suitable value of $r = 3$, for which we expect not to reach consensus in the deterministic limit, and the metastable interfaces between phases of opposite spins to exist, allowing domain coarsening to take place.

3.6.1 Simulation Details

In order to test our analysis and probe the behaviour of the model system, we perform Monte Carlo simulations of the stochastic dynamics given by the master equation (3.9) using random sequential updating and averaging over many realisations, as reviewed in section 2.11.2. As there is always the same number of constituents at each site N, this gives the correct sampling for each spin to update once on average in a timestep.

3.7 Identifying the Ordering Dynamics

As far as we are aware this is the first model of its kind which facilitates the independent control of the diffusion, potential and noise strengths. We have fixed the deterministic behaviour by fixing the static potential (3.5) through holding r constant. On a finite system, and with $a > 0$, $b = 0$ in (3.4), the system eventually ends up in one of the globally absorbing states (i.e., all $\phi_i = 1$ or all $\phi_i = -1$) [32]. We now examine how the ordering dynamics in the high (small h) and low (large h) noise regimes.

One way to identify the coarsening regime is to examine the density of interfaces as a function of time [34, 32]. This is defined as

$$\rho(t) = \frac{1}{4L^2} \sum_{\langle i,j \rangle} (1 - \phi_i \phi_j) \tag{3.25}$$

on the square lattice in two dimensions, in which the sum is over distinct nearest-neighbour pairs. As previously discussed, for the Ising model $\rho(t) \sim t^{-1/2}$ [39], while for the voter model, $\rho(t) \sim 1/\ln(t)$ [70] in 2D. We can detect and verify this behaviour directly from Monte Carlo simulations, by keeping track of the number of interfaces between a spin and its neighbours on the same site and at the nearest neighbouring sites.

3.7.1 Low Noise Regime

In the large h regime, from the theory of phase ordering kinetics we anticipate a domain growth driven by surface tension. This is because the deterministic limit $h \to \infty$ corresponds to the time-dependent Ginzburg-Landau equation, obtained from the Landau free energy functional for the Ising model with a non-conserved order parameter [39]. When the noise amplitude is small, we do not expect the distinction between additive and multiplicative noise to be important, and without the square root multiplicative factor to the noise, (3.24) is recognisable as model A of the Ising model [69].

This leads us to predict that we will observe algebraic coarsening in the low noise, large h, regime. From the left panel of figure 3.5, we confirm this as we observe $\rho(t) \sim t^{-\nu}$ with the measured exponent ν ranging from $0.45 - 0.50$ in the large h region. These measured exponents are consistent with those reported

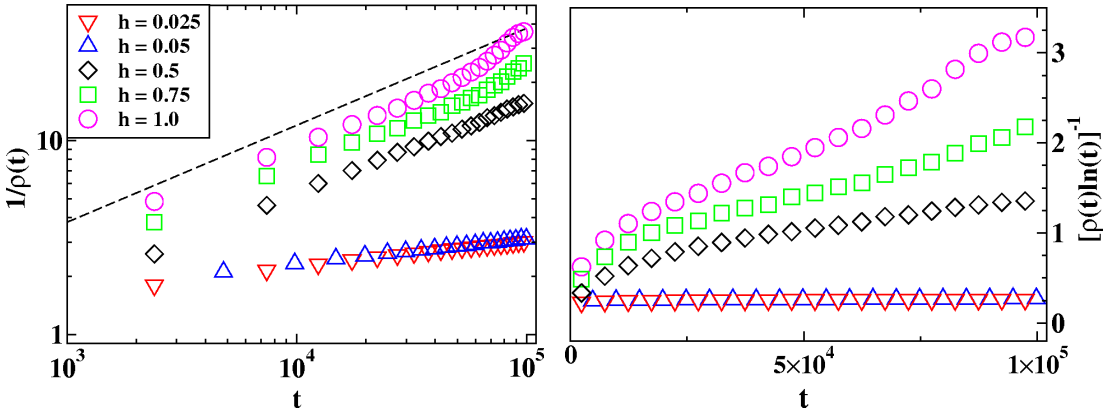

Figure 3.5: Interfacial density ρ as a function of time t in Monte Carlo simulations of the microscopic model. Left: $1/\rho(t)$ is plotted on logarithmic axes, such that a straight line indicates algebraic coarsening. For large h, and at times before the onset of finite-size effects, the gradient is consistent with the Ising model value of $\frac{1}{2}$ (dashed line). Right: $[\rho(t)\ln t]^{-1}$ plotted on linear axes. A constant asymptote, seen for small h, indicates logarithmic coarsening.

from other microscopic models with an effective surface tension by Dall' Asta and Galla [76], and Castellano and Castello [78]. We remark that the deviation from the expected $t^{-1/2}$ law seen at late times for large h is a finite-size effect caused by the periodic boundary conditions in the simulation, when a domain grows large enough to coalesce with a periodic image of itself.

However the left hand panel of figure 3.5 also shows that as h becomes smaller this exponent deviates largely from $\nu = 0.5$ to a typical range $0.15 - 0.20$, which suggests that the coarsening due to surface tension is not the dominant ordering mechanism in a higher noise regime.

3.7.2 High Noise Regime

From the study of a closely related system, it can be shown using the method of Möhle [87], that in the limit $h \to 0$ the purely fluctuation-driven dynamics of the voter model are formally recovered. The dynamics of the voter model is a system driven purely by interfacial noise. In the Al Hammal Langevin equation (3.4) if the potential term is removed, one recovers the Langevin equation for the voter model originally proposed by Dickman [66, 67] and subsequently verified by Dornic *et al* [68]. We consider taking the limit $h \to 0$ in the context of our model's dynamics. A spin will undergo the local update more and more times between

two instances of the diffusive update as h gets smaller, leading to a separation of timescales for the two processes. This scenario, we argue, is akin to that presented by Möhle [87], describing a Markov process with a fast and a slow mode. After copying a spin from a neighbouring site, on the slow timescale of this mode, the next time the same site copies from another site, it will have fully ordered to either $\phi_i = \{-1, 1\}$. The phase space is therefore reduced to sites only occupying the fully ordered configurations, making the model resemble a single spin-per-site model with the effective dynamics of the voter model.

Therefore we expect to see voter-like coarsening for some sufficiently small h, where the density of interfaces decays logarithmically in 2D. We see confirmation of this in the right hand panel of figure (3.5) for the smallest values of h. However as h increases the logarithmic nature of the evolution of $\rho(t)$ breaks down.

In summary, we observe Ising-like, algebraic coarsening driven by a surface tension in the low noise (high h) regime and voter-like, logarithmic coarsening due to interfacial noise in the high noise (low h) regime. We now want to establish whether this change in phase ordering dynamics is a sharp transition or a smooth crossover, and if the former, what the mechanism for a transition would be.

3.8 Mapping to a Thermal Diffusion Process

The multiplicative noise in the Langevin equation (3.18) makes interpretation of the stochastic dynamics difficult as it stands. Our physical intuition is strongest when the noise is additive, and the dynamics can be viewed in terms of diffusion in a potential. To this end, we transform the local magnetisation ϕ_i to a variable θ_i such that the FPE (3.13) has a diffusion term $\mathcal{B}_i(\{\theta\})$ that is independent of the coordinates θ_i. This technique has previously been used for models with a single absorbing state [88], and a derivation of the transformation is given in section 2.10.

The appropriate transformation is

$$\theta_i = \sin \phi_i \,, \tag{3.26}$$

with the resulting FPE corresponding uniquely (à la Itô) to the set of Langevin equations

$$\dot{\theta}_i = -V_{\mathrm{D}}'(\theta_i) + \eta \,, \tag{3.27}$$

one for each site i, and where η is the usual thermal (Gaussian white) noise. The potential V_{D} has the form

$$V_{\mathrm{D}}(\theta) = \ln\left[\left(\frac{1-\sin\theta}{1+\sin\theta}\right)^{\frac{1}{2}hz\bar{m}}(\cos\theta)^{\frac{1}{2}-hz}\right] + \frac{hr}{8}\cos 2\theta \tag{3.28}$$

where

$$\bar{m} = \frac{1}{z}\sum_{j}\phi_j \tag{3.29}$$

is the mean magnetisation of the z sites that are neighbours of site i. We note that the L^2 separate Langevin equations are coupled because $\bar{m}$ depends on the values of θ at neighbouring sites.

The subscript D here is used to emphasise the crucial difference between this potential, felt by a thermal diffusion process, and the static potential (3.5) whose derivative gives the deterministic term in the Langevin equation (3.4). The shape of V_{D} gives insight into the stability of a microscopic configuration under the stochastic dynamics, and that this shape changes with the noise strength h in a non-trivial way. On first inspection, this *diffusion potential* V_D seems very complex and to analytically find how its shape varies with h is not an easy task. However, as we now show, for our purposes it suffices to look at the behaviour near the boundaries in order to deduce the three distinct qualitative shapes that V_D may take.

Under the variable transformation (3.26), the local absorbing states $\phi_i = \pm 1$ become $\theta_i = \pm\frac{\pi}{2}$. We now consider a mean-field analysis by having only one active site i with $\theta_i = \theta$, while holding all other θ_j fixed. In particular this means the local neighbourhood and hence the local magnetisation $\bar{m}$ (3.29) is held constant. Taking the case $\bar{m} < 0$, we examine the form of V_D near the right hand boundary at $\theta = \frac{\pi}{2}$. First we rewrite the potential as

$$V_D(\theta) = \frac{h\bar{m}z}{2}\ln(1-\sin\theta) - hz\ln(\cos\theta) + \frac{1}{2}\ln(\cos\theta) - \frac{h\bar{m}z}{2}\ln(1+\sin\theta) + \frac{hr}{8}\cos 2\theta. \tag{3.30}$$

Near $\theta = \frac{\pi}{2}$ we can write

$$\begin{aligned}\ln(1-\sin\theta) &= \ln(1-(1-\cos^2\theta)^{\frac{1}{2}}) \\ &\approx \ln(1-(1-\frac{1}{2}\cos^2\theta)) = \ln(\frac{1}{2}\cos^2\theta) \sim \ln(\cos^2\theta) \end{aligned} \tag{3.31}$$

where the final form is the limiting behaviour as we take $\theta \to \frac{\pi}{2}$. Using this we can express V_D near $\theta = \frac{\pi}{2}$ using (3.30) as

$$V_D(\theta) \sim \left(\frac{1}{2} - hz\right)\ln(\cos\theta) + \frac{hz\bar{m}}{2}\ln(\cos^2\theta) \tag{3.32}$$

$$= \left(\frac{1}{2} - hz(1+\bar{m})\right)\ln(\cos\theta). \tag{3.33}$$

Now formally taking the limit we find

$$\lim_{\theta\to\frac{\pi}{2}} V_D(\theta) = \begin{cases} -\infty & \text{if} \quad h < h_- \\ \\ \infty & \text{if} \quad h > h_- \end{cases} \tag{3.34}$$

where

$$h_\pm = \frac{1}{2z(1\pm\bar{m})}\,. \tag{3.35}$$

Following the exact same procedure, we find analogously for the left hand barrier $\theta = -\frac{\pi}{2}$:

$$\lim_{\theta\to-\frac{\pi}{2}} V_D(\theta) = \begin{cases} -\infty & \text{if} \quad h < h_+ \\ \\ \infty & \text{if} \quad h > h_+ \end{cases}\,. \tag{3.36}$$

From this we have learnt that as θ approaches either boundary point $\theta = \pm\frac{\pi}{2}$ at some fixed local magnetisation $\bar{m}$, V_D diverges logarithmically. Depending on the values of h and $\bar{m}$, the divergence can be either towards $+\infty$ or $-\infty$. Considering the case $\bar{m} < 0$, we find that the divergence is towards $+\infty$ at the right boundary when $h > h_-$, and towards $-\infty$ for smaller values of h. Similarly, at the left boundary, the divergence is towards $+\infty$ when $h > h_+$. The three possible combinations of boundary divergence are as shown in Fig. 3.6. To do this analysis we considered that the fixed local magnetisation $\bar{m} < 0$. If we repeat the procedure for the case $\bar{m} > 0$ we find analogous shapes of the potential, due to the symmetry

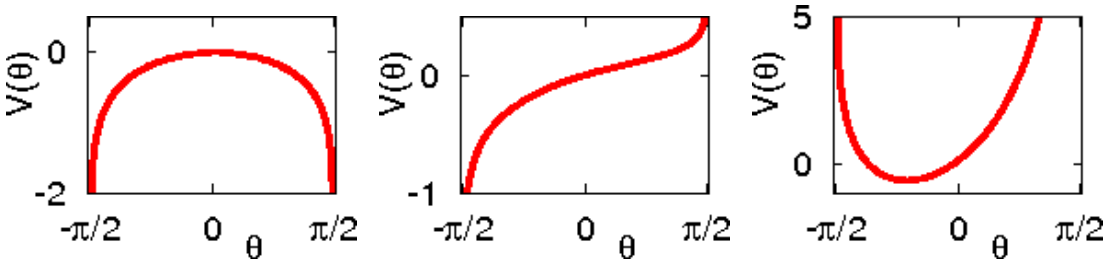

(a) $h < h_-$ (b) $h_- < h < h_+$ (c) $h > h_+$

Figure 3.6: Shape of the diffusion potential V_D at increasing h. Here, $h_\pm = [2z(1 \pm \bar{m})]^{-1}$, $z = 4$ and $\bar{m} = -0.5$.

$\theta_i \to -\theta_i$ and $\bar{m} \to -\bar{m}$.

We want to know what the different distinct shapes of the diffusion potential in different noise regimes tells us about the coarsening dynamics. We can reconcile the shape of the potential 3.6(a) with our observation of voter-like coarsening in the low h, high noise regime. A microscopic spin configuration is determined by the value of $\bar{m} \in [-1, 1]$. Taking a fully ordered local neighbourhood $\bar{m} = -1$, for which h_- is minimal, there always exists an h such that

$$h < h_- = \frac{1}{4z} = 0.0625. \tag{3.37}$$

Therefore, for $h < \frac{1}{4z}$, there are always minima of the diffusion potential at the boundaries, and a single maximum in between (since there are at most two extrema in the interior region). Thus the diffusion of θ is at any instant biased towards a locally absorbing state at $\theta_i = \pm\frac{\pi}{2}$. Once a locally absorbing state is reached, the deterministic force in (3.24) vanishes. Then, all that remains is the Langevin equation for the voter model [66, 67]. This leads us to suggest that voter coarsening should be seen over some *finite* range of h, at least up to $h = \frac{1}{4z}$.

Given the abruptness in the change in shape of V_D as h increases through h_-, the observation of Ising-like coarsening for larger values of h in figure 3.5 and the fact that the deterministic limit of (3.18) and model A for the Ising model are equivalent, we believe there is the possibility of a transition to Ising-like coarsening at some non-zero value of h, perhaps in the vicinity of $h = \frac{1}{4z}$.

3.9 Droplet Simulation

In order to confirm whether a transition exists, we look for evidence from Monte Carlo simulation of the stochastic dynamics. We have already found evidence for the different ordering regimes from simulation, as shown in figure 3.5. However, while those simulations identify the transitional region in which the coarsening dynamics change, in order to identify a sharp transitional value of h, akin to the value h_- from our diffusion potential analysis, something more definitive is required.

The simulations in figure 3.5 were generated by starting with a random initial condition, where each spin is equally likely to be up or down. Now we will adopt a highly ordered initial condition, that of a droplet, analogous to that used by Dornic *et al* in [34] and displayed in figure 3.1. All the sites within a given radius of the centre of the square lattice are fully ordered with up spins, while those outside are fully ordered down.

The reason for adopting this is that by measuring the time evolution of the global magnetisation, for which the total number of up spins

$$M_u(t) = \frac{1}{L^2} \sum_i n_i \tag{3.38}$$

is a suitable definition, we can identify both Ising-like and voter-like coarsening.

3.9.1 Voter-Like Behaviour

A key characteristic of the voter-like dynamics is m-conservation [8, 70, 71], meaning that on average we expect

$$\frac{d\langle M_u \rangle}{dt} = 0 \, . \tag{3.39}$$

This we can readily identify from simulation.

3.9.2 Ising-Like Behaviour

The calculation we give here is adapted from Bray's review of phase ordering dynamics [39]. For systems with a non-conserved order parameter field $\phi(\mathbf{r}, t)$, such as the magnetisation in the sub critical Ising model, an appropriate equation

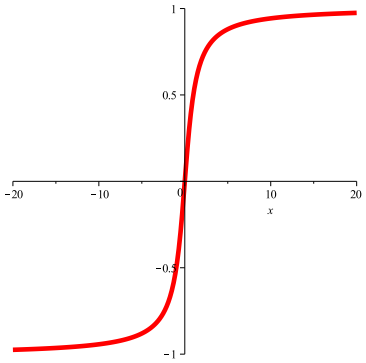

Figure 3.7: The schematic form of the order parameter $f(x)$. It has a large derivative at 0 as it the function moves sharply between ± 1.

for the time evolution of the field is

$$\partial_t \phi = D\nabla^2 \phi - V'(\phi) \tag{3.40}$$

where $V(\phi)$ is a symmetric well defined potential. For a 2D circular domain of radius $R(t)$, i.e. a droplet, if the radius is much bigger than the interface width between the two phases then we can make an ansatz of the form, using polar coordinates (r, θ),

$$\phi(r, t) = f(r - R(t)) \tag{3.41}$$

where $x = r - R(t)$ is the distance form the interface. A schematic form of $f(x)$ is displayed in figure 3.7. Loosely, it has the form

$$f(x) = \begin{cases} -1 & x > 0 \\ 1 & x < 0 \end{cases} \tag{3.42}$$

and its derivative is maximal about $x = 0$.

Writing (3.40) in polar coordinates

$$\frac{\partial \phi}{\partial t} = D\left[\frac{\partial^2 \phi}{\partial r^2} + \frac{1}{r}\frac{\partial \phi}{\partial r}\right] - \sigma V'(\phi), \tag{3.43}$$

substituting in the ansatz (3.41) gives

$$-f'\dot{R} = D\left[f'' + \frac{1}{r}f'\right] - V'(f). \tag{3.44}$$

Multiplying through by f' and rearranging gives

$$0 = Df'f'' + \left(\frac{D}{r} + \dot{R}\right)(f')^2 - f'V'(f). \tag{3.45}$$

Now we integrate this through the interface with $x \in [-w, w]$, $w \gg 1$. The latter two terms give:

$$\int_{-w}^{w} V'(f)f'dx = V(f)\Big|_{-\infty}^{\infty} = 0$$

as the potential is symmetric and the fully ordered phases have the same potential, $V(1) = V(-1)$;

$$\int_{-w}^{w} f''f'dx = \frac{1}{2}(f')^2\Big|_{-\infty}^{\infty} = 0\ .$$

The first term gives

$$\int_{-\infty}^{\infty} dx \left[\frac{D}{x+R} + \dot{R}\right](f')^2 = 0\ . \tag{3.46}$$

We see from figure 3.7 that the dominant contribution to this integral comes from the neighbourhood of $x = 0$, and therefore the integral will not be zero unless we have

$$\frac{D}{R} + \dot{R} = 0 \tag{3.47}$$

which yields the final expression

$$R^2(t) = R_0^2 - 2Dt\ . \tag{3.48}$$

So under surface tension we expect the radius of the droplet to decay from its initial value R_0 linearly with time, the rate being set by the diffusion D. As the initial condition confines all the up-spins to lie inside the droplet, we see that the global magnetisation $M_u(t) \sim R(t)$ because as the droplet shrinks, so too proportionately will the number of up-spins. From the discretisation of section 3.5 we know that $D \sim h$, and so we arrive at the scaling form for the time evolution of the magnetisation

$$M_u(t) = M_0 - ct \tag{3.49}$$

where $M_0 = M_u(0)$ is the initial magnetisation and the rate of the linear decay c

has the scaling form

$$c \sim \frac{h}{L^2} \, . \tag{3.50}$$

This linear decay rate c is our order parameter for Ising-like coarsening. In the low h voter regime we expect m-conservation to hold and so from (3.39) we expect c to be zero. Above a certain value of h we expect to find Ising-like coarsening, giving us a non-zero value of c according to (3.50).

3.9.3 Simulation Results

In figure 3.8(a) is the time evolution of the average magnetisation $\langle M_u(t) \rangle$ obtained from Monte Carlo simulation of the stochastic dynamics with the droplet initial condition. We see the expected linear decay at high h and m-conservation at low h. To each stochastic realisation of $M_u(t)$ we fit a linear function. An estimate of c, and an error, can be computed from the mean and standard deviation of the measured gradients. We can compare results from different system sizes L by taking the initial droplet radius R_0 proportional to L, and by plotting cL^2 against h test our hypothetical scaling form (3.50).

These results are shown in figure 3.8(b). The expected linear increase of c with h from (3.50) is observed. Crucially, we find that the intercept is not at $h = 0$, but at some positive value of h, below which c is consistent with zero. This suggests that there is indeed a transition between voter-like and Ising-like coarsening dynamics at some $h = h^* > 0$. A least-squares linear fit to the data yields an estimate of $h^* \approx 0.059$, which is close to the value $h_- = \frac{1}{4z} = 0.0625$ suggested by the analysis of the diffusion potential. One possibility for this observed non-zero critical value of h could be due to a finite-size effect in the simulation. If such an effect were present we would expect the h-axis intercept to regress to zero as L increased. By plotting the data for several different system sizes and observing a scaled data collapse in figure 3.8(b), we rule out this possibility.

3.10 Discussion and Conclusion

We have presented evidence for a purely noise-induced transition in the ordering dynamics in systems with two symmetric absorbing states for a non-trivial value of the inverse noise strength h, from Ising-like coarsening under surface tension

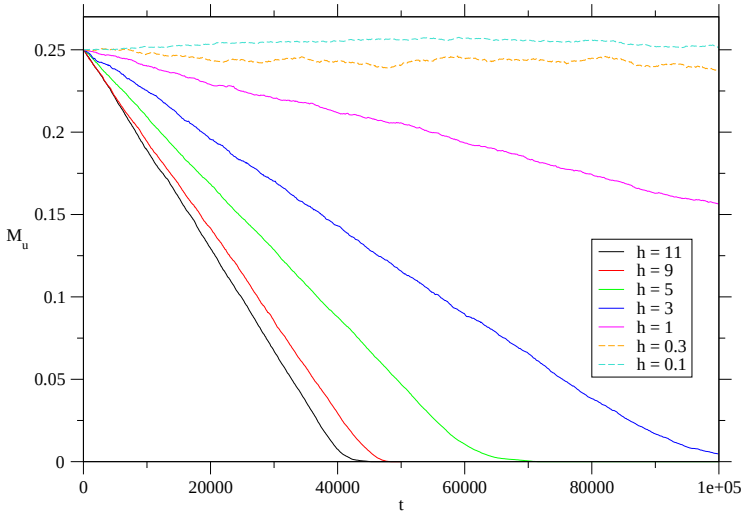

(a) The time evolution of the average magnetisation $\langle M_u(t) \rangle$ for a range of values of the noise strength parameter h for system size $L = 60$, averaged over 100 runs. For high h (low noise) we can see clearly the linear decay of as expected, whereas for low h (high noise) we can see evidence of m-conservation, indicative of the voter model.

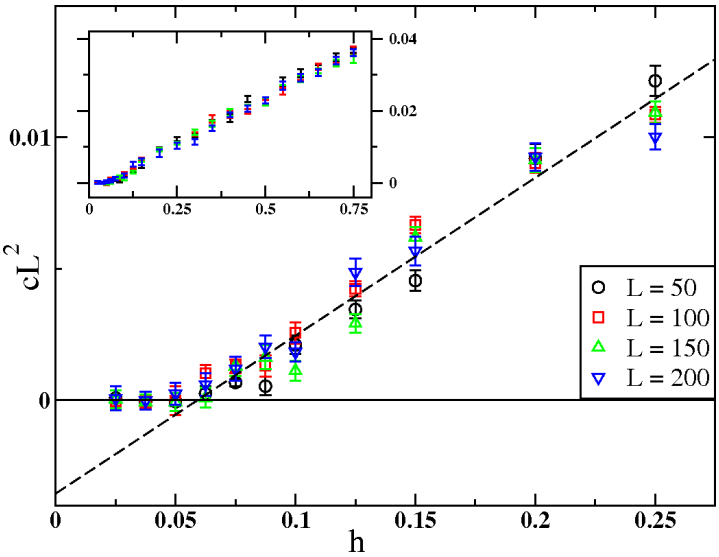

(b) Droplet shrinking rate, c, as a function of inverse noise strength h at a range of system sizes L. Each data point is obtained from a sample of 100 simulation runs. The same is shown in the inset over a larger range of h.

Figure 3.8: Results from Monte Carlo simulation of the stochastic dynamics with a droplet initial condition.

in a low noise regime, to ordering driven by interfacial noise like that of the voter model, when the noise is sufficiently strong. Through a mean-field mapping of the non-equilibrium stochastic dynamics to a thermal diffusion process, we found a physical mechanism for this transition. Once the noise is sufficiently strong, we find that *locally*-absorbing states are entered with ease. This makes the force term in the governing Langevin equation (3.24), which provides a surface tension at the interface, vanish. Consequently, the only way for the system to order is through interfacial fluctuations, a mode of domain coarsening exhibited by the voter model.

This noise-induced dynamical transition has not been predicted by any other models of systems with symmetric absorbing states. Though several microscopic models whose stochastic dynamics are mesoscopically described by the phenomenological Langevin equation (3.4) proposed by Al Hammal *et al* have been proposed, none allow an independent study of the noise, as the deterministic and stochastic contributions to the dynamics are often not independent. We constructed a model specifically to avoid such a shortcoming, which facilitates a study of the role the multiplicative noise can play in the dynamics of such systems.

We believe the discrete space in our model has been key to our observation of the transition. The physical mechanism we propose for the transition relies on the discrete nature of the model, which allows that a locally-absorbing state can be reached more quickly than the diffusion process connecting neighbouring sites. However in taking the spatial continuum limit of $\delta \to 0$, any finite transition point $h^* > 0$ collapses onto a zero diffusion constant, $D = 0$. While a previous field-theoretic renormalisation group treatment of Dall' Asta and Galla [76] on the Langevin equation (3.4) did not reveal the noise strength as a relevant quantity, it is not incompatible with our observed transition in the ordering dynamics at a critical value of the noise strength h. It is an interesting open question whether such a transition can be realised in a future field-theoretic treatment of the phenomenological Langevin equation (3.4) of Al Hammal *et al*.

As an extension to this work, it would be interesting to find if the demographic noise strength can lead to other macroscopic effects of the dynamics of a spatially discrete system, or even dictate its long term fate. It is known that the demographic noise plays a key role in keeping the existence and

stability of spatially extended predator-prey metapopulations [50] as well as their synchronisation [52]. The stability arises from a complex interplay of the spatial heterogeneity, the noise strength and migration rate [53]. By construction of a model similar to that presented here, which allowed independent control of these parameters, an insight into the framework and phase portrait of the observed rich behaviour of such systems may be possible

A final general implication of this work relates to a question first investigated twelve years ago by Dornic *et al* in [34]. It is: which qualitative features, such as symmetries and conservation laws, determine the dynamical universality class of systems with multiple absorbing states? We have shown that even in a subclass of models which have the same qualitative properties, but different noise strengths, the macroscopic ordering dynamics can be different. In particular, strong noise leads to the m-conservation characteristic of the voter model being an emergent consequence of the stochastic dynamics. To develop a better general understanding of non-equilibrium phase transitions and critical phenomena, one may need to determine whether other cases exist in which such conservation laws emerge.

In conclusion, we have found that the multiplicative form of the demographic noise can play a crucial role in the macroscopic ordering dynamics of systems with two symmetric absorbing states. We uncovered this result by taking an individual based modelling approach to the constructing the dynamics of the system. As well as deriving from this the deterministic rate equations, it also allows us to derive the form of the demographic noise, and crucially its amplitude, which we are able to control independently of the deterministic contribution.

Chapter 4

Currents in Finite Populations About a Stable Fixed Point

In the previous chapter we witnessed the consequences that demographic noise can have in the ordering dynamics of a system out of equilibrium. For multi-dimensional systems, it is generally the case that non-equilibrium probability currents flow in the steady state. In this chapter we study whether probability currents can be macroscopically observable in finite-size populations. We do so by means of an individual based model which we analyse through a van Kampen expansion of the governing master equation. The deterministic dynamics evolve the system to a stable fixed point in the 2D configuration space, the simplest such behaviour for studying the manifestation and possible effects of a probability current. We derive the conditions for a probability current to flow, and introduce a noise-controlled mechanism into the model which allows the system to evolve to a non-equilibrium steady state. We confirm the existence of a probability current through Monte Carlo simulation of the stochastic dynamics and by calculating the frequency of the closed elliptical orbits of the current velocity.

4.1 Introduction

The paradigmatic example of an individual based model (IBM) approach for studying the role noise can play in a finite population is the phenomenon of stochastic amplification discovered by McKane and Newman [44]. The authors were interested in looking for a novel mechanism which could give rise to cycling behaviour in an interacting population. The example they studied was a predator-prey system [23], which comprises two competing populations, one of which can reproduce at the expense of the other. In modelling such an ecological system, the essential processes which must be included are: prey reproduction, predator and prey mortality and the predator-prey interaction. Incorportating these features lead to the famous Lotka-Volterra equations which, however, by themselves in a mean-field treatment do not lead to cycles [42, 43, 23]. For that, further processes are required such as satiation of the predator population, which imposes a carrying capacity on the predator population. Including these leads to stable limit cycle solutions, such as seen in the Holling-Tanner model [89, 90]. McKane and Newman argued that given cycles are ubiquitous in nature, on scales of many differing orders of magnitude, there may be a simpler mechanism which gives rise to them, not requiring the inclusion of more subtle biological processes. This view had previously been expressed by Nisbet and Gurney, who believed that an interplay of the noise with the deterministic behaviour of a predator-prey system was a more likely scenario to give rise to cycles, rather than having to accommodate limit cycles in the deterministic dynamics [91].

The authors of [44] incorporated the simplest biological processes given above into an IBM, which described well-mixed patch population with a conserved size N. A van Kampen expansion of the master equation was implemented, as outlined in section 2.8. The mean-field equations recovered are the Volterra equations, which predict the system to evolve to a fixed point in the steady state. Taking the linear Fokker-Planck equation (FPE) for the fluctuations about the mean densities for each population, the authors calculated the power spectra for the fluctuations by transforming the equivalent Langevin equations. These display a resonance in the spectrum at a non-zero frequency. The amplitude of this resonance is then large enough to be relevant on the mean-field level of the system size expansion which then gives rise to macroscopic cycles. In the neighbourhood of the the fixed point the deterministic trajectory is a focus, following a decaying

spiral into it. Periodically the system is perturbed by the stochastic resonance a macroscopic distance out from the fixed point, meaning the trajectory then rejoins the deterministic focus. This behaviour persists indefinitely leading to a cycling behaviour in the time series of the population densities, the frequency of which is that of the decaying spiral.

We observe that while the resonance of the demographic noise plays a key role in this observed cycling behaviour, of equal importance is the deterministic spiral. In the language of Tomé and de Oliveira [92], the demographic noise converts the deterministic, damped oscillations of the spiral, to undamped oscillations in the form of phase-forgetting quasicycles. This mechanism of stochastic amplification has been realised in models of systems as diverse as gene regulation [45] and measles epidemics [93].

The importance of this work is that it establishes a generic mechanism for sustained population cycles in predator-prey systems. The periodic orbits present in the deterministic Lotka-Volterra system, for example, are not robust to modifications of the dynamics or noise [23]. Intrinsic demographic noise has been shown to destabilise marginally stable predator-prey cycles [53, 94, 95], shifting the phase space trajectory between different limit cycle orbits until eventually one crosses an absorbing state where a species becomes extinct. The need for models in which cycles are robustly observed arises from the fact that some natural populations indeed exhibit cyclicity in abundances. For example, voles and lemmings exhibit complex multi-year cycles [96, 97]. It is unlikely that such behaviour is achieved by fine-tuning of parameters with highly specific values that happen to favour cyclicity.

In this chapter, we investigate a potential and hitherto unexplored mechanism for generating cycles in a population dynamical system without parameter tuning. It is based on the observation that when one has more than one stochastic variable (as is the case in a multi-species population dynamics) a *non-equilibrium steady state* that exhibits cyclic probability currents in configuration space typically arises. We want to find out whether these abstract cycles can be manifested as macroscopically observable cycles in species abundances. This is a reasonable hypothesis since it is known that in *physical* systems, such currents are directly observable in experiments on optically-trapped colloids [98]. There, the presence of a current was inferred from the persistent bias seen in the evolution of the

polar coordinate of the colloid's motion.

Central to our considerations is the question of whether a non-equilibrium steady state can be attributed solely to the form and nature of the noise. As we have just discussed, the demographic noise plays a key part in sustaining cycling behaviour and keeping finite-size systems driven out of equilibrium [44]. A more general question we wish to address is: under what conditions does a population reach a steady state in thermal equilibrium? We present the simplest two-species population dynamical model as a candidate for observing these currents macroscopically, and derive the most general conditions under which a non-equilibrium steady state can be permitted.

A final motivation of this study comes from the technical aspect of the stochastic resonance mechanism. As mentioned, this was uncovered following a power spectrum analysis of the Langevin equations describing the dynamics of the fluctuations about the centre of the stable focus. Given the equivalence of the Fokker-Planck formalism under Itô calculus in IBMs, we wish to learn if similar information can be obtained from the FPE.

4.2 The Stable Fixed Point (SFP) Model

We wish to investigate the importance of demographic noise in influencing the dynamics of non-equilibrium systems and to see if it alone can be responsible for some macroscopic phenomena not observable in a deterministically analogous system, in particular focussing on cycles in ecological population models. To this end, we wish to study a system similar to the stochastic predator-prey model of [44]. As already discussed, the cycles observed there are due to an interplay of a stochastic resonance due to the noise, and an stable deterministic spiral. We propose a model which deterministically quickly relaxes to a stable node, which then allows a clean study of the effect of noise on the subsequent dynamics of the system.

The model we use is the stable fixed point (SFP) model which we introduced in section 2.7.1. To recap, it comprises two competing species A and B with species number n and m respectively residing on a non-spatial patch with conserved size $N = n + m + e$ where e is the number of empty sites on the patch. We denote rate constants for processes of species A with a 1 and for species B with

a 2. Individuals of both species reproduce with rate a_i, while each can die due to: (i) natural death with rate d_i; (ii) predation from the other species with rate p_i; (iii) cannibalism from another of its species with rate c_i, where $i = \{1, 2\}$. This gives us the transition rates for the model:

$$\begin{aligned} T(n+1, m|n, m) =& 2a_1 \frac{n}{N}(N - n - m) \\ T(n, m+1|n, m) =& 2a_2 \frac{m}{N}(N - n - m) \\ T(n-1, m|n, m) =& d_1 n + c_1 \frac{n(n-1)}{N} + 2p_1 \frac{nm}{N} \\ T(n, m-1|n, m) =& d_2 m + c_2 \frac{m(m-1)}{N} + 2p_2 \frac{nm}{N} \,, \end{aligned} \tag{4.1}$$

and the corresponding master equation using the step operator $\hat{\mathcal{E}}$ is

$$\begin{aligned} \frac{dP(n,m)}{dt} =& (\hat{\mathcal{E}}_n^{-1} - 1)T(n+1, m|n, m)P(n, m) \\ &+ (\hat{\mathcal{E}}_n^{1} - 1)T(n-1, m|n, m)P(n, m) \\ &+ (\hat{\mathcal{E}}_m^{-1} - 1)T(n, m+1|n, m)P(n, m) \\ &+ (\hat{\mathcal{E}}_m^{1} - 1)T(n, m-1|n, m)P(n, m) \,. \end{aligned} \tag{4.2}$$

4.2.1 van Kampen Expansion

Because we are interested in looking at fluctuations about some steady state determined by the deterministic dynamics, it is appropriate to analyse the model using the van Kampen system size expansion. Following the procedure outlined in section 2.8, we write the ansatz

$$\begin{aligned} n &= N\rho(t) + \sqrt{N}\,\xi \\ m &= N\sigma(t) + \sqrt{N}\,\eta \end{aligned} \tag{4.3}$$

which gives us the new stochastic variables ξ and η to describe the fluctuations about the mean-field values ρ and σ. Applying this transform to the master

equation (4.2) gives us the expansion

$$\frac{\partial \Pi}{\partial t} - \sqrt{\Omega}\,\dot{\rho}\frac{\partial \Pi}{\partial \xi} - \sqrt{\Omega}\,\dot{\sigma}\frac{\partial \Pi}{\partial \eta} = \tag{4.4}$$
$$\left(-\frac{1}{\sqrt{N}}\frac{\partial}{\partial \xi} + \frac{1}{2N}\frac{\partial^2}{\partial \xi^2} + \dots\right) N2a\left[\rho + \frac{\xi}{\sqrt{N}}\right]\left[1 - \rho - \sigma - \frac{1}{\sqrt{N}}(\xi + \eta)\right]\Pi$$

$$+\left(\frac{1}{\sqrt{N}}\frac{\partial}{\partial \xi} + \frac{1}{2N}\frac{\partial^2}{\partial \xi^2} + \dots\right) N\left[\rho + \frac{\xi}{\sqrt{N}}\right]\left[d + 2p(\sigma + \frac{\eta}{\sqrt{N}}) + c(\rho + \frac{\xi}{\sqrt{N}})\right]\Pi$$

$$+\left(-\frac{1}{\sqrt{N}}\frac{\partial}{\partial \eta} + \frac{1}{2N}\frac{\partial^2}{\partial \eta^2} + \dots\right) N2a\left[\sigma + \frac{\rho}{\sqrt{N}}\right]\left[1 - \rho - \sigma - \frac{1}{\sqrt{N}}(\xi + \eta)\right]\Pi$$

$$+\left(\frac{1}{\sqrt{N}}\frac{\partial}{\partial \eta} + \frac{1}{2N}\frac{\partial^2}{\partial \eta^2} + \dots\right) N\left[\sigma + \frac{\eta}{\sqrt{N}}\right]\left[d + 2p(\rho + \frac{\xi}{\sqrt{N}}) + c(\sigma + \frac{\eta}{\sqrt{N}})\right]\Pi\,.$$

4.2.2 Mean-Field Analysis

The equations of motion governing the deterministic behaviour are obtained by gathering the terms of $\mathcal{O}(N^{1/2})$. We have from (4.4)

$$\begin{aligned}-\dot{\rho}\partial_\xi \Pi - \dot{\sigma}\partial_\eta \Pi = {} & [-2a_1\rho(1 - \rho - \sigma) + d_1\rho + c_1\rho^2 + 2p_1\rho\sigma]\partial_\xi \Pi \\ & + [-2a_2\sigma(1 - \rho - \sigma) + d_2\sigma + c_2\sigma^2 + 2p_1\rho\sigma]\partial_\eta \Pi\end{aligned} \tag{4.5}$$

which in order to satisfy we must have the rate equations

$$\begin{aligned}\dot{\rho} &= \rho[2a_1 - d_1 - 2(a_1 + p_1)\sigma - (2a_1 + c_1)\rho] \\ \dot{\sigma} &= \sigma[2a_2 - d_2 - (2a_2 + c_2)\sigma - 2(a_2 + p_2)\rho]\,.\end{aligned} \tag{4.6}$$

In order to keep the deterministic behaviour of the model neutral we will set the rates for each process as equal, i.e. $a_1 = a_2 \equiv a$ etc. This shows that we do not have a preference or selection bias for either species.

Fixed Points

We now look to find the fixed points of (4.6). From inspection, we have the three fixed points (ρ_*, σ_*):

$$(0, 0) \tag{4.7}$$

$$\left(0, \frac{2a-d}{2a+c}\right) \tag{4.8}$$

$$\left(\frac{2a-d}{2a+c}, 0\right) \tag{4.9}$$

The first of these is clearly the absorbing state at the origin which is the extinction of both species. The other are fixed points where one species has gone extinct. We find the final fixed point from simultaneously solving the linear equations in the square brackets, yielding the fixed point (ρ_*, ρ_*) where

$$\rho_* = \frac{2a-d}{(2p-c)(4a+2p+c)} \ . \tag{4.10}$$

In order for this fixed point to exist in the system we shall impose $2a > d$ and $2p > c$.

Linear Stability

To find the evolution of the deterministic dynamics we study the stability of each of the fixed points. We do this by examining the eigenvalues of the linearised matrix, or Jacobian matrix, A for the system of equations (4.6):

$$A = \begin{pmatrix} 2a-d-2(a+p)\sigma_* - 2(2a+c)\rho_* & -2(a+p)\rho_* \\ -2(a+p)\sigma_* & 2a-d-2(a+p)\rho_* - 2(2a+c)\sigma_* \end{pmatrix} \tag{4.11}$$

We find that the fixed point at the origin (4.7) has eigenvalues $\lambda_- = \lambda_+ = 2a-d$, meaning it is repulsive. For the two single species fixed points (4.8) and (4.9) the eigenvalues are

$$\lambda_\pm = \frac{2a-d}{2a+c}\Big[a+p \pm (a-p+c)\Big] \tag{4.12}$$

which means they are either repulsive nodes or saddle points depending on the parameter values. For the parameter regime we will work with, they are saddle

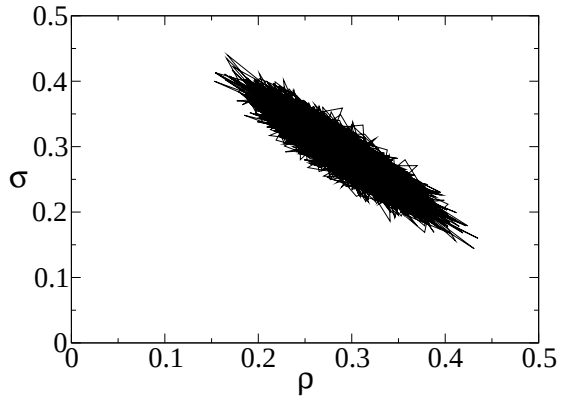

Figure 4.1: The phase portrait of the two population densities ρ and σ. For the parameters $a = 2.1$, $d = 0.5$, $c = 2.5$, $p = 0.9$ the system evolves to the fixed point at $\rho = \sigma = 0.29$ and then diffuses about it.

points. For the fixed point (4.10) the linearised matrix is

$$A = -\rho_* \begin{pmatrix} 2a + c & 2(a + p) \\ 2(a + p) & 2a + c \end{pmatrix} \tag{4.13}$$

with eigenvalues

$$\begin{aligned} \lambda_+ &= -(4a + 2p + c)\rho_* \\ \lambda_- &= -(c - 2p)\rho_* \, . \end{aligned} \tag{4.14}$$

Both of these are negative and so the fixed point is stable. Therefore deterministically we expect the system to evolve to the stable node (4.10).

4.2.3 Monte Carlo Simulation of the System

Using the Gillespie algorithm, as detailed in section 2.11.1, we can simulate the stochastic dynamics (4.1) to see if the deterministic behaviour of the system we predict is borne out. In figure 4.1 we see that the system does evolve to the fixed point predicted by (4.10). Once there the system is then free to diffuse about it. We see immediately this diffusion is skewed to act more in one particular direction. Because of the double symmetry of the form of the linearised matrix, where $A_{11} = A_{22}$ and $A_{12} = A_{21}$, the corresponding eigenvectors $\mathbf{e}_\pm$ of the eigenvalues

$\lambda_{\pm}$ (4.14) are

$$\begin{aligned}\mathbf{e}_{+} =& \frac{1}{\sqrt{2}}(1,1)\\ \mathbf{e}_{-} =& \frac{1}{\sqrt{2}}(-1,1)\end{aligned} \tag{4.15}$$

We see from figure 4.1 that the diffusion is elongated in the direction of $\mathbf{e}_2$, which tallies with the fact that the associated eigenvalue $|\lambda_-| < |\lambda_+|$ and so the restoring force is weaker in this direction compared to its perpendicular axis.

4.2.4 Nullcline

We can describe this elongated diffusion more formally by describing the dynamics about the fixed point in terms of a slow manifold dynamics as done very recently by Constable *et al* in [99]. The basic idea is to exploit a separation in timescales: in a diagonalised system, the variables are cast as fast or slow depending on how quickly they relax to the fixed point according to their eigenvalues derived from linear stability analysis. The variables whose eigenvalues are large and negative can be held constant as they will fix first. Then the remaining active, or *slow*, variables can be described as acting on a subspace of the phase space called the slow manifold [100]. To estimate the slow manifold, Constable *et al* use the nullcline of the deterministic system, a surface on which the forces are zero [101]. They find for a similar population dynamical model to ours, for a system with a stable fixed point, that the diffusion can be approximated as acting over a hyperbolic nullcline.

Following the same method, we derive the form of the nullcline for the SFP model from the defining equation

$$\dot{\rho} + \dot{\sigma} = 0\ . \tag{4.16}$$

Plugging in (4.6) gives

$$A\rho^2 + 2B\rho\sigma + A\sigma^2 + C\rho + C\sigma = 0 \tag{4.17}$$

with $A = 2a + c$, $B = 2(a + p)$ and $C = -(2a - d)$. Rewriting this as

$$\begin{pmatrix} \rho & \sigma \end{pmatrix} \begin{pmatrix} A & B \\ B & A \end{pmatrix} \begin{pmatrix} \rho \\ \sigma \end{pmatrix} + C\rho + C\sigma = 0\,, \tag{4.18}$$

we diagonalise the matrix by introducing the variable transformation

$$\begin{pmatrix} \rho \\ \sigma \end{pmatrix} = \frac{1}{\sqrt{2}} \begin{pmatrix} 1 & -1 \\ 1 & 1 \end{pmatrix} \begin{pmatrix} u \\ v \end{pmatrix} \tag{4.19}$$

to the new variables (u, v) which are the principal axes of the eigenvalues (4.15). This yields

$$\begin{pmatrix} u & v \end{pmatrix} \begin{pmatrix} P_1 & 0 \\ 0 & P_2 \end{pmatrix} \begin{pmatrix} u \\ v \end{pmatrix} + \sqrt{2}Cu = 0 \tag{4.20}$$

with $P_1 = A + B$, $P_2 = A - B$. Multiplying this out and completing the square gives

$$P_1 \left(u + \frac{C}{\sqrt{2}P_1} \right)^2 + P_2 v^2 - \frac{C^2}{2P_1} = 0\,, \tag{4.21}$$

which can be written in the canonical form of the equation of an ellipse

$$\frac{(u - u_0)^2}{R_u^2} + \frac{(v - v_0)^2}{R_v^2} = 1\,, \tag{4.22}$$

where

$$u_0 = \frac{-C}{\sqrt{2}P_1} = \frac{2a - d}{\sqrt{2}(4a + 2p + c)} = \frac{\rho_*}{\sqrt{2}} \tag{4.23}$$

$$v_0 = 0 \tag{4.24}$$

$$R_u = \left| \frac{C}{\sqrt{2}P_1} \right| = \frac{2a - d}{\sqrt{2}(4a + 2p + c)} \tag{4.25}$$

$$R_v = \left| \frac{C}{\sqrt{2P_1P_2}} \right| = \frac{2a - d}{\sqrt{2(4a + 2p + c)(c - p)}} \tag{4.26}$$

In figure 4.2 we superimpose the elliptical nullcline and the simulation of the stochastic dynamics. Analogously to what was found in [99], we see the diffusion could be approximated as diffusing on the slow manifold approximated by the nullcline. Here, for the SFP model we will not pursue this slow manifold approach, but we will make use of it for for a different model in chapter 5.

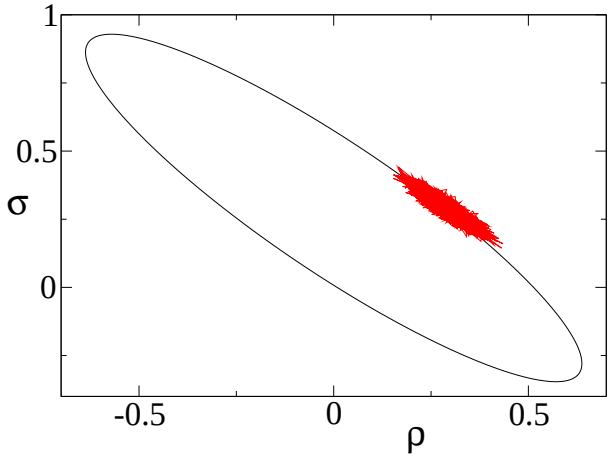

Figure 4.2: Superposition of the elliptical nullcline (4.22) and a simulation of the stochastic dynamics with parameters $a = 2.1$, $d = 0.5$, $c = 2.5$, $p = 0.9$.

4.2.5 Fokker-Planck Equation

To describe the fluctuations due to the noise about the stable fixed point, described by the stochastic variables $\boldsymbol{\xi} = (\xi, \eta)$, we return to the van Kampen expansion (4.4). Collecting the terms of $\mathcal{O}(N^0)$ we find a linear FPE, giving the evolution of the distribution of the fluctuations $P(\xi, \eta)$. We have, using Einstein notation,

$$\frac{\partial P(\xi,\eta)}{\partial t} = \frac{\partial}{\partial \xi_i}\left(\gamma_{ij}\xi_j P\right) + D_{ij}\frac{\partial^2 P}{\partial \xi_i \partial \xi_j} \tag{4.27}$$

where the drift matrix γ and the diffusion matrix D are given by

$$\gamma = -A = \rho_* \begin{pmatrix} 2a+c & 2(a+p) \\ 2(a+p) & 2a+c \end{pmatrix} \tag{4.28}$$

$$D = 2a\rho_* \frac{c+2(p+d)}{4a+2p+c} \begin{pmatrix} 1 & 0 \\ 0 & 1 \end{pmatrix} \equiv D_{eq} \begin{pmatrix} 1 & 0 \\ 0 & 1 \end{pmatrix} . \tag{4.29}$$

4.3 The Steady State

We are interested in studying our SFP model in the long time limit, when the system has relaxed to its steady state. We digress here to review the important concept of detailed balance. When detailed balance holds, the system reaches

thermal equilibrium in the steady state, and a probability current is necessarily not permitted. Conversely, when detailed balance is broken, in the steady state a current can flow, and so the system is driven into a non-equilibrium steady state (NESS). To explore the flow of a probability current as a possible mechanism for cycles and other macroscopic dynamical phenomena, we must establish how the conditions for detailed balance are codified in a Fokker-Planck formalism. In doing so, we also look to find what rules the noise must adhere to, and learn how it can be used to drive the system to a NESS.

4.3.1 Detailed Balance

A FPE can be expressed as a continuity equation

$$\frac{\partial P(\mathbf{x},t)}{\partial t} = -\frac{\partial}{\partial x_i} J_i(\mathbf{x},t) \tag{4.30}$$

where we recognise $\mathbf{J}$ as the probability current. Comparing this with the FPE obtained in a Kramers-Moyal expansion (2.30) we write this current as

$$J_i = \alpha_i P - \frac{\partial}{\partial x_j}\alpha_{ij} P \ . \tag{4.31}$$

A system is in thermal equilibrium if in the steady state, where $\partial_t P = 0$, the current is zero everywhere. This is a manifestation of detailed balance being satisfied [54]. When one is dealing with systems that are defined by their dynamics, rather than by appealing to an energy function, a steady state in which the current is non-zero is most likely. In order to satisfy the continuity equation (4.30) in the steady state we require that the current is divergence free.

In a one-dimensional (1D) system—by which we refer to the size of the phase space—it is possible to make a change of variable such that these conditions are satisfied, unless a current is enforced on the system by virtue of periodic boundary conditions, or driving of the system at the boundaries. If the system has natural boundary conditions, where the probability and the current vanish at the boundaries, then necessarily the current must be zero everywhere in the steady state [26]. In two or more dimensions, however, detailed balance is typically only satisfied if it is imposed from the outset, as is appropriate for systems that are at thermal equilibrium. In particular, in two dimensions (2D), the vanishing of a

divergence implies that 'streamlines' following the probability current form closed loops in the 2D phase space within the boundaries of the system, regardless of whether the system has natural, periodic or driven boundary conditions [54].

For the system to be in thermal equilibrium in the steady state two conditions must be satisfied by the drift and diffusion matrices [54]. The first is the *potential condition* which requires that the drift forces in the equivalent Langevin equation can be derived from a potential $V(\mathbf{x})$:

$$\dot{x_i} = \alpha_i(\mathbf{x}) + \eta_i(t) \equiv -\frac{\partial V(\mathbf{x})}{\partial x_i} + \eta_i(t) \ . \tag{4.32}$$

We see that this means we require $\alpha_i = \partial_{x_i} V$. Differentiating by x_j this becomes

$$\frac{\partial \alpha_i}{\partial x_j} = \frac{\partial^2 V}{\partial x_j \partial x_i} \ . \tag{4.33}$$

Alternatively by relabelling $i \leftrightarrow j$ we can write this as

$$\frac{\partial \alpha_j}{\partial x_i} = \frac{\partial^2 V}{\partial x_i \partial x_j} \ . \tag{4.34}$$

As the order of partial differentiation is irrelevant, equating these two expressions shows that to obey the potential condition we that the drift terms satisfy

$$\frac{\partial \alpha_i}{\partial x_j} = \frac{\partial \alpha_j}{\partial x_i} \ . \tag{4.35}$$

The second condition we require for no current to flow is that the we have thermal noise, which requires the diffusion matrix D to be equivalent to the identity matrix $D_{ij} = d\delta_{ij}$, where d is some diffusion constant. If both the potential and thermal condition are met, the steady-state probability distribution is given by the Boltzmann distribution

$$P(\mathbf{x}) = \frac{1}{Z} e^{-V(\mathbf{x})/D} \ . \tag{4.36}$$

with normalisation constant Z [54].

4.3.2 Application to a Linear Fokker-Planck Equation

We want to translate these conditions for detailed balance for the case where the stochastic dynamics are acting in the neighbourhood of a deterministic fixed point, a problem studied more generally by Kwon *et al* [102, 103, 104]. Using the linear noise expansion of the van Kampen expansion, the FPE is linear (2.76). The thermal noise condition needs no translating as it is trivial to identify whether a matrix is proportional to the identity matrix. Identifying $\alpha_1 \equiv \alpha_{1,0}$ and $\alpha_2 \equiv \alpha_{0,1}$, from inspection of (2.76) and (2.77) we see that the potential condition is satisfied if γ is symmetric, i.e. $\gamma_{12} = \gamma_{21}$.

We can also obtain a direct expression for the current $\mathbf{J}$ for a linear FPE. Such an FPE is of the form of that for the Ornstein-Uhlenbeck process which has been studied extensively as a model for describing Brownian motion [105, 26]. For a general n-dimensional vector x the solution to the linear FPE (using Einstein notation)

$$\frac{\partial P(\mathbf{x})}{\partial t} = \frac{\partial}{\partial x_i}\gamma_{ij}x_j P + D_{ij}\frac{\partial^2}{\partial x_i \partial x_j}P \tag{4.37}$$

in the steady state, $\partial_t P_S = 0$, is the multivariate normal distribution

$$P_S(\mathbf{x}) = \frac{1}{Z}e^{-\frac{1}{2}x_k S_{kl} x_l} \tag{4.38}$$

where the matrix S is the inverse of the covariance matrix: $S^{-1}_{kl} = \mathrm{cov}(x_k, x_l)$ [54]. Substituting this Gaussian ansatz into (4.37) we can find how S relates to the drift and diffusion matrices γ and D. Solving in the steady state, at long enough time that the system has deterministically reached its fixed point, we will evaluate the two terms in (4.37) separately. The first term is

$$\begin{aligned}\frac{\partial}{\partial x_i}\gamma_{ij}x_j P_S &= \gamma_{jj}P_S - \frac{1}{2}\gamma_{ij}x_j(S_{ik}x_k + x_k S_{ki})P_S \\ &= \Big[\gamma_{ii} - \frac{1}{2}x_j(\gamma^T_{ji}S_{ik} + S_{ji}\gamma_{ik})x_k\Big]P_S\end{aligned} \tag{4.39}$$

where we have used the fact that $S_{ij} = S_{ji}$ and relabelled $j \leftrightarrow k$ in the final term.

The second term gives, making use of the fact $D_{ij} = D_{ji}$,

$$\begin{aligned} D_{ij}\frac{\partial^2}{\partial x_i \partial x_j}P_S &= -\frac{\partial}{\partial x_i}D_{ij}S_{jk}x_k P_S \\ &= \big[-D_{ij}S_{ji} + D_{ij}S_{jk}x_k S_{il}x_l \big] P_S \\ &= \big[-(DS)_{ii} + x_j S_{ji} D_{il} S_{lk} x_k \big] P_S \end{aligned} \tag{4.40}$$

where in the final line we relabelled $l \leftrightarrow j$ in the second term. Putting these two expressions back into (4.37) the steady-state equation is now

$$(\gamma - DS)_{ii}P_S - x_j \left[\frac{1}{2}(\gamma^T S)_{jk} + \frac{1}{2}(S\gamma)_{jk} - (SDS)_{jk} \right] x_k P_S = 0 \tag{4.41}$$

which can only be satisfied if the following two relations hold:

$$\gamma^T S + S\gamma = 2SDS \tag{4.42}$$

$$\mathrm{Tr}(DS - \gamma) = 0. \tag{4.43}$$

Plugging the Gaussian solution (4.38) into the the expression for the current from the continuity equation for a linear FPE,

$$J_i = \gamma_{ij} P_S - D_{ij}\frac{\partial}{\partial x_j}P_S \,, \tag{4.44}$$

gives

$$J_i = (DS - \gamma)_{ij} x_j P_S \,. \tag{4.45}$$

We see then that the current will be zero in the steady state, and the system will be in thermal equilibrium, if

$$S = D^{-1}\gamma \,. \tag{4.46}$$

This is consistent with the two conditions for detailed balance. To see this we transpose it to get $S = \gamma^T D^{-1}$, using the fact that S and D are symmetric. Equating these equivalent expressions for S and rearranging we see that we must have

$$\gamma D = D\gamma^T \tag{4.47}$$

which is true when $\gamma_{ij} = \gamma_{ji}$ and $D_{ij} = d\delta_{ij}$.

4.3.3 Solving the Linear Fokker-Planck Equation Explicitly

It is in fact possible to solve the linear FPE (4.37) directly using the method of characteristics. While this is mentioned by Risken in [54], it is not done explicitly, and having been unable to find such a derivation we present our own version here. The reason for doing so is that it will give us a direct way to calculate the matrix S appearing in the steady-state Gaussian distribution (4.38), which is crucial in subsequent calculations. A different method of how to construct this matrix is given by Kwon *et al* [102], who refer to S as the *cost matrix*. However the method still boils down to diagonalisation and matrix decomposition, and does not prove to be a faster method than the one we present here.

Formally, writing the probability distribution as $P(\mathbf{x}) \equiv P(\mathbf{x}, t|\mathbf{x}', t')$ we define the Fourier transform

$$P(\mathbf{x}, t|\mathbf{x}', t') = \frac{1}{(2\pi)^N} \int_{-\infty}^{\infty} \mathrm{d}^N k \; e^{ik_m x_m} \tilde{P}(\mathbf{k}, t|\mathbf{x}', t') \; . \tag{4.48}$$

Using this, the linear FPE (4.37) is transformed to the first-order partial differential equation

$$\frac{\partial \tilde{P}(\mathbf{k}, t|\mathbf{x}', t)}{\partial t} = -\gamma_{ij} k_j \frac{\partial \tilde{P}}{\partial k_i} - D_{ij} k_i k_j \tilde{P} \tag{4.49}$$

which we now solve using the methods of characteristics [106]. Defining our initial time $t' = 0$, we have the initial conditions $P(\mathbf{x}, 0|\mathbf{x}', 0) = \delta(\mathbf{x} - \mathbf{x}')$. This gives the equivalent initial condition in k-space $\tilde{P}(\mathbf{k}, t|\mathbf{x}', t) = e^{-ik_j x'_j}$.

We are required to solve the coupled ordinary differential equations

$$\frac{dt}{dr} = 1 \tag{4.50}$$

$$\frac{dk_i}{dr} = \gamma_{ji}^T k_i \, , \qquad i = 1, \ldots, N \tag{4.51}$$

$$\frac{d\tilde{P}}{dr} = -k_i D_{ij} k_j \; . \tag{4.52}$$

As we have a linear partial differential equation then the characteristic curves are given parametrically by $(k_1(0), k_2(0) \ldots, k_N(0), \tilde{P}(0)) = (s_1, s_2, \ldots, s_N, e^{-is_j x'_j})$

[106]. This gives the initial conditions

$$t(r,0) = 0 \tag{4.53}$$
$$k_i(r,0) = s_i\,, \qquad i = 1,\ldots,N \tag{4.54}$$
$$\tilde{P}(r,0) = e^{-is_jx'_j} \tag{4.55}$$

The solution to (4.50) is simply $t(r) = r + c(r)$. Applying the initial condition (4.53) gives $r = t$ which requires no work to invert. The solution to (4.51) is

$$k_i(r,s) = \sum_j c_j e^{r\lambda^{(j)}} v_i^{(j)} \tag{4.56}$$

where c_j are constants of integration and $\{\lambda^{(j)}, \mathbf{v}^{(j)}\}$ are the eigenvalue-eigenvector pairs of γ^T. Introducing the matrices

$$V_{ij} = v_i^{(j)} \tag{4.57}$$
$$\Gamma_{ij} = e^{r\lambda^{(j)}}\delta_{ij} \tag{4.58}$$

we can express k_i as

$$k_i(r,s) = c_j V_{ip}\Gamma_{pj}\,. \tag{4.59}$$

Applying the initial condition (4.54) we have

$$k_i(r,0) = s_i = c_j V_{ij} \tag{4.60}$$

which we invert to find the constant vector $\mathbf{c}$. This gives us the solution

$$\mathbf{k}(r,s) = V\Gamma V^{-1}\mathbf{s} \tag{4.61}$$

which it is straightforward to invert to find $\mathbf{s}(k,t)$. Now that we have solved (4.50) and (4.51) and can go between $(t,\mathbf{k}) \leftrightarrow (r,\mathbf{s})$, we are able to solve (4.52) and find the solution in terms of t and $\mathbf{k}$. The solution is of the form

$$\tilde{P}(r,\mathbf{s}) = C\exp\left(-\int \mathrm{d}r\; k_i D_{ij} k_j\right) \tag{4.62}$$

where C is the integration constant. To do this integral we express the integrand

by writing k in terms of s using (4.61) and we use the definition of Γ (4.58):

$$k_i D_{ij} k_j = V_{ia} e^{r\lambda^{(b)}} \delta_{ab} V^{-1}_{bc} s_c D_{ij} V_{jw} e^{r\lambda^{(y)}} \delta_{wy} V^{-1}_{yz} s_z \tag{4.63}$$

Combining the exponentials this is simple to integrate over r. Reordering the terms it is

$$\int \mathrm{d}r \; k_i D_{ij} k_j = \frac{s_c (V^{-1})^T_{cb} \Gamma_{ba} V^T_{ai} D_{ij} V_{jw} \Gamma_{wy} V^{-1}_{yz} s_z}{\lambda^{(a)} + \lambda^{(w)}} \; . \tag{4.64}$$

Defining the matrix

$$\beta_{ij} = \frac{(V^T D V)_{ij}}{\lambda^{(i)} + \lambda^{(j)}} \tag{4.65}$$

and again using (4.61) to switch between s and k we can now write (4.62) as

$$\tilde{P}(r, \mathbf{s}) = C \exp\left[-k_i (V^{-1})^T_{ia} \beta_{ab} V^{-1}_{bj} k_j\right] \; . \tag{4.66}$$

Applying the initial conditions (4.54) and (4.55) gives us for the integration constant

$$C = \exp(-i s_j x'_j) \exp(s_i (V^{-1})^T_{ia} \beta_{ab} V^{-1}_{bj} s_j) \; . \tag{4.67}$$

Transforming s to k and plugging this back in gives us the expression for $\tilde{P}$:

$$\tilde{P}(t, \mathbf{k}) = \exp\left(-i k_j m_j - \frac{1}{2} k_i \sigma_{ij} k_j\right) \tag{4.68}$$

where we define

$$\mathbf{m} = V \Gamma^{-1} V^{-1} \mathbf{x}' \tag{4.69}$$

$$\sigma = 2 (V^{-1})^T (\beta - \Gamma^{-1} \beta \Gamma^{-1}) V^{-1} \; . \tag{4.70}$$

The only thing we require now is to compute the Fourier transform (4.48):

$$P(\mathbf{x}, t | \mathbf{x}', t') = \frac{1}{(2\pi)^N} \int_{-\infty}^{\infty} \mathrm{d}^N k \; \exp\left(i (x_j - m_j) k_j - \frac{1}{2} k_i \sigma_{ij} k_j\right) \; . \tag{4.71}$$

This is a standard multi-dimensional Gaussian integral for a symmetric positive-definite matrix σ [107] with solution

$$P(\mathbf{x}, t | \mathbf{x}', t') = \frac{1}{(2\pi)^{N/2} \sqrt{\det \sigma}} \exp\left[-\frac{1}{2} (m_i - x_i) \sigma^{-1}_{ij} (m_j - x_j)\right] \; . \tag{4.72}$$

The final consideration we make is to find obtain the long time behaviour, when P has reached its steady-state distribution. The time dependence enters into the matrix Γ (4.58), and we see that as $t \to \infty$, $\Gamma^{-1} \to 0$, which by (4.69) means $\mathbf{m} \to 0$.

We summarise this method of solution in the box below. It gives us a way to explicitly calculate the matrix of the Gaussian distribution for the steady state (4.75) from knowledge of the drift matrix γ and diffusion matrix D of a system described by a linear FPE (4.73).

For an N-dimensional linear Fokker-Planck equation

$$\frac{\partial P(\mathbf{x})}{\partial t} = \frac{\partial}{\partial x_i}\gamma_{ij}x_j P + D_{ij}\frac{\partial^2}{\partial x_i \partial x_j}P \tag{4.73}$$

the solution in the steady state is

$$P_S(\mathbf{x}) = \frac{1}{(2\pi)^{N/2}\sqrt{\det \sigma}} \exp\left[-\frac{1}{2}x_i \sigma^{-1}_{ij} x_j\right] \tag{4.74}$$

where:

$$\sigma = 2(V^{-1})^T \beta V^{-1} \; ; \tag{4.75}$$

$$\beta_{ij} = \frac{(V^T D V)_{ij}}{\lambda^{(i)} + \lambda^{(j)}} \; ; \tag{4.76}$$

$\{\lambda^{(j)}, \mathbf{v}^{(j)}\}$ are the eigenvalue-eigenvector pairs of γ^T and $V_{ij} = v_i^{(j)}$.

4.3.4 Consistency Check

We can check that this result satisfies the criteria for detailed balance (4.46) derived earlier. For the potential condition we have $\gamma = \gamma^T$. This means that the matrix V will be orthogonal and so $V^{-1} = V^T$. Applying this and the thermal noise condition $D_{ij} = d\delta_{ij}$ where d is a constant to (4.76) gives

$$\beta = \frac{d}{2\lambda^{(i)}}\delta_{ij} = \frac{d}{2}\Lambda^{-1} \tag{4.77}$$

where $\Lambda = \mathrm{diag}(\lambda^{(1)}, \lambda^{(2)}, \ldots, \lambda^{(N)})$.

Plugging this into (4.75) gives

$$\sigma = d\ V\Lambda^{-1}V^T\ . \tag{4.78}$$

From the spectral theorem of diagonalisation [108] we have the relation

$$\Lambda = V^T\gamma^T V \tag{4.79}$$

which we substitute into (4.78). Cancelling terms and using the symmetric property of γ gives

$$\sigma = d\gamma^{-1} = D\gamma^{-1}\ . \tag{4.80}$$

Inverting this we find the equivalence with the Gaussian ansatz matrix S in (4.38),

$$S \equiv \sigma^{-1} = \gamma D^{-1} = D^{-1}\gamma \tag{4.81}$$

where in the final step we have used the fact D is proportional to the identity matrix. We see that we have recovered the constraint (4.46) on S for detailed balance to hold and thermal equilibrium be reached in the steady state.

4.4 The SFP Steady State

Now that we have established the criteria for whether or not a system described by a linear FPE is in thermal equilibrium or not, we apply it to the SFP model. From inspection of the FPE (4.27) we see that both detailed balance conditions are satisfied: $\gamma_{12} = \gamma_{21}$ and $D_{ij} = D_{eq}\delta_{ij}$. This means in the steady state we expect no current to flow. Intuitively this seems correct as the SFP model is neutral, with no selection bias favouring either species.

4.4.1 Breaking Detailed Balance

In order for the system to evolve instead to a NESS, we must induce a current to flow by breaking the neutrality of the model. To do so we could introduce some new processes to the model or make the rates of one of the existing processes different for each species. As we wish to study effects purely due to the noise, doing either requires some thought. We wish to break the detailed balance by

violating the thermal noise condition, while keeping the potential condition intact and the deterministic behaviour of the system unchanged.

This is achievable by not just differentiating one of the rate constants, but by transforming each of them by a systematic linear displacement. Introducing the parameters r_1 and r_2 for species A and B respectively, we transform the rate constants for the processes given in (4.1) as

$$a \to a - r_i\,, \quad d \to d - 2r_i\,, \quad p \to p + r_i\,, \quad c \to c + 2r_i\,. \tag{4.82}$$

Substituting this into the rate equations (4.6) and the drift matrix (4.28) leaves them invariant. The diffusion matrix (4.29) however becomes

$$D_{ij} = [D_{eq} + 2r_i\rho_*(2\rho_* - 1)]\,\delta_{ij} \tag{4.83}$$

meaning that if $r_1 \neq r_2$ then $D_{11} \neq D_{22}$, making the noise athermal which violates detailed balance.

4.5 Measuring the Current

Now that we have found a way to induce a current to flow in the steady state, we wish to observe it in the system. We must define an appropriate measure which signifies the presence of a current. As mentioned earlier, in a study of a physical system of an optically trapped colloid [98], a persistent non-zero angular velocity was measured in the thermal motion, from which a probability current was inferred to be flowing. We will also use the average angular velocity as a yardstick, and measure it in two ways: (i) from finding the analytical form of the closed current cycle, and (ii) by direct measurement from Monte Carlo simulation of the master equation (4.2).

4.5.1 Solving the Planar Autonomous System

Returning to our notation of $\boldsymbol{\xi}$ to describe fluctuations about the stable fixed point in the SFP model, we can express the current in the steady state in terms of a velocity by writing

$$J(\boldsymbol{\xi}) = \dot{\boldsymbol{\xi}} P_S(\boldsymbol{\xi})\,. \tag{4.84}$$

Using our expression for the current derived for a linear FPE (4.45) we see this gives us the planar autonomous system

$$\dot{\boldsymbol{\xi}} = (DS - \gamma)\boldsymbol{\xi} \equiv W\boldsymbol{\xi} \,. \tag{4.85}$$

If the detailed balance condition (4.46) holds then $W = 0$ and so the velocity is zero. When $r_1 \neq r_2$ and $W \neq 0$, we can solve the planar autonomous system (4.85) by diagonalising W. We calculate the eigenvalues using

$$\lambda_\pm = \frac{\operatorname{Tr} W}{2} \pm \frac{\sqrt{(\operatorname{Tr} W)^2 - 4 \det W}}{2} \,. \tag{4.86}$$

We know by the constraint (4.43) imposed by the Gaussian form of the steady-state distribution P_S that $\operatorname{Tr} W = 0$. Therefore we have two purely imaginary eigenvalues: $\lambda_\pm = \pm i\omega$ where $\omega = \sqrt{\det W}$.

For planar autonomous systems whose trajectories are centres, the solutions to (4.85) can be expressed as [108]

$$\boldsymbol{\xi}(t) = \cos(\omega t)\mathbf{c}_1 + \sin(\omega t)\mathbf{c}_2 \tag{4.87}$$

where the constant vectors $\mathbf{c}_1$ and $\mathbf{c}_2$ are set by the initial conditions:

$$\mathbf{c}_1 = \boldsymbol{\xi}(0) = (\xi_0, \eta_0) \tag{4.88}$$

$$\mathbf{c}_2 = \frac{1}{\omega} W \mathbf{c}_1 \,. \tag{4.89}$$

Writing the matrix W as

$$W = \begin{pmatrix} q & u \\ z & -q \end{pmatrix} , \tag{4.90}$$

we express the general solution as

$$\boldsymbol{\xi}(t) = \begin{pmatrix} \xi_0 \cos(\omega t) + \frac{1}{\omega}(q\xi_0 + u\eta_0)\sin(\omega t) \\ \eta_0 \cos(\omega t) + \frac{1}{\omega}(z\xi_0 - q\eta_0)\sin(\omega t) \end{pmatrix} . \tag{4.91}$$

These solutions tell us that the steady-state currents form closed loops that are ellipses in the 2D phase space of (ξ, η), with the particular trajectory in the phase portrait selected by the initial condition. In figure 4.3 is displayed the vector field defined by (4.85) along with a particular solution of the form (4.91).

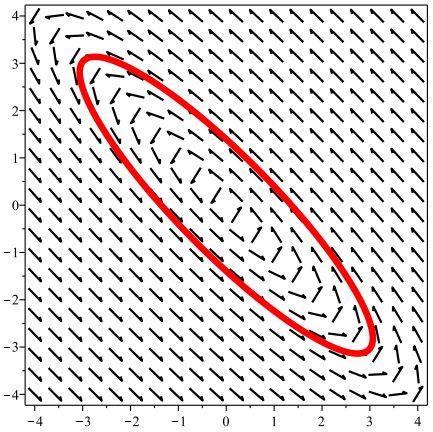

Figure 4.3: Field plot of the planar autonomous system (4.85) overlaid with a particular solution of the form (4.91). The parameters are $a = 3.1$, $d = 1.0$, $c = 3.5$, $p = 1.2$, $r_1 = 0.0$ and $r_2 = -0.6$ with $c_1 = 0, c_2 = 10.3$ for the red ellipse.

The important thing to take from this analysis is the frequency of the elliptical orbit, which we see clearly from the form of the solution (4.91) is ω. This frequency is the angular velocity associated with the elliptical probability current which we denote by ω_E and is, from before, given by

$$\omega_E = \sqrt{\det W} \, . \tag{4.92}$$

In order to calculate this we use the mathematical software Maple(TM) to calculate W, which involves constructing the matrix S by the method of characteristics solution given by (4.73 – 4.76).

4.5.2 Measuring an Angle From Simulation

To verify the existence of the elliptical steady-state current we need to measure the average angular velocity directly from Monte Carlo simulations of the stochastic dynamics. This requires us to calculate the angular position of the system about the stable fixed point in the Cartesian coordinate system of the species population numbers in the simulation.

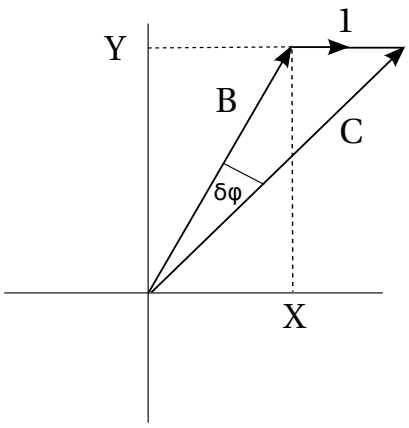

Figure 4.4: Schematic of how the change in angle $\delta\phi$ is calculated in terms of the state of the system before the update, **B**, and after, **C**. This example is of the birth of an A, meaning $X(t+\tau) = X(t) + 1$.

Defining a coordinate system with a shifted origin to the stable fixed point,

$$X = n - n_* \tag{4.93}$$

$$Y = m - m_* \tag{4.94}$$

with $n_* = m_* = N\rho_*$, we can measure the total angular displacement $\phi(t)$ which is positive in the anti-clockwise direction and quantifies the total distance travelled. After each update of the simulation we update the angle by

$$\phi(t+\tau) = \phi(t) + \delta\phi \; . \tag{4.95}$$

Defining by $\mathbf{B} = (X(t), Y(t))$ the state of the system at the start of the update, and by $\mathbf{C} = (X(t+\tau), Y(t+\tau))$ the state of the system at the end of the update as in the schematic given in figure 4.4, we can calculate the change in ϕ using the cosine rule:

$$\cos(\delta\phi) = \frac{B^2 + C^2 - 1}{2BC} \; . \tag{4.96}$$

As the model involves only one-step processes of a birth or a death of an A or B in an update, the vector $\mathbf{C} - \mathbf{B}$ is always of length 1.

What we measure is not the actual polar coordinate $\theta \in [-\pi, \pi]$, but the aggregate angle ϕ which will be non-zero if there is a persistent current present in

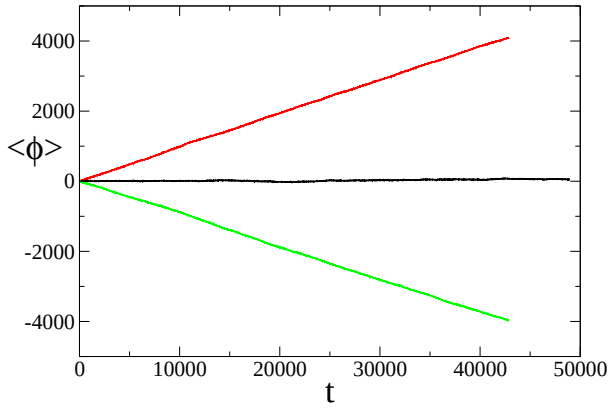

Figure 4.5: Time evolution of the total average angular displacement $\langle\phi(t)\rangle$ measured by simulation of the stochastic dynamics (4.1) by the Gillespie algorithm. The parameters are $a = 2.1$, $d = 0.5$, $c = 2.5$, $p = 0.9$. For the red line (top) $r_1 = -0.6$, $r_2 = 0$, the black line (middle) $r_1 = r_2 = 0$, the green line (bottom) $r_1 = 0$, $r_2 = -0.6$. Each is averaged over 100 runs.

the system. In figure 4.5 is plotted the the time evolution of the ensemble average $\langle\phi\rangle$. We see that we have the linear relation

$$\langle\phi(t)\rangle \sim \omega_G t \tag{4.97}$$

for some constant angular velocity which we denote ω_G. Furthermore, we observe that the criterion for no current to flow, $r_1 = r_2$, holds as the (black) central plot has a gradient consistent with a zero angular velocity. For the parameters quoted in the figure we find by linear regression that the average angular velocity has a magnitude of $\omega_G = 0.97$ for the (red) top and (green) bottom plots. We also see that the direction of circulation is determined by the athermality of the noise, i.e. if D_{11} is larger or smaller than D_{22}.

Using the same parameter set, we calculate the angular velocity obtained from the frequency of the elliptical orbit (4.92) to be $\omega_E = \pm 0.98$, where the sign is again indicative of the direction of circulation according to whether $r_1 > r_2$ or vice-versa.

4.6 Discussion and Conclusion

Our aim in this chapter has been to understand the conditions under which a non-equilibrium steady-state current in a finite population may be visible macroscopically, and if such currents could facilitate cycling behaviour in the population densities. We have observed through what we believe to be the simplest candidate model of species competition that a system may sustain a non-equilibrium steady state due to the form of the noise alone. This is manifested in the flow of a probability current whose presence we have inferred through a persistent non-zero average angular velocity in 2D state space. We find very good agreement between the two measurements made: calculating the frequency of the elliptical orbits the currents form in order to be divergence free in 2D, and by direct measurement of the ensemble average of the angular velocity from Monte Carlo simulation of the model's dynamics using the Gillespie algorithm.

By breaking the symmetry of the fluctuations by violating detailed balance, we observe a driven motion around the stable fixed point, which is in either the clockwise or anti-clockwise direction depending on the relative magnitude of the non-equilibrium parameters r_1 and r_2. Observing this long-time biased diffusion due to the athermality of the demographic noise is analogous to the fluctuating motion observed experimentally for the optically trapped colloid in [98]. However, a crucial feature of the dynamics is that one does not observe cyclicity in population abundances in *single realisations* of the stochastic dynamics on short timescales. More precisely, it is not possible to see the precession of a single orbit over a 2π interval. One must either perform an average over long times or an large ensemble to uncover systematic cyclicity. This means we do not observe global cycles as behaviour in the sense of McKane and Newman. Indeed, for the dynamics of the SFP model, there is no resonance in the power spectrum of the noise, and therefore no stochastic amplifications resulting in large deviations from the deterministic fixed point values of the species populations.

To observe any form of damped or undamped oscillations, Tomé and de Oliveira argue that one must have an underlying mechanism in the deterministic dynamics [92]. Here we have found this is indeed the case - we postulated whether a non-equilibrium current could fulfil this role in the absence of a deterministic component. This is not the case in terms of observing macroscopic oscillations with a well-defined frequency. Instead on short timescales we only observe

standard non-cyclic fluctuations consistent with Gaussian noise. Therefore we find that the presence of a non-equilibrium probability current due to the athermality of the noise could not be advanced in this case as a sole explanation for cyclic behaviour in natural populations, as observed in single field experiments.

This leads us to consider the question: is it possible to set up a population dynamical model in such a way that the flow of a noise-induced probability current does lead to cyclic behaviour being observed in a single trajectory over short times? When faced with the notion of an elliptical probability current flowing about the stable fixed point, conceptually one is drawn to thinking the fluctuations follow a fixed orbital path. Instead as is clear from figure 4.1 the system diffuses noisily about the fixed point. The definition of an angle about the fixed point is tenuous as the system can diffuse very close to and even jump over this origin, making the notion of an orbit implausible. This is the case both when the system is in thermal equilibrium and when a current is flowing, one being indistinguishable from the other. In the next chapter we look to overcome this obstacle by having a truly fixed orbital path, allowing us to study whether cycling behaviour can be observed due to the flow of a non-equilibrium steady-state current.

Chapter 5

Currents in Finite Populations Along a Circular Manifold

In the previous chapter we found for the stable fixed point (SFP) model that the flow of a steady-state probability current could not by itself give rise to macroscopically observable cycles. In this chapter we introduce an individual based, population dynamical model which is explicitly constructed to allow the system to follow a fixed radial orbit. It comprises two competing species, whose deterministic dynamics are such that the population resides on a stable circular manifold. As the population is finite, the system then diffuses around the manifold. Our major assumption is to neglect any diffusion off the manifold in the radial direction and model the diffusive motion as a one-dimensional motion in the polar direction ϕ. We induce a current to flow by dethermalising the demographic noise, which leads to a biased diffusion around the manifold resulting in quasicycles in the two-dimensional (2D) phase space of the population densities. We measure the current directly from the full 2D dynamics using the Gillespie algorithm, numerical integration of the polar 1D Langevin equation, and by considering a thermal diffusion process and calculating Kramers escape rates. We find broad agreement between these measurements, and find the system is well described by a 1D non-equilibrium steady state.

5.1 Introduction

In the stable fixed point (SFP) model of chapter 4 we studied the effects a probability current in the steady state can have on the macroscopic dynamics of a two-species population. An obfuscating factor in our considerations was the ill-defined closed orbit the current followed. We found that the proposed mechanism, due purely to the athermal form of the noise, by itself is not enough to sustain cycling behaviour—there must be some deterministic component. In other ecological models, most commonly this has been provided by a deterministic spiral, or focus, as in predator-prey systems [23] which give rise to damped oscillations. These are a feature only at short times which have attenuated in the steady state. In the last decade, multiple studies of the effects of demographic noise have shown how combinations of stochastic and deterministic effects can combine to sustain macroscopically observable cycles in populations [44, 53, 92, 94, 109]. Crucial to these studies have been the taking of an individual based model (IBM) approach, in which knowledge of the deterministic behaviour and fluctuations about it are obtained from the same common source, the stochastic dynamics that define the model, and encapsulated in the master equation.

We now look to introduce a component to the deterministic dynamics in order to facilitate cyclic behaviour. But rather than introduce a spiral, which allows overdamped oscillations which may or may not become undamped due to the noise [92], we impose a fixed orbital trajectory for the current to follow. What is needed is for the dynamics to be repelled from some origin, so that an orbit may then be set up about it. In particular, if the dynamics are constructed such that the deterministic forcing vanishes along some closed line (or manifold) in phase space, and such that the dynamics are attracted onto the manifold from outside, then it could in principle be possible for non-equilibrium fluctuations to generate a biased diffusion on the manifold. If so, in general we would expect to observe cycles about the circular manifold.

In this chapter we present what we believe to be the simplest model to achieve this, which on the deterministic level introduces a stable circular continuous manifold of fixed points, which lie at a fixed radius away from a repulsive node. We admit from the perspective of modelling real biological populations, the dynamics required to generate such a property in the deterministic behaviour are somewhat

contrived. However, from the more fundamental perspective of non-equilibrium statistical mechanics, we believe that this is the simplest such system that admits macroscopically observable quasicycles arising from non-equilibrium probability currents. It is also a natural extension of *quasi-neutral* models of population dynamics from open to closed neutral manifolds [110].

In studying the stochastic dynamics on the circular manifold we will carry out a dimensional reduction akin to a slow manifold analysis in order to describe the athermal biased diffusion, a purely noise-induced phenomenon, about the circular manifold. In doing so we can not only find whether cycles are possible, but also test the validity of describing 2D systems in terms of slow and fast variables, as done similarly in [95, 99].

5.2 The Circular Manifold (CM) Model

The new model we construct has a similar patch dynamics to that of the SFP model, the framework of which is detailed in section 2.7.1. The only major difference is now we do not conserve the total number of sites on the non-spatial patch. In other words, the patch can accommodate an indefinitely large number of both species. The population is kept finite however by the necessarily more complex interactions we admit to the model.

Defining the intensive population numbers $x_A = X_A/K$, $x_B = X_B/K$ where K is the carrying capacity, both species undergo the following birth and death processes:

$$\begin{aligned}
T(X_A+1, X_B|X_A, X_B) &= bx_A\left(2 + 3x_A^2 + x_B^2 + 2x_Ax_B\right) && \text{birth of A}\\
T(X_A, X_B+1|X_A, X_B) &= bx_B\left(2 + 3x_B^2 + x_A^2 + 2x_Ax_B\right) && \text{birth of B}\\
T(X_A-1, X_B|X_A, X_B) &= bx_A\left(a + (4-a)x_A + 2x_B + x_A^3 + x_Ax_B^2\right) && \text{death of A}\\
T(X_A, X_B-1|X_A, X_B) &= bx_B\left(a + (4-a)x_B + 2x_A + x_B^3 + x_Bx_A^2\right) && \text{death of B}
\end{aligned} \tag{5.1}$$

where $b \equiv b(K)$ and a are constants.

To interpret these transition rates in terms of biological processes, we note that a term in $x_A^n x_B^m$ corresponds to an interaction between n individuals of species A and m individuals of species B. So, for example, the birth of A

at a rate proportional to x_A^3 would arise from some interaction between three individuals of species A, i.e., some cooperative interaction. Likewise, a birth rate for A proportional to $x_A x_B^2$ would arise through some interaction between individuals of species B: for example, the cooperative production of some resource by individuals of B that is beneficial to A. The higher-order terms in the death rates serve to stop the population sizes running out of control: they can therefore be interpreted as some kind of resource depletion implied by large populations. Thus although the combination of processes that yields a circular stable manifold is somewhat specific, the biological principles involved (cooperative behaviour and resource depletion) are not entirely unreasonable.

For analysis purposes the useful quantities obtained from the rates are the moments of δx_A and δx_B. From these we will find the rate equations for the mean-field analysis of the deterministic behaviour of the system, and the jump moments of the Fokker-Planck equation (FPE) derived from a Kramers-Moyal expansion of the master equation, as detailed in section 2.7.1. They are given by

$$\langle (\delta x_A)^i (\delta x_B)^j) \rangle = \sum_{X'_A, X'_B} (\delta x_A)^i (\delta x_B)^j T(X'_A, X'_B | X_A, X_B) \tau \tag{5.2}$$

where $X'_{A/B} = X_{A/B} \pm 1$ and $T(X'_A, X'_B | X_A, X_B)\tau$ is the probability that x_A and/or x_B changes by $\pm 1/K$ in an infinitesimal time τ. We write the moments in terms of the extensive variables b and K, and the intensive variables x_A and x_B via the functions $M_{i,j}(x_A, x_B)$:

$$\langle (\delta x_A)^i (\delta x_B)^j) \rangle = \frac{b}{K^{i+j}} M_{i,j} \tau \ . \tag{5.3}$$

We find for the first and second moments:

$$\begin{aligned}
M_{1,0} &= x_A \left(2 - a - (4-a)x_A - 2x_B + 3x_A^2 + x_B^2 + 2x_A x_B - x_A^3 - x_A x_B^2\right) \\
M_{0,1} &= x_B \left(2 - a - (4-a)x_B - 2x_A + 3x_B^2 + x_A^2 + 2x_A x_B - x_B^3 - x_B x_A^2\right) \\
M_{2,0} &= x_A \left(2 + a + (4-a)x_A + 2x_B + 3x_A^2 + x_B^2 + 2x_A x_B + x_A^3 + x_A x_B^2\right) \\
M_{0,2} &= x_B \left(2 + a + (4-a)x_B + 2x_A + 3x_B^2 + x_A^2 + 2x_A x_B + x_B^3 + x_B x_A^2\right) \\
M_{1,1} &= 0 \ .
\end{aligned} \tag{5.4}$$

5.2.1 Mean-Field Analysis

The deterministic behaviour can be found from the rate equations for $\langle x_A \rangle$ and $\langle x_B \rangle$:

$$\begin{aligned} \frac{d\langle x_A \rangle}{dt} &= \lim_{\tau \to 0} \frac{\langle x_A(t+\tau) \rangle - \langle x_A(t) \rangle}{\tau} = M_{1,0} \\ \frac{d\langle x_B \rangle}{dt} &= \lim_{\tau \to 0} \frac{\langle x_B(t+\tau) \rangle - \langle x_B(t) \rangle}{\tau} = M_{0,1} \,, \end{aligned} \tag{5.5}$$

can be computed using (5.4). In the mean-field limit $K \to \infty$ where we neglect fluctuations, $\langle x_A(t) \rangle \equiv x_A(t)$ and we find after some algebra:

$$\begin{aligned} \dot{x}_A &= b x_A (x_A - 1)[a - (x_A - 1)^2 - (x_B - 1)^2 \,] \\ \dot{x}_B &= b x_B (x_B - 1)[a - (x_A - 1)^2 - (x_B - 1)^2 \,] \,. \end{aligned} \tag{5.6}$$

Defining the polar coordinates r and ϕ via

$$\begin{aligned} x'_A &\equiv x_A - 1 = r \cos(\phi) \\ x'_B &\equiv x_B - 1 = r \sin(\phi) \,, \end{aligned} \tag{5.7}$$

we find that the fixed points of (5.6) are

$$(x_A = 0, x_B = 0) \tag{5.8}$$

$$(x_A = 1, x_B = 0) \tag{5.9}$$

$$(x_A = 0, x_B = 1) \tag{5.10}$$

$$(x_A = 1, x_B = 1) \tag{5.11}$$

$$r = r_0 = \sqrt{a} \,. \tag{5.12}$$

To find the nature of these fixed points we must evaluate the linearised stability matrix L,

$$L = b \begin{pmatrix} (2x_A - 1)(a - r^2) - 2x_A(x_A - 1)^2 & 2x_A(x_A - 1)(x_B - 1) \\ 2x_B(x_A - 1)(x_B - 1) & (2x_B - 1)(a - r^2) - 2x_B(x_B - 1)^2 \end{pmatrix}$$

for each in turn. The fixed point (5.8) is an absorbing state at the origin where

both species are extinct. Its linear stability is given by the eigenvalues of

$$L = b \begin{pmatrix} -(a-2) & 0 \\ 0 & -(a-2) \end{pmatrix} \tag{5.13}$$

which we can read off as L is diagonal. We see that for $a < 2$ both eigenvalues are positive and the fixed point will be repulsive. The fixed point (5.11) sits at the centre of the polar coordinate system defined in (5.7). Physically this means that (K, K) is the centre of the circle in the extensive system. It has the diagonal stability matrix

$$L = b \begin{pmatrix} a & 0 \\ 0 & a \end{pmatrix} \tag{5.14}$$

which means it will also be a repulsive fixed point, as desired, for any positive $a > 0$. Two fixed points (5.9) and (5.10) sit on the A and B axis respectively, which are absorbing for the respective species. They have diagonal stability matrices

$$L = b \begin{pmatrix} \pm(a-1) & 0 \\ 0 & \mp(a-1) \end{pmatrix} \tag{5.15}$$

which will make them saddle points if we choose $0 < a < 1$. Finally, we have the fixed point (5.12), which is in fact a continuous circular manifold of fixed points, located at fixed radius r_0 from the centre (5.11). The stability matrix is

$$L = -2b \begin{pmatrix} x_A^*(x_A^*-1)^2 & x_A^*(x_A^*-1)(x_B^*-1) \\ x_B^*(x_A^*-1)(x_B^*-1) & x_B^*(x_B^*-1)^2 \end{pmatrix} \tag{5.16}$$

where (x_A^*, x_B^*) are points which lie on the circular manifold. This matrix has zero determinant, which means using (4.86) that the eigenvalues are $\{0, \mathrm{Tr}\, A\}$. For any permitted population densities, i.e. those that are non-negative, $\mathrm{Tr}\, A < 0$ and so the circular manifold is stable, having a restoring force in the radial direction off the manifold, and no force acting in the ϕ-direction around the manifold, precisely what we set out to obtain.

To summarise, we find that at the level of the deterministic equations, the system evolves to a fixed point on the circular manifold if we have $0 < a < 1$. The fixed point that is reached would be determined by the initial conditions. For finite K however, we expect the system to evolve to the neighbourhood of the manifold,

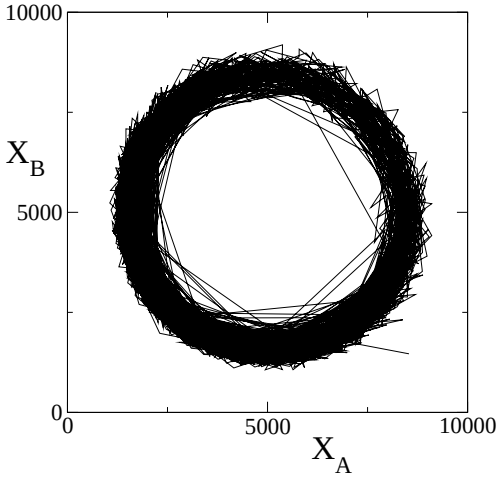

Figure 5.1: Typical dynamical trajectory of the system defined by $X_A(t)$ and $X_B(t)$ and the transition rates given in (5.1). These data were obtained by simulation using the Gillespie algorithm of the master equation with parameters $K = 5000$, $b = K^2$, $a = 0.5$.

and then diffuse about it. A typical snapshot of the evolution of the system is given in figure 5.1: this indeed shows that the occupied region of phase space is a circular annulus of large radius relative to its width.

The CM model as defined by (5.1) is neutral, in the sense that relabelling A to B in the birth rate for A say, gives the birth rate for B. There is no selection bias for one of the species and the rates of birth and death are equivalent. The neutrality is made more explicit by the fact each species has the same locus of fixed points, and deterministically both relax to reside on the circular manifold. This is a natural extension of *quasi-neutral* models of population dynamics from open to closed neutral manifolds. In [110], Parsons and Quince study a model of a non-spatial population with two species, each of which undergo the same birth and death processes. Their model is non-neutral in the sense that the birth and death rate differ for each species. However, when the ratios of these two parameters are the same for both species, deterministically both population densities evolve to reside at a stable linear manifold, made up of a continuum of fixed points. In this sense the model is said to be quasi-neutral.

5.3 Reduction to a One-Dimensional Diffusion

Due to the mean-field behaviour of the CM model, the stochastic dynamics of the system are now restricted to act on a circular annulus, as seen in figure 5.1. In order to analyse the diffusion about it, we now reduce the full dynamics in the two-dimensional space spanned by x_A and x_B to the diffusion of the angular coordinate ϕ in a polar coordinate system defined in (5.7), whose origin is the centre of the circular manifold. A similar approach was used by Parker and Kamenev in studying the stability of a stochastic Lotka-Volterra model [95]. There, as the angular component of the motion relaxes rapidly, it can be integrated out of the probability distribution, allowing the dynamics of the 2D system to be described by the 1D stochastic radial motion between the deterministic limit cycles. In contrast, our main assumption in this study is to neglect diffusion in the radial r direction off the stable circular manifold. That is, we assume that the restoring force that acts perpendicular to the manifold is sufficiently strong that any deviation away from the manifold does not contribute to the dynamics in an important way. In doing so, we are casting the circle as a slow manifold of the stochastic dynamics, a technique also employed in [99, 111, 112]: the fast variable r relaxes quickly to the circle, leaving the dynamics of the slower variable ϕ, which has a zero eigenvalue, to be constrained to lie on the circular manifold.

We note, however, that lateral diffusion off a manifold has been seen to enter into an effective description on an open manifold [110]. Here, our aim is to see how well we can understand the full two-dimensional diffusion within a highly simplified approximation, and in particular any sustained angular velocity due to the presence of a probability current in the steady state, leading to cyclic behaviour.

In a very recent piece of work [99], the authors studied the dynamics of a two-species population which deterministically evolves to reside at a fixed point on a stable hyperbolic manifold. They carried out a similar dimensional reduction to that presented here and found it to be a good approximation of the full 2D dynamics. However a crucial difference is that the hyperbola has natural boundary conditions. As mentioned in section 4.3.1, for a 1D system with natural boundary conditions the current must vanish at the boundaries. Therefore the system cannot support a sustained constant current in the steady state as it must be zero everywhere on the hyperbola.

5.3.1 The Polar Fokker-Planck Equation

In order to study the diffusion in the ϕ direction around the manifold, we wish to derive a polar Fokker-Planck equation (FPE) for the evolution of the probability density $P(\phi, t)$. To do so we terminate the Kramers-Moyal forward expansion

$$\frac{\partial P(\phi,t)}{\partial t} = \sum_{n=1}^{\infty} \frac{(-1)^n}{n!} \left(\frac{\partial}{\partial \phi}\right)^n \alpha_n(\phi) P(\phi,t) \tag{5.17}$$

at the second term, as we detailed in section 2.7.1. This truncation is valid if α_1 and α_2 are the only non-zero jump moments as defined by

$$\alpha_n = \lim_{\tau \to 0} \frac{\langle [\phi(t+\tau) - \phi(t)]^n \rangle}{\tau} \equiv \lim_{\tau \to 0} \frac{\langle (\delta\phi)^n \rangle}{\tau} \ . \tag{5.18}$$

To find an expression for $\delta\phi$ we use the schematic of figure 4.4 to find a relation in terms of of δx_A and δx_B. It is

$$\delta\phi(\delta x'_A, \delta x'_B | x'_A, x'_B) = \tan^{-1}\left(\frac{x'_B + \delta x'_B}{x'_A + \delta x'_A}\right) - \tan^{-1}\left(\frac{x'_B}{x'_A}\right) \ , \tag{5.19}$$

where the first term on the right hand side is the angle defined after an update and the second is the angle before, defined from the origin at the centre of the manifold using the polar coordinates defined by (5.7). Taylor expanding to second order in $\delta x'_A$ and $\delta x'_B$ about $\delta x'_A = \delta x'_B = 0$ and keeping terms up to order δ^2 yields

$$\begin{aligned} \delta\phi = &- \frac{x'_B}{r^2}(\delta x'_A) + \frac{x'_A}{r^2}(\delta x'_B) \\ &+ \frac{x'_A x'_B}{r^4}\left((\delta x'_A)^2 - (\delta x'_B)^2\right) + \frac{(x'_B)^2 - (x'_A)^2}{r^4}(\delta x'_A \delta x'_B) \ . \end{aligned} \tag{5.20}$$

Applying the polar transformation (5.7) and averaging gives

$$\langle \delta\phi \rangle = \frac{b}{K^2}\left[\frac{\sin(2\phi)}{2r_0^2}\Big(M_{2,0} - M_{0,2}\Big)\right]\tau \tag{5.21}$$

$$\langle (\delta\phi)^2 \rangle = \frac{b}{K^2}\left[\frac{\sin^2(\phi) M_{2,0} + \cos^2(\phi) M_{0,2}}{r_0^2}\right]\tau \ , \tag{5.22}$$

where we use the definitions of the moments (5.2) and the fact that deterministically we are at a fixed point so $\langle \delta x_A \rangle = \langle \delta x_B \rangle = 0$. For the higher-order jump moments we can infer from (5.3) and (5.4) that to leading order in K

$$\langle (\delta\phi)^n \rangle \sim bK^{-n} G_n(x_A, x_B)\tau, \quad n \geq 3 \tag{5.23}$$

where G_n are functions of the intensive variables, independent of K. Using (5.18), we have from the above expressions for the moments that

$$\alpha_1, \alpha_2 \sim \lim_{b\to\infty} \frac{b}{K^2} \tag{5.24}$$

$$\alpha_n \sim \lim_{b\to\infty} \frac{b}{K^n}, \quad n \geq 3\,. \tag{5.25}$$

The change in limit is an observation that the rates defined in (5.1) scale with b and so the time τ until an event happens scales like $1/b$. This means that in order to have a non-zero first and second jump moment with higher-order jump moments vanishing we should choose $b = K^2$.

Therefore we have the 1D polar FPE describing the diffusion about the circular manifold

$$\frac{\partial P(\phi,t)}{\partial t} = -\frac{\partial}{\partial\phi}\Big[f(\phi)P\Big] + \frac{1}{2}\frac{\partial^2}{\partial\phi^2}\Big[g^2(\phi)P\Big] \tag{5.26}$$

where the drift term f and the diffusion term g are

$$\begin{aligned} f(\phi) &= \frac{\sin(2\phi)}{2r_0^2}\Big(\langle(\delta x_A)^2\rangle - \langle(\delta x_B)^2\rangle\Big) \\ &= \frac{1}{4r_0^2}\Big(2r_0(12+r_0^2)[\sin(\phi)-\cos(\phi)] + 4r_0(6+r_0^2)[\sin(3\phi)+\cos(3\phi)] \\ &\qquad + 20r_0^2\sin(4\phi) + 2r_0^3[\sin(5\phi)-\cos(5\phi)]\Big)\,, \end{aligned} \tag{5.27}$$

$$\begin{aligned} g^2(\phi) &= \frac{1}{r_0^2}\Big(\sin^2(\phi)\langle(\delta x_A)^2\rangle + \cos^2(\phi)\langle(\delta x_B)^2\rangle\Big) \\ &= \frac{1}{4r_0^2}\Big(64 + 28r_0^2 + r_0(56+6r_0^2)[\sin(\phi)+\cos(\phi)] \\ &\qquad + 4r_0(6+r_0^2)[\sin(3\phi)-\cos(3\phi)] \\ &\qquad + 24r_0^2\sin(2\phi) - 20r_0^2\cos(4\phi) - 4r_0^2[\sin(5\phi)-\cos(5\phi)]\Big)\,. \end{aligned} \tag{5.28}$$

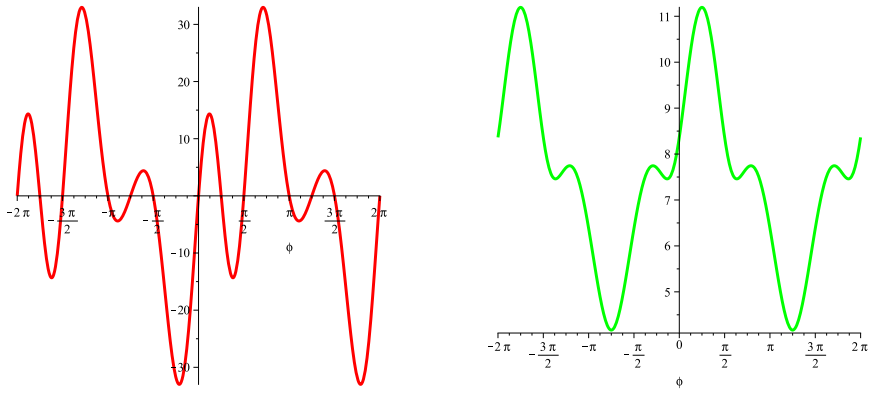

(a) $f(\phi)$ (b) $g(\phi)$

Figure 5.2: The drift term f and the diffusion term g of the Langevin equation (5.29) for $a = 0.5$.

Using the Itô prescription (2.86) we can write the equivalent Langevin equation

$$\dot{\phi} = f(\phi) + g(\phi)\ \eta_\phi \tag{5.29}$$

where η_ϕ is Gaussian white noise with zero mean and unit variance. As one would expect, f and g are 2π-periodic as can be seen in figure (5.2).

5.4 The Steady State

A key feature of the Langevin equation (5.29) is that the noise is multiplicative. The criteria for a non-equilibrium steady state (NESS) with a current to exist in a system with a FPE of the form (5.26) with periodic boundary conditions are more easily checked in the case where the noise is additive. Therefore we will use the transformation defined in section 2.10 which will do just that. The required change of variable is

$$\theta(\phi) = \sqrt{2D} \int_0^\phi \frac{d\phi'}{g(\phi')}\,, \tag{5.30}$$

under which the FPE (5.26) becomes

$$\partial_t Q(\theta, t) = -\partial_\theta \left(F(\theta)Q\right) + D\partial_\theta^2 Q \tag{5.31}$$

describing the time evolution of the probability density $Q(\theta, t)$ where now the diffusion is a constant D and the drift force $F(\theta)$ is

$$F(\theta) = \sqrt{2D}\ \left(\frac{f(\phi)}{g(\phi)} - \frac{1}{2}\partial_\phi g(\phi)\right)\Bigg|_{\phi=\phi(\theta)} . \tag{5.32}$$

The corresponding Langevin equation (à la Itô) is

$$\dot{\theta} = F(\theta) + \sqrt{2D}\ \eta_\theta\ . \tag{5.33}$$

In this transformation one can choose D arbitrarily. For completeness we will proceed with arbitrary D, but in numerical calculations will set it to unity.

Unfortunately, it is difficult to obtain an analytic expression for $F(\theta)$, as one needs to evaluate the integral (5.30) and invert the resulting expression to obtain the function $\phi(\theta)$ that appears in (5.32). It is however possible to determine whether the drift force $F(\theta)$ is conservative, and hence infer whether the system will reach thermal equilibrium, without an explicit expression for this function.

First, we note that $F(\theta)$ is conservative if the work done in one circulation of the manifold vanishes, i.e., if

$$\oint \mathrm{d}\theta\ F(\theta) = 0\ . \tag{5.34}$$

We can write an ansatz for F:

$$F(\theta) = \omega - \partial_\theta V(\theta)\,, \tag{5.35}$$

where the first term ω is a constant, non-equilibrium driving force and the second term is a conservative force derived from a potential $V(\theta)$. To determine whether $\omega = 0$, formally, we should be able to write $F(\theta)$ as a Fourier series

$$F(\theta) = \frac{1}{2}a_0 + \sum_{n=1}^{\infty}\left[a_n \cos\left(\frac{n\theta}{T}\right) + b_n \sin\left(\frac{n\theta}{T}\right)\right] \tag{5.36}$$

where, using (5.30),

$$T = \frac{\sqrt{2D}}{2}\int_{-\pi}^{\pi}\frac{\mathrm{d}\phi}{g(\phi)} \tag{5.37}$$

is the half-width of the transformed interval $[-\pi, \pi]$, viz, $T = \theta(\pi) - \theta(0)$. (We

can take $\theta(0) = 0$ with no loss of generality). The coefficients are given in the usual way as

$$a_n = \frac{1}{T}\int_{-T}^{T} \mathrm{d}\theta\, F(\theta) \cos\left(\frac{n\theta}{T}\right) \tag{5.38}$$

$$b_n = \frac{1}{T}\int_{-T}^{T} \mathrm{d}\theta\, F(\theta) \sin\left(\frac{n\theta}{T}\right) . \tag{5.39}$$

Comparing (5.35) and (5.36) we see that $\omega = a_0/2$. So the question of whether $F(\theta)$ is conservative and hence whether the system is reaches thermal equilibrium is equivalent to finding if a_0 is zero.

Taking

$$a_0 = \frac{1}{T}\int_{-T}^{T} \mathrm{d}\theta\, F(\theta) \tag{5.40}$$

we apply the change of variable (5.30):

$$a_0 = \frac{1}{T}\int_{\phi(-T)}^{\phi(T)} \mathrm{d}\phi\, F(\theta[\phi]) \frac{\mathrm{d}\theta}{\mathrm{d}\phi} . \tag{5.41}$$

By definition $\phi(\pm T) = \pm\pi$, $F(\theta[\phi])$ can be obtained directly by (2.96), formally via $\phi(\theta[\phi]) = \phi$, and we know the Jacobian of the transformation. So,

$$a_0 = \frac{\sqrt{2D}}{T}\int_{-\pi}^{\pi} \mathrm{d}\phi \left(\frac{f(\phi)}{g(\phi)^2} - \frac{\mathrm{d}}{\mathrm{d}\phi}\ln g(\phi)\right) \tag{5.42}$$

$$= \frac{\sqrt{2D}}{T}\int_{-\pi}^{\pi} \mathrm{d}\phi\, \frac{f(\phi)}{g(\phi)^2} , \tag{5.43}$$

since the second term vanishes due to the periodicity of $g(\phi)$.

Although we have successfully side-stepped the problem of evaluating $\phi(\theta)$, it remains the case that the integral (5.43) does not have a convenient closed form. However we can determine whether it is zero by finding if the integrand

$$h(\phi) = \frac{f(\phi)}{g^2(\phi)} \tag{5.44}$$

is odd over the limits of integration. In figure 5.2 we see that f is odd and g is

even about $\phi = \pi/4$. This implies that h is also odd about $\pi/4$, namely:

$$h(\phi) = -h\left(\frac{\pi}{2} - \phi\right) . \tag{5.45}$$

Due to the 2π-periodicity of h we can write (5.43) as

$$a_0 = \int_{-\pi}^{\pi} \mathrm{d}\phi \; h(\phi) = \int_{-\frac{3\pi}{4}}^{\frac{5\pi}{4}} \mathrm{d}\phi \; h(\phi) = \int_{\frac{\pi}{4}}^{\frac{5\pi}{4}} \mathrm{d}\phi \; h(\phi) + \int_{-\frac{3\pi}{4}}^{\frac{\pi}{4}} \mathrm{d}\phi \; h(\phi) . \tag{5.46}$$

Changing variable to $\beta = \pi/2 - \phi$ in the second integral we have

$$a_0 = \int_{\frac{\pi}{4}}^{\frac{5\pi}{4}} \mathrm{d}\phi \; h(\phi) + \int_{\frac{\pi}{4}}^{\frac{5\pi}{4}} \mathrm{d}\beta \; h\big(\frac{\pi}{2} - \beta\big) . \tag{5.47}$$

Now applying (5.45) we see that $a_0 = 0$.

Intuitively it seems correct that the system reaches thermal equilibrium as the model defined by the processes in (5.1) is neutral and each species undergoes the same processes at equivalent rates.

5.4.1 Breaking Detailed Balance

The insight that is gained from this analysis is that we now know in order to reach a NESS, we must introduce processes which will enter the drift term f and the diffusion g in such a way as to make the integrand in (5.43) not be odd. In order to adhere to our central study of the effects that noise can have in the dynamics and fate of non-equilibrium systems, we wish to do this in such a way so that the deterministic contribution is unaffected. Therefore whatever change to the model's dynamics (5.1) we make, we wish the drift term f to be unaffected. To this end we introduce the following extra rates to the CM model:

$$\begin{aligned}
T(X_A + 1, X_B | X_A, X_B) &= b(p_1 x_A x_B^3 + p_2 x_a^3 x_B) \\
T(X_A, X_B + 1 | X_A, X_B) &= b(p_1 x_A x_B^3 + p_2 x_a^3 x_B) \\
T(X_A - 1, X_B | X_A, X_B) &= b(p_1 x_A x_B^3 + p_2 x_a^3 x_B) \\
T(X_A, X_B - 1 | X_A, X_B) &= b(p_1 x_A x_B^3 + p_2 x_a^3 x_B) .
\end{aligned} \tag{5.48}$$

These new rates cancel in the first moments $\langle \delta x_A \rangle$ and $\langle \delta x_B \rangle$ and so leave the deterministic equations (5.5) unaltered. The second moments accrue the extra terms

$$\langle (\delta x_A)^2 \rangle = \frac{b}{N_0^2} \Big[2p_1 x_A x_B^3 + 2p_2 x_A^3 x_B \Big] \tau \tag{5.49}$$

$$\langle (\delta x_B)^2 \rangle = \frac{b}{N_0^2} \Big[2p_1 x_A x_B^3 + 2p_2 x_A^3 x_B \Big] \tau \ . \tag{5.50}$$

Substituting these into (5.27) leaves f as it was. However the form of g will change. The two new parameters p_1 and p_2 will determine the magnitude and direction of the probability current. The new terms that appear in our expression for g (5.28) are

$$2p_1 \sin^2(\phi)(1 + r\cos(\phi))(1 + r\sin(\phi))^3 + 2p_2 \cos^2(\phi)(1 + r\sin(\phi))(1 + r\cos(\phi))^3 \ .$$

From this we see that g will only remain even about $\pi/4$ as long as $p_1 = p_2$. Therefore as long as $p_1 \neq p_2$ a probability current will flow in the steady state. This condition breaks the neutral selection of the model as the rates of birth and death for each species are no longer exactly equivalent. However *quasi-neutrality* is maintained in the sense that the deterministic behaviour of both species is the same [110, 113], each evolving to reside on the common circular manifold.

5.5 Measuring the Current

Having now established a mechanism in the multiplicative noise of the CM model for inducing a probability current to flow in the steady state, we now look to establish its existence. We present three different approaches to measuring the current. We follow the same principle for the SFP model of chapter 4 in expressing the current as

$$J(\phi, t) = P(\phi, t)\omega \tag{5.51}$$

where P is the probability density and ω is the average angular velocity, and we infer the flow of a current from a non-zero ω.

The first method is the same as that used in section 4.5.2, which uses Monte Carlo simulation of the dynamics for the full problem. The second

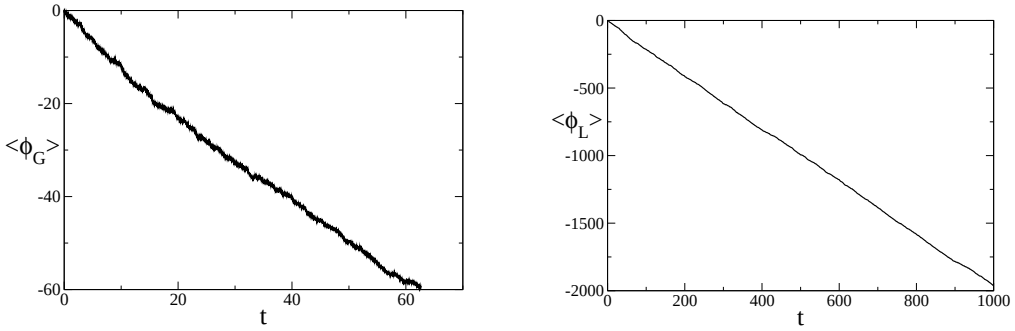

(a) Simulation (b) Numerical Integration

Figure 5.3: Plot of the time evolution of the average aggregate angle obtained from: (a) simulation of the 2D stochastic model using the Gillespie algorithm; (b) numerical integration of the 1D polar Langevin equation. For each, the parameters are $K = 5000$, $b = K^2$, $a = 0.5$, $p_1 = 20$ and $p_2 = 0$, and the average is taken over 100 runs.

is to numerically integrate the Langevin equation within the one-dimensional reduction. This will also provide an assessment of the validity of the 1D reduction approximation, and thereby revealing any error that is introduced in this procedure. The third method is to appeal to Kramers' escape-rate theory to estimate the current. Our expectation is these methods trade accuracy for precision and (in the latter case) analytical insight.

5.5.1 Monte Carlo Simulation

Using the Gillespie algorithm the stochastic model as defined by the rates in (5.1) and (5.48) can be simulated. We measure the total angular displacement $\phi_G(t)$ which is positive in the anti-clockwise direction and quantifies the total distance travelled, as previously described in section 4.5.2. For each update

$$\phi_G(t+\tau) = \phi_G + \delta\phi \tag{5.52}$$

where $\delta\phi$ is calculated using (5.19). In figure 5.3(a) we plot the angular displacement and find that

$$\langle \phi_G(t) \rangle \sim \omega_G \, t \; . \tag{5.53}$$

For the parameters quoted, linear regression of the data yields $\omega_G = -0.97$.

5.5.2 Numerical Integration of the Langevin Equation

The average velocity can also be calculated from direct numerical integration of the quasi-1D Langevin equation (5.29). We do so using the integration scheme [54]

$$\phi_L(t+dt) = \phi_L(t) + f(\phi_L)dt + g(\phi_L)\sqrt{dt}\ \eta_\phi\ . \tag{5.54}$$

For the same set of parameter values of previously, we find an ensemble-averaged angular displacement shown in figure 5.3(b). This time we find that $\omega_L = -1.27$, in reasonable agreement with the simulations of the full 2D diffusion. (See below for a more detailed discussion of the different methods for estimating the current.)

5.5.3 Kramers' Escape-Rate Theory

Our final approach makes use of the transformation of the diffusion with multiplicative noise to a diffusion with additive noise described in Section 5.3. This allows us to estimate the non-equilibrium current via calculations of escape rates over potential barriers as done by Kramers [114], following closely the presentation of the method in [54].

The potential $\Phi(\theta)$ that we are required to calculate is

$$\Phi(\theta) = -\int^{\theta} d\theta' F(\theta')\ . \tag{5.55}$$

From earlier discussion, one would expect $\Phi(\theta)$ to only be a true potential if $F(\theta)$ is conservative. However, using the ansatz (5.35) in (5.55) we have

$$\Phi(\theta) = -\omega_\theta \theta + V(\theta) \tag{5.56}$$

up to an irrelevant constant. We know $V(\theta)$ is periodic as it can be expressed as a Fourier series (5.36). Therefore in the domain of θ, V will be monotonically shifted by $\omega\theta$, which we interpret as our potential $\Phi(\theta)$.

Given the form of f and g derived for this model it is not possible to perform the transformation from ϕ to θ in (5.30), or compute the integral in (5.55) to obtain Φ. By approximating the function g with a mathematically tractable function we are able to make some progress in analytically approximating these required expressions.

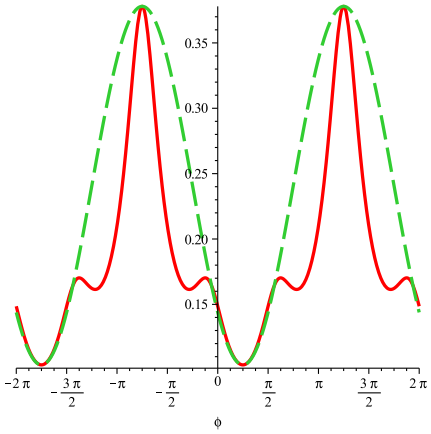

Figure 5.4: The inverted diffusion term $1/g$ (red, solid) and its approximation G (green, dashed).

Approximating $\theta(\phi)$ and $\Phi(\theta)$

Here we present the technical details of our approximations for the variable transformation and the potential. We are faced with the task of computing

$$\Phi(\theta) = -\int^{\theta} \mathrm{d}\theta' \; F(\theta') \tag{5.57}$$

$$= -\sqrt{2D}\int^{\theta} \mathrm{d}\theta' \; \left(\frac{f(\phi)}{g(\phi)} - \frac{1}{2}\partial_\phi g(\phi)\right)\Big|_{\phi=\phi(\theta')} . \tag{5.58}$$

Applying the same change of variable as in (5.41), (5.42) we have

$$\Phi(\theta) = -\sqrt{2D}\int^{\phi(\theta)} \mathrm{d}\phi \; \left(\frac{f(\phi)}{g^2(\phi)} - \frac{1}{2}\frac{\partial_\phi g(\phi)}{g(\phi)}\right) . \tag{5.59}$$

The form of $g(\phi)$ as it is given in (5.28) makes the above integral intractable. We therefore make the approximation $G(\phi) \approx G_g(\phi) = 1/g(\phi)$ where G has the form

$$G(\phi) = c_G + A_G \cos(\phi - b_G) . \tag{5.60}$$

The phase b_G is set to by matching numerically the position of the first extremum of G_g and G for $\phi > 0$. The other two parameters are set by making the maximum and minimum values of G_g and G the same. We illustrate this approximation for a typical g in figure 5.4. Applying the approximation $G(\phi) \approx 1/g(\phi)$ our

expression (5.59) becomes

$$\Phi_\theta(\theta) = -\sqrt{2D}\int^{\phi(\theta)} \mathrm{d}\phi \ \left(f(\phi)G(\phi)^2 + \frac{1}{2}\frac{\partial_\phi G(\phi)}{G(\phi)} \right) . \tag{5.61}$$

It is possible to numerically integrate this integral by computer, in our case using Maple(TM). However, to evaluate it in the θ coordinate we must have an analytical form of $\phi(\theta)$ to substitute into it.

The transformation from θ to ϕ in (5.30) does not have a closed form for the exact $g(\phi)$ derived for this model so we approximate it by

$$\theta(\phi) \approx \theta_G(\phi) = \sqrt{2D}\int_0^\phi d\phi' G(\phi') \tag{5.62}$$

which using (5.60) gives

$$\theta_G(\phi) = \sqrt{2D}(c_G\phi - A_G\sin(\phi - b_G) - A_G\sin(b_G)) . \tag{5.63}$$

This functional relation is shown in figure B5.5(a). What we really require is the inverted form of this relation, giving us ϕ in terms of θ. The inversion is not possible, however we can approximate it via

$$\theta_t = \sqrt{2D}\int_0^\phi \frac{\mathrm{d}\phi}{c_t + A_t\cos(\phi)} . \tag{5.64}$$

This integral has the solution

$$\theta_t(\phi) = \frac{2\sqrt{2D}}{c_t\sqrt{1-a_t}}\tan^{-1}\left(\frac{1-a_t}{\sqrt{1-a_t^2}}\tan\left(\frac{\phi}{2}\right)\right) \tag{5.65}$$

where $c_t = A_t/c_t$. We need to approximate the values c_t and a_t to give a good fit with the form of $\theta(\phi)$ from (5.63).

We do this by matching the linear gradient and the curvature near $\phi = 0$ of $\theta_G(\phi)$ and $\theta_t(\phi)$. The slope we match by finding the straight line gradient between two points that lie on $\theta_t(\phi)$ and making it equal to slope of the constant term in (5.63). Choosing the two points $\phi = -\pi$ and $\phi = \pi$ we have from (5.65) that

$$\theta_t(\pm\pi) = \pm\frac{\sqrt{2D}\ \pi}{c_t\sqrt{1-a_t^2}} . \tag{5.66}$$

Matching the gradients:

$$\frac{\theta_t(\pi) - \theta_t(-\pi)}{2\pi} = \sqrt{2D}\ c_G \tag{5.67}$$

yields

$$c_G = \frac{1}{c_t\sqrt{1-a_t^2}}\ . \tag{5.68}$$

To match the curvature near the origin we rearrange (5.65) to

$$\tan\left(\frac{c_t\sqrt{1-a_t^2}}{\sqrt{2D}}\ \frac{\theta_t}{2}\right) = \frac{1-a_t}{\sqrt{1-a_t^2}}\tan\left(\frac{\phi}{2}\right)\ . \tag{5.69}$$

Substituting θ_G for θ_t using (5.63) gives

$$\begin{aligned}&\tan\left(\frac{c_t\sqrt{1-a_t^2}}{\sqrt{2D}}\ \frac{\theta_G}{2}\right) = \\ &\tan\left(\frac{c_t\sqrt{1-a_t^2}}{2\sqrt{2D}}\ \left[\sqrt{2D}(c_G\phi - A_G\sin(\phi - b_G) - A_G\sin(b_G))\right]\right)\ .\end{aligned} \tag{5.70}$$

Now setting the above two expressions equal and Taylor expanding about $\phi = 0$ we have

$$\frac{1-a_t}{\sqrt{1-a_t^2}}\ \frac{\phi}{2} = \frac{c_t\sqrt{1-a_t^2}}{2}\Big(c_G - A_G\cos(b_G)\Big)\phi \tag{5.71}$$

which upon matching coefficients gives

$$\frac{1}{c_t(1+a_t)} = c_G - A_G\cos(b_G)\ . \tag{5.72}$$

We can solve (5.68) and (5.72) simultaneously to find c_t and a_t for the approximate transformation (5.65). A comparison of the two approximate transformations are given in figure B5.5(b). We can invert (5.65) and find the functional form we require:

$$\phi(\theta) = 2\frac{\sqrt{1-a_t^2}}{1-a_t}\tan^{-1}\left(\frac{c_t\sqrt{1-a_t^2}}{\sqrt{2D}}\frac{\theta}{2}\right)\ . \tag{5.73}$$

Finally, we need to find the limits of the domain in the θ variable. Substituting

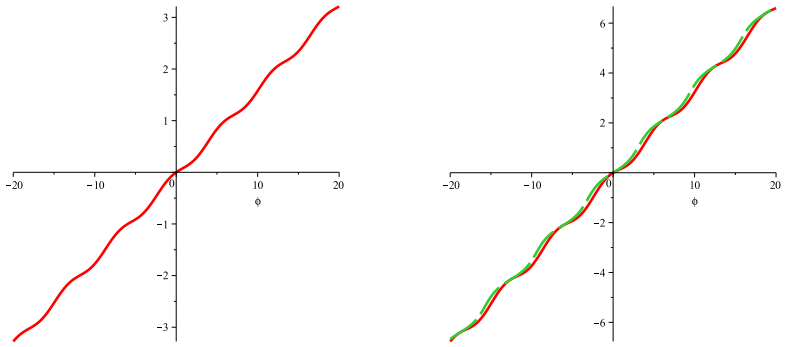

(a) $\theta_G(\phi)$ (b) $\theta_G(\phi)$ and $\theta_t(\phi)$

Figure 5.5: Comparison of the two approximations of the transformation $\theta_G(\phi)$ (red, solid) and $\theta_t(\phi)$ (green, dashed).

the ϕ limits $\pm\pi$ into (5.65) we find $\theta \in [-\theta_0, \theta_0]$, with

$$\theta_0 = \frac{\sqrt{2D}}{c_t\sqrt{1-a_t^2}} \,. \tag{5.74}$$

The Static Potential

In figure 5.6 are typical examples of $\Phi(\theta)$ according to different values of the non-equilibrium parameters p_1 and p_2. The thermal equilibrium condition $p_1 = p_2$ is shown in figure 5.6(a). In this case there is no current flowing and the potential $\Phi(\theta)$ is periodic. However in the non-equilibrium cases shown in figures 5.6(b) and 5.6(c) we see that $\Phi(\theta)$ is not periodic. Though as the domain of of the potential is only $\theta \in [-\theta_0, \theta_0]$, as defined in (5.74), it is only important that the upper and lower limits of the domain are the same to satisfy the periodic boundary conditions of the system. The absolute value of a potential is not important for deriving the force for it, so we do not require $\Phi(\theta)$ to be periodic to regard it as being a potential.

The Escape Rate

Each of the potentials in figure 5.6 are characterised by having a minimum between two barriers. We can derive the escape rate of a particle over these barriers; here we will do so for the right side barrier of the potential displayed in figure 5.6(c). We denote the position of the minimum in the well by θ_W, the top

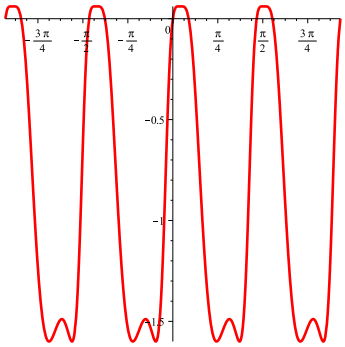

(a) $p_1 = 0,\ p_2 = 0$

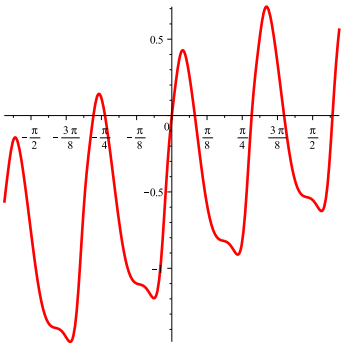

(b) $p_1 = 20,\ p_2 = 0$

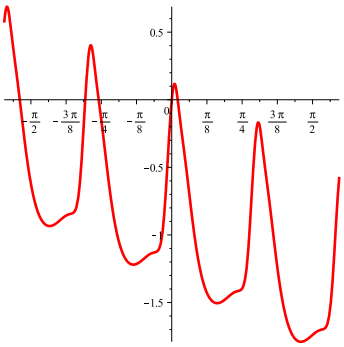

(c) $p_2 = 0,\ p_2 = 20$

Figure 5.6: $\Phi(\theta)$ for different values of the current parameters p_1, p_2 with $a = 0.5$.

of the barrier by θ_B and the next minimum to the right of the barrier by A. For the FPE (2.95) in a non-equilibrium steady state the probability current

$$J = -\partial_\theta \Phi_\theta(\theta) Q_S(\theta) - D\partial_\theta Q_S(\theta) \tag{5.75}$$

can be written as

$$J = -De^{-\Phi_\theta/D} \frac{\partial}{\partial\theta}\left[e^{\Phi_\theta/D} Q_S\right] . \tag{5.76}$$

Integrating between θ_W and A we have

$$J\int_{\theta_W}^{A} \mathrm{d}\theta\ e^{\Phi_\theta/D} = D\left[e^{\Phi_\theta(\theta_W)/D} Q_S(\theta_W) - e^{\Phi_\theta(A)/D} Q_S(A)\right] . \tag{5.77}$$

If the barrier height $\Delta\Phi = \Phi(\theta_B) - \Phi(\theta_W)$ is much greater than the diffusion D then the particle is far more likely to be found in the well about θ_W. This means

we neglect the second term in the square brackets in (5.77), giving

$$J = \frac{D\ Q_S(\theta_W)\ \mathrm{e}^{\Phi(\theta_W)/D}}{\int_{\theta_W}^{A} \mathrm{d}\theta\ e^{\Phi_\theta/D}}\ . \tag{5.78}$$

The current can be expressed as the probability p of being in the well at θ_W multiplied by the escape rate r from the well. Taking $\theta_1 < \theta_W < \theta_2$ to define the domain of the well we write

$$p = \int_{\theta_1}^{\theta_2} \mathrm{d}\theta\ Q_S(\theta)\ . \tag{5.79}$$

From (5.76) the stationary distribution is

$$Q_S(\theta) = Ne^{-\Phi(\theta)/D} - Je^{-\Phi(\theta)/D} \int^{\theta} \mathrm{d}\theta'\ \frac{e^{\Phi(\theta')/D}}{D}\ . \tag{5.80}$$

As we are interested in the stationary distribution in the well we introduce $Q_S(\theta_W)$ by eliminating the normalisation constant N:

$$Q_S(\theta) = Q_S(\theta_W)e^{-[\Phi(\theta)-\Phi(\theta_W)]/D} - \frac{Je^{-\Phi(\theta)/D}}{D}\left[\int^{\theta} \mathrm{d}\theta'\ e^{\Phi(\theta')/D} - \int^{\theta_W} \mathrm{d}\theta'\ e^{\Phi(\theta')/D}\right] \tag{5.81}$$

Using this we can now write

$$p = Q_S(\theta_W)e^{\Phi(\theta_W)/D} \int_{\theta_1}^{\theta_2} \mathrm{d}\theta\ e^{-\Phi(\theta_W)/D} \tag{5.82}$$

where the contribution from the square bracket terms in (5.81) is negligible when considering the contribution from the domain of the well. Combining this with (5.78) we can express the escape rate as

$$\frac{1}{r} = \frac{p}{J} = \frac{1}{D} \int_{\theta_1}^{\theta_2} \mathrm{d}\theta\ e^{-\Phi(\theta)/D} \int_{\theta_W}^{A} \mathrm{d}\theta\ e^{\Phi(\theta)/D}\ . \tag{5.83}$$

We Taylor expand each integrand in the above expression, the first about θ_W,

the second about θ_B:

$$\Phi(\theta) \approx \Phi(\theta_W) + \frac{\Phi''(\theta_W)}{2}(\theta - \theta_W)^2 \tag{5.84}$$

$$\Phi(\theta) \approx \Phi(\theta_B) - \frac{|\Phi''(\theta_B)|}{2}(\theta - \theta_B)^2 \ . \tag{5.85}$$

Using these second order expansions, we can extend the boundaries of each integral to $\pm\infty$, meaning that to both integrals in (5.83) are now Gaussian. Computing them leads to the final expression for the escape rate

$$r \approx \frac{1}{2\pi}\sqrt{\Phi''(\theta_W)|\Phi''(\theta_B)|}\ e^{-\Delta\Phi/D} \ . \tag{5.86}$$

To find the value of these escape rates, we numerically compute the value of the second derivatives at the minima and maxima after explicitly constructing the potential $\Phi(\theta)$ using the mathematical software Maple (TM).

Denoting by r^- and r^+ the escape rate for the left and right barrier respectively, we express the average change in θ due to hopping over the right or left barrier in a time τ as

$$\langle \delta\theta \rangle = (r^+\Delta_\theta - r^-\Delta_\theta)\tau \tag{5.87}$$

where $\Delta_\theta = 2\theta_0$ is the distance between wells, i.e. the period of the system. In the limit $\tau \to 0$ this gives the average angular velocity

$$\omega_K = \Delta_\theta(r^+ - r^-) \ . \tag{5.88}$$

It is clear from (5.86) that a current exists due to the difference in the height of the two barriers. When the system is in thermal equilibrium as in figure 5.6(a) there is no current as we are equally likely to hop left or right around one circuit. With the parameter set used before, and setting $D = 1$, we find $\omega_K = -0.83$. Again, this value is in reasonable agreement with those previously obtained by other means.

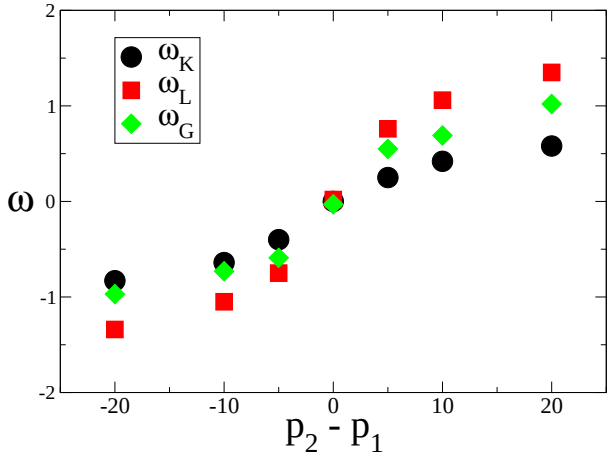

Figure 5.7: Overlay of the different measurements of ω using the three distinct methods of section 5.5 plotted against a relative measure of the non-equilibrium current $p_2 - p_1$. For each data point either p_1 or p_2 is zero.

5.5.4 Comparison of the Three Measurements

To better understand how well the currents obtained via these different approaches correspond with each other, we compare in Figure 5.7 these measures for different values of the p parameter which controls the extent to which detailed balance is violated. We see that all three measurements obey the same qualitative trend, and remain within an order of magnitude of each other.

This validates our principal approximation to reduce the full two-dimensional system to one dimension, that of the polar angle ϕ, by neglecting radial diffusion. In particular, we note that the 1D criterion for a non-equilibrium steady state $p_1 = p_2$ is borne out by simulations of the full 2D dynamics. The difference in the dynamic measurements, ω_L is larger than ω_G, is understandable as while we neglect any radial diffusion in the 1D treatment, it is still present in the simulations, as witnessed in figure 5.1. We expect time spent diffusing radially to slow the rate of polar diffusion.

The main assumption of the Kramers escape rate calculation is that the ratio of the barrier size $\Delta\Phi$ to the diffusion constant D is very large. In practice, we set $D = 1$, and it is not possible to tune the model to allow us to independently control the barrier height and the diffusion strength. Typically, we find that the ratio is $2 < \Delta\Phi/D < 3$, which is a likely cause of the quantitative discrepancy between this method of obtaining ω with the other two.

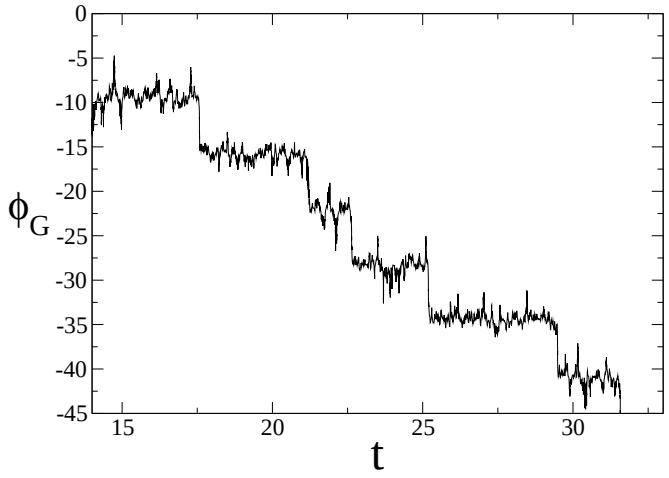

Figure 5.8: A single realisation of ϕ_G obtained by simulation of the stochastic dynamics with parameters: $K = 5000$, $b = K^2$, $a = 0.5$, $p_1 = 20$, $p_2 = 0$.

5.6 Discussion and Conclusion

In the work presented here we have observed cycling behaviour in a multi-dimensional population dynamical model which is driven by the presence of a probability current in the steady state. We have demonstrated that this current is a feature induced purely through the form of the demographic noise inherent in the finite population. The cyclicity is facilitated by the deterministic dynamics being neutral on some closed manifold in configuration space. Then, by dethermalising the multiplicative noise, a probability current can be induced to flow around the manifold, resulting in a sustain non-zero angular velocity which gives rise to global quasicycles in the 2D phase space of the system. Although, the specific interactions that yield such a structure are somewhat contrived from a purely biological viewpoint, here we have used them to highlight some interesting features of stochastic dynamical systems from the perspective of non-equilibrium statistical mechanics.

Most notably, the stochastic trajectories along the manifold are somewhat complex, as figure 5.8 shows. We see that the system tends to diffuse over a small region of the phase space before sharply jumping a distance of approximately 2π radians, i.e. a full circuit of the manifold. The origin of this motion can be understood from the potential picture after mapping to additive (thermal) noise as described in section 5.3. After transforming the multiplicative noise,

the deterministic equations acquire additional terms that can be interpreted as a constant driving force acting in a periodic potential with multiple maxima and minima on the manifold. The dynamics will reside for some time in a potential minimum before escaping over one of the barriers to a neighbouring minimum. Since the potential is periodic, one eventually returns to the same minimum (hence the 2π jump). The driving force leads to an asymmetry in the barrier heights, which in turn yields a systematic current in one direction around the circle (i.e., a 'cycle', albeit not a strictly periodic one). We note that such step motion on a closed manifold we demonstrate in figure 5.8 is a more generic feature found in stochastic systems which permit mean-field limit cycles [115, 116].

This analysis leads us to believe that in general the closed manifold does not have to be neutrally stable in order to observe this cycling behaviour, as long as the manifold itself is attractive from the outside. In such an instance, the non-zero angular velocity generated by the probability current would still drive the system over potential barriers, but now they barriers are due to the deterministic forces acting on the manifold. While the timescale for passing over a barrier would increase markedly, quasicycles would still be generically observable in a system with athermal noise whose deterministic dynamics evolve to a closed manifold.

The observation of quasicycles due to a noise-induced non-conservative driving force highlights the importance of the form of the demographic noise that is manifest in these stochastic population models. In the polar Langevin equation (5.29) the non-equilibrium processes given in (5.48) only appear in the diffusion term g. Therefore if one naively assumed the noise to be thermal, i.e. g is constant, integrating up the drift force f would yield a periodic potential similar to the one displayed in figure 5.6(a), and one would conclude no current is flowing. We see that stochastic effects alone are responsible for a current to flow in the system, keeping the system out of equilibrium.

In the context of modelling population dynamical systems more generally, our findings further showcase the advantages of taking an IBM approach to modelling finite population dynamics. The deterministic and stochastic contributions to the dynamics can be derived from the defined stochastic processes of the model, so one can analytically understand and also control the effects of noise. We have found that finite-size populations in which the dynamics are non-neutral, never relax fully to equilibrium, but instead inhabit a steady state where their is a thermal

bias in the fluctuations due to the presence of a non-equilibrium probability current.

In this work we resorted to a number of approximations to compute the steady-state current in the dynamical system. The first of these was a reduction to a single-coordinate description by disregarding one of the degrees of freedom in the system. Sophisticated methods have been applied to integrate out this degree of freedom in the context of quasi-neutral diffusion along an open interval [110] (as opposed to one that is closed/periodic, as here). It would be of interest to see if similar methods can be applied to determine what is lost in such a dimensional reduction, as this may be of utility in understanding high-dimensional stochastic dynamical systems more generally. Moreover, we made various approximations in order to apply Kramers' escape rate theory to diffusion on the manifold: it may be that more direct approaches to estimating the current in such systems can be found. Finally, and more generally, it would be interesting to establish if there are other ways that a non-equilibrium current may enter into the macroscopic dynamics of a stochastic population dynamical system in ways that are not immediately evident from their deterministic counterparts.

Chapter 6

Synchronisation in a Metapopulation

In this chapter we return to the study of spatially extended systems as in chapter 3, analysing a model which consists of a multi-patch network of populations coupled through migration. We examine the onset of synchronisation between the patches, whose local dynamics are that of the circular manifold (CM) model of chapter 5. We derive a governing set of Langevin equations to describe the quasicycles at each patch. Analytically, we perform a quantitative study of the relationship between the synchronisation of the patches and the coupling migration rate q by conducting a stability analysis of the global coherent state, where all the patches are fully synchronised. We compare this to two empirical methods for measuring the synchronisation of the system from Monte Carlo simulations of the stochastic dynamics, finding good qualitative agreement over the domain of q for which the system crosses over from being unsynchronised to fully coherent.

6.1 Introduction

In the previous chapter we studied the circular manifold (CM) model of a non-spatial, single patch population with two competing species A and B. We observed cycling behaviour in the species densities due to two mechanisms of the defining dynamics given by the birth and death processes. Firstly, the deterministic dynamics constrain the population to reside on a circular annulus in the two-dimensional (2D) phase space, with a radius greater than its width, as witnessed in figure 5.1. Then, the stochastic dynamics of the fluctuations can be controlled to dethermalise the demographic noise, inducing a steady-state probability current to flow. This in turn leads to a non-zero angular velocity which gives a biased diffusion about the manifold, resulting in quasicycles.

The analysis of the CM model was founded on a dimensional reduction, describing the dynamics about the manifold through the polar coordinate ϕ. An obvious, interesting extension to the CM model, is to consider a metapopulation comprising several such single patch systems, which are coupled through the migration of each species between different patches. Intuitively, we would expect to see some level of synchronisation in the phase of each patch given by its angular position ϕ_i on the circular manifold.

In general, spatially extended models have become a major area of study in population biology in the past two decades [56], leading to the unveiling of a variety of observed macroscopic behaviour in the persistence of cycles [52, 53], and, more fundamentally, in the long term extinction or survival of a population [51]. In studying cycling behaviour in spatially extended finite population dynamical models, there is a complex interplay between three factors: (i) the diffusion due to migration of the species between patches [117]; (ii) the intrinsic, demographic noise due to the stochasticity of the finite local patch populations [92], and (iii) the synchronisation between local cycles of the patch populations [53].

For example, Abta *et al* found in a multi-patch stochastic predator-prey model, by tuning of the migration and noise strength parameters, a regime where sustained cycles are permitted at each patch of the system [52]. However, in order to explain this behaviour from a paradigmatic toy model, they argue that a missing mechanism is desynchronisation between the cyclic frequencies of each patch. Schematically, this is facilitated by the orbiting frequencies being phase

space dependent, allowing the noise to desynchronise the patches. The migration then counteracts this by decreasing the concentration gradient between the two patch velocities, restoring each to an invariant manifold in phase space, away from the absorbing states.

The complex interactions of these different processes highlights the fact that if one wishes to consider the role synchronisation can play in stochastic metapopulations, it is also necessary to measure and quantify it, as the relative strength of each of the three factors can prove to be key in determining the macroscopic dynamical behaviour. In a recent study of the effects of demographic noise in a metapopulation of predator-prey patches, Lai *et al* derived a measurement of the synchronisation in the system through the probability distribution of pairwise phase differences [50].

In this chapter we conduct a quantitative study of synchronisation in the spatially extended CM model due to the coupling from migration. We begin by deriving the coupled Langevin equations governing the system's dynamics. This is followed by a brief review of the Kuramoto model, a well studied model for synchronisation whose conceptual framework we adopt to describe our system. We then proceed to measure the synchronisation through a stability analysis of the global coherent state, where each patch population has the same phase (angular position) on the common circular manifold. Finally, we develop two empirical methods for measuring the synchronisation from Monte Carlo simulations of the stochastic dynamics of the multi-patch CM model, which we compare with that obtained from our linear stability treatment.

Naively one might assume that in the limit of fast migration the metapopulation behaves as an effective single patch population which exhibits the same macroscopic behaviour with a global dynamics analogous to the single patch dynamics. Recently, Khasin *et al* showed that even for the simplest case of a single species dynamics on a network of patches, if the carrying capacities of each patch are different, then only if the rates of the birth and death dynamics obey a certain scaling form will this be the case [118]. With this in mind, in order to study as cleanly as possible the relation between migration and synchronisation we extend the CM model in the simplest fashion possible, taking the migration rates to be symmetric between each pair of patches, assigning each patch the same carrying capacity and the same CM model local dynamics and parameters.

6.2 The Multi-Patch CM Model

We begin by spatially extending the CM model of section 5.2. To do so, our model system becomes a network, or lattice. At each site is a non-spatial patch with the same carrying capacity K, with a population comprising two species which undergo the same birth and death processes defined by the transition rates (5.1). The spatial component now enters by the process of migration, which allows constituents of both species to move between different patches. The allowed migrations are governed by the topology of the lattice. In this work we will use the simplest case of a fully connected lattice, meaning that both species at a site i can move to reside at any other site j.

6.2.1 Migration Transition Rates

The probability density P now describes the probability that at a given time t the system is in a state defined by the patch population densities $x_i = n_i/K$ and $y_i = m_i/K$:

$$P(x_1, y_1, x_2, y_2, \ldots, x_L, y_L) \equiv P(\mathbf{x}, \mathbf{y}) \,. \tag{6.1}$$

To keep things manageable we write transition rates in such a way as to only indicate which components of the system have changed. So for example, the transition rate for the birth of an A at site i given the system is in a state $(\mathbf{n}, \mathbf{m})$ is expressed as $T(n_i + 1|\mathbf{n}, \mathbf{m})$.

We introduce migration in the simplest way, as a neutral and linear process. The probability of an A moving from a site i to a site j is proportional to the number of A at site i:

$$T(n_i + 1, n_j - 1|\mathbf{n}, \mathbf{m}) = \frac{bq}{z} x_j \,, \tag{6.2}$$

where q is the migration rate constant, which is the same for migration between any two sites, and $z = L - 1$ is the number of nearest neighbours of the source site i. The parameter b is that common to all processes in the CM model (5.1) and is used to set the continuous-time limit. As explained in section 5.3.1 we set $b = K^2$. The division by z tells us that the migration is neutral as the A at site i choose uniformly randomly which site to migrate to. For the migration to be a neutral process which favours neither species, analogously we have the transition

rate for species B from a site i to a site j given by

$$T(m_i + 1, m_j - 1|\mathbf{n}, \mathbf{m}) = \frac{bq}{z} y_j \ . \tag{6.3}$$

These new processes give rise to the first and second Cartesian moments of δx_i and δy_i in an update time τ,

$$\begin{aligned} \langle \delta x_i \rangle &= \frac{bq\tau}{Kz} \sum_{j \neq i} (x_j - x_i) \\ \langle \delta y_i \rangle &= \frac{bq\tau}{Kz} \sum_{j \neq i} (y_j - y_i) \ . \end{aligned} \tag{6.4}$$

6.2.2 Sub-Deterministic Migration

We must consider how to scale the migration rate q with the system size K. At the mean-field level, adding the contributions (6.4) from migration to the local deterministic dynamics of a population (5.6) at a site i gives the new rate equations,

$$\begin{aligned} \dot{x}_i &= x_i(x_i - 1)[a - (x_i - 1)^2 - (y_i - 1)^2 \ ] + \frac{q}{z} \sum_{j \neq i} (x_j - x_i) \\ \dot{y}_i &= y_i(y_i - 1)[a - (x_i - 1)^2 - (y_i - 1)^2 \ ] + \frac{q}{z} \sum_{j \neq i} (y_j - y_i) \ . \end{aligned} \tag{6.5}$$

When $Q = 0$, we know that each patch population will evolve to reside on a common circular manifold. We want to maintain this behaviour in the presence of migration. Therefore we need a weak form of migration, not acting at the leading order in K, so it can treated as a sub-deterministic process which is neglected in the above mean-field equations. We can achieve this by scaling the migration rate q with the carrying capacity K as

$$q \to \frac{q}{K} \ . \tag{6.6}$$

6.3 Multi-Patch Fokker-Planck Equation

Following the same procedure for the single patch CM model in section 5.3.1, we derive a polar Fokker-Planck Equation (FPE) to describe the diffusion in the ϕ-direction about the circular manifold for each patch. To do so we must find what contribution the migration process make to the polar jump moments α_i of the Kramers-Moyal expansion given by

$$\alpha_n^{(i)} = \lim_{\tau \to 0} \frac{\langle (\delta\phi_i)^n \rangle}{\tau} \,. \tag{6.7}$$

This means we need to find the moments of the change in ϕ in a time τ due to migration, and consider which terms are non-zero when the continuous-time limit is taken. It turns out we can find out both of these things by considering just the contributions from the first-order moments. With the transformation to polar coordinates defined as

$$\begin{aligned} x_i' &\equiv x_i - 1 = r_i \cos(\phi_i) \\ y_i' &\equiv y_i - 1 = r_i \sin(\phi_i) \,, \end{aligned} \tag{6.8}$$

we write the Cartesian first moments, using the scaled form of Q (6.6), as

$$\begin{aligned} \langle \delta x_i \rangle &= \frac{b\tau}{K^2} \frac{q r_0}{z} \sum_{j \neq i} [\cos(\phi_j) - \cos(\phi_i)] \\ \langle \delta y_i \rangle &= \frac{b\tau}{K^2} \frac{q r_0}{z} \sum_{j \neq i} [\sin(\phi_j) - \sin(\phi_i)] \end{aligned} \tag{6.9}$$

where r_0 is the radius of the circular manifold. As each site has the same carrying capacity and local dynamics with the same rates, then r_0 is the same assumed fixed radius for each circular manifold. In other words, the oscillators reside on a common circular manifold of radius r_0.

Using an equivalent expression for $\delta\phi_i$ from (5.20), we have for the first moment

$$\langle \delta\phi_i \rangle = -\frac{y_i'}{r_i^2} \langle \delta x_i' \rangle + \frac{x_i'}{r_i^2} \langle \delta y_i' \rangle + \frac{x_i' y_i'}{r_i^4} \left(\langle (\delta x_i')^2 \rangle - \langle (\delta y_i')^2 \rangle \right) \,.$$

Considering the first two terms, plugging in (6.9) and transforming to polar

coordinates using (6.8) we find

$$\langle \delta\phi_i \rangle = \frac{b\tau}{K^2}\frac{q}{zr_0^2}\sum_{j\neq i}\Big(r_0^2\cos(\phi_i)[\sin(\phi_j)-\sin(\phi_i)] - r_0^2\sin(\phi_i)[\cos(\phi_j)-\cos(\phi_i)]\Big) \tag{6.10}$$

which after some use of trigonometric addition formulae can be written as

$$\langle \delta\phi_i \rangle = \frac{b\tau}{K^2}\frac{q}{z}\sum_{j\neq i}\sin(\phi_j-\phi_i)\ . \tag{6.11}$$

In defining the continuous-time scale for the local dynamics of the CM model in section 5.3.1, we set $b \equiv K^2$ so that

$$\alpha_1(\phi_i) = \lim_{\tau\to 0}\frac{\langle \delta\phi_i\rangle}{\tau} \sim \lim_{b\to\infty}\frac{b}{K^2} \tag{6.12}$$

is finite. Therefore we do the same here, giving the non-zero contribution to the first jump moment from the migration

$$\alpha_1^{(i)}(\phi_i) = \frac{q}{z}\sum_{j\neq i}\sin(\phi_j-\phi_i)\ . \tag{6.13}$$

Furthermore, we see that there will be no contribution to the first-order or second-order polar jump moments from the second-order Cartesian moments due to migration as they scale with K as b/K^3.

Adapting the one patch FPE (5.26), we have the FPE describing the polar diffusion about the circular manifolds of each patch

$$\frac{\partial P(\{\phi_i\},t)}{\partial t} = \sum_i\Bigg(-\frac{\partial}{\partial\phi_i}\Big[f(\phi_i)P\Big] + \frac{1}{2}\frac{\partial^2}{\partial\phi_i^2}\Big[g^2(\phi_i)P\Big] - \frac{q}{z}\sum_{j\neq i}\frac{\partial}{\partial\phi_i}\Big[\sin(\phi_j-\phi_i)P\Big]\Bigg) \tag{6.14}$$

where the local, single patch functions f and g are the same as those given in (5.27) and (5.28) respectively.

6.4 A Langevin Description of Synchronisation

The equivalent set of Langevin equations to the FPE (6.14) under the Itô prescription are

$$\phi_i = f(\phi_i) + \frac{q}{z}\sum_j \sin(\phi_j - \phi_i) + g(\phi_i)\eta_i \tag{6.15}$$

where the stochastic variables η_i are Gaussian white noise with zero mean and unit variance.

This is the governing set of equations we shall use to explore how the diffusion of each patch population can become synchronised around the manifold. To make our language more concise and relate it to other studies of synchronisation phenomena, we now refer to the diffusion at each patch about the common circular manifold as the oscillator at site i whose phase is given by ϕ_i. Having made the migration a sub-deterministic process, in this regime it is clear from inspection of the second term of (6.15) to expect the migration to make the oscillators more similar, and that their phases will synchronise for some sufficiently strong coupling strength q. Our aim is to study the emergence of synchronisation between the oscillators, finding how it depends on q. To do so we need to develop meaningful quantitative definitions and measurements of synchronisation in the system. We proceed to begin with by studying the Langevin equations (6.15) describing the system dynamics, after first reviewing a commonly studied model of synchronisation.

6.4.1 The Kuramoto Model of Synchronisation

A paradigmatic model of synchronisation is the Kuramoto model, named after Kuramoto who first solved it in the mean-field limit [119, 120]. The model consists of a system of N coupled oscillators whose phases are denoted by $\theta_i \in [-\pi, \pi]$. In the basic deterministic model, the dynamics are defined by the first-order rate equations

$$\dot{\theta}_j = \omega_j + \sum_{k=1}^{N} Q_{jk} \sin(\theta_k - \theta_j) \ . \tag{6.16}$$

The first term is the natural frequency of each oscillator while the second term is the coupling between the oscillators, which tends to synchronise them according

to the coupling matrix Q_{ij}.

To quantify the synchronisation, an appropriate order parameter is the complex valued s [47], defined as

$$s = \frac{1}{N}\sum_{k=1}^{N} e^{i(\theta_k - \psi)} \tag{6.17}$$

where

$$\psi = \frac{1}{N}\sum_{k=1}^{N} \theta_k \tag{6.18}$$

is the average phase and $i = \sqrt{-1}$. The order parameter (6.17) gives the level of synchronicity by assigning a value of $0 \leq s \leq 1$. If the oscillators are unsynchronised, we can assume they are uniformly distributed about the unit circle. Defining the uniform spacing as $\Delta = 2\pi/N$ then we can express each oscillator's position as $\theta_k = k\Delta$. Using this in (6.17) we have

$$se^{i\psi} = \frac{1}{N}\sum_{k} e^{ik\Delta} \, . \tag{6.19}$$

Taking the large N limit, we replace this sum with an integral and compute

$$\begin{aligned} se^{i\psi} = \frac{1}{N}\int_0^N \mathrm{d}k \; e^{ik\Delta} &= \frac{1}{Ni\Delta}(e^{iN\Delta} - 1) \\ &= \frac{1}{Ni\Delta}(e^{2\pi i} - 1) \\ &= 0 \, . \end{aligned} \tag{6.20}$$

As $e^{i\psi} \neq 0$, this means that $s = 0$ for the incoherent, unsynchronised state. On the other hand, if all the oscillators are fully synchronised, then we have $\theta_j = \theta$ for all j. This gives an average phase of $\psi = \theta$ and the order parameter (6.17) becomes

$$se^{i\theta} = e^{i\theta} \tag{6.21}$$

meaning $s = 1$. Between these two extremes of incoherence and synchronisation any interim value of $0 < s < 1$ represents a state of partial synchronisation [47].

The version of the model solved by Kuramoto is the mean-field version of (6.16) in the limit of $N \to \infty$ many oscillators, with $Q_{jk} = Q/N$. The

natural frequencies of the oscillators ω_j are drawn from a unimodal probability distribution $g(\omega)$ with zero mean, i.e. a Gaussian distribution. Here we do not reproduce the mathematical derivation of the main result, details of which can be found in a review of Kuramoto systems by Acebrón *et al* [47], but instead simply quote it: there exists a transition from incoherence to partial synchronisation at a critical value of the coupling constant Q_c, encapsulated in the critical scaling law

$$s = \sqrt{\frac{16(Q - Q_c)}{\pi Q_c^4 g''(0)}}\,, \tag{6.22}$$

where Q_c is determined by the unimodal distribution as

$$Q_c = \frac{2}{\pi g(0)}\,. \tag{6.23}$$

We wonder if any similar transitional behaviour can be observed in our multi-patch CM model. At first glance the two systems seemed very similar when comparing their governing dynamical equations. For the multi-patch CM Langevin equations (6.15), remarkably the sub-deterministic migration process has resulted in a sinusoidal coupling term identical to that for the Kuramoto model (6.16) for the mean-field case. However there are two principle differences between the two models. Firstly our model considers a relatively small number of oscillators making up a metapopulation, not a large, possibly infinite, coupled system. Secondly, the frequencies of each oscillator in our model are not constant, rather there is a diffusive motion in a periodic 1D potential, which can be dethermalised to give a non-zero angular velocity or frequency. Schematically, in our model we have $\omega_i(\phi_i)$, i.e. position dependent velocities, compared to the constant frequencies of the Kuramoto model, drawn from a probability distribution. This is an important distinction: as we mentioned in the introduction to this chapter, recently Abta *et al* have shown that desynchronisation due to gradients between phase space dependent oscillator frequencies plays a crucial role in the stability of cycles and the long-time survival of spatial predator-prey systems [52, 53].

For these reasons it is therefore not possible to repeat the analysis of the mean-field Kuramoto model for our system. Instead, we now proceed to develop our own analytical and empirical techniques to study the synchronisation.

6.5 The Eigenvalue Landscape Function Method

While the Kuramoto model has helped with our conceptual understanding of how to study synchronicity for a system of coupled oscillators, we now develop our own method for trying to study synchronisation in our system, in particular probing the relationship with the coupling strength due to migration q. The basic premise of the method is to construct a linear stability analysis of the fully synchronised state of the system.

6.5.1 Multiplicative to Additive Noise

We know well from previous chapters the importance the multiplicative form of the demographic noise can have on the dynamics of finite systems. Therefore we take our governing set of Langevin equations for the coupled patch populations (6.15) and perform a variable transformation to a system of Langevin equations with additive noise terms. The transformation is the same as that for for the single patch CM model in section 5.4. Defining the new variables

$$\theta_i = \int^{\phi} \frac{\mathrm{d}\phi_i'}{g(\phi_i)} \tag{6.24}$$

and using the details of the transformation in section 2.10 we have

$$\dot{\theta}_i = F(\theta_i) + \frac{q}{zg(\theta_i)} \sum_j \sin(\theta_j - \theta_i) + \eta_i \tag{6.25}$$

where

$$F(\theta) = \left(\frac{f(\phi)}{g(\phi)} - \frac{1}{2} \partial_\phi g(\phi) \right) \Bigg|_{\phi=\phi(\theta)} . \tag{6.26}$$

We now proceed to analyse the deterministic dynamics of these Langevin equations, neglecting the effects of the additive Gaussian noise terms. While at first glance this seems to run contrary to our main aim of studying the effects of noise in the dynamics of complex systems, we see from the above expression for $F(\theta_i)$ that the new Langevin equations (6.25) describing the dynamics of the system contain the multiplicative factors of the noise,

$$g(\theta_i) \equiv g(\phi_i) \Big|_{\phi_i=\phi_i(\theta_i)} \tag{6.27}$$

found in the original Langevin equations (6.15). Therefore the behaviour we observe in the new deterministic dynamics of the transformed system is a direct consequence of the multiplicative form of the demographic noise in the original.

In order to make progress, in producing plots and performing numerical calculations, we once again have to resort to the approximation schemes for the variable transformation (6.24) and of the multiplicative noise factor (6.27). These approximations are the same as detailed in section 5.5.3 which were used to facilitate analysis of the single patch population for the CM model.

6.5.2 Change of Variables

When the system is fully synchronised we refer to it as being in the coherent state. Here, oscillators all have the same phase $\theta_i = \theta \ \forall i$, and so the average phase

$$\psi = \frac{1}{L}\sum_{j=1}^{L}\theta_j = \theta \ . \tag{6.28}$$

We now investigate the stability of this coherent state as described by $\psi = \theta$. To do so we perform the change of variables,

$$\left.\begin{aligned} \psi &= \frac{1}{L}\sum_{j=1}^{L}\theta_j \\ \chi_i &= \theta_i - \theta_1 \ , \quad i = 2, \ldots, L \end{aligned}\right\} \tag{6.29}$$

for which the inverse transformation is,

$$\left.\begin{aligned} \theta_1 &= \psi - \frac{1}{L}\sum_{j=2}^{L}\chi_j \\ \theta_i &= \chi_i + \psi - \frac{1}{L}\sum_{j=2}^{L}\chi_j \ , \quad i = 2, \ldots, L \end{aligned}\right\} \ . \tag{6.30}$$

Applying this change of variables to the deterministic part of the Langevin equations (6.25) yields the rate equations

$$\dot{\psi} = \frac{1}{L}\sum_j F(\theta_j) + \frac{q}{zg(\theta_i)}\sum_j \sin(\theta_j - \theta_i) \tag{6.31}$$

$$\dot{\chi}_i = F(\theta_i) - F(\theta_1) + q\sum_{j=1}^{L}\left[\frac{1}{zg(\theta_i)}\sin(\theta_j - \theta_i) - \frac{1}{zg(\theta_1)}\sin(\theta_j - \theta_1)\right] . \tag{6.32}$$

The coherent state is now equivalently defined by

$$\theta_j = \theta\,, \quad i = 1, \ldots, L \tag{6.33}$$

$$\psi = \theta \tag{6.34}$$

$$\chi_i = 0\,, \quad i = 2, \ldots, L\,. \tag{6.35}$$

In the coherent state the system is reduced to an effective single oscillator whose phase is given by ψ. The coherent state is not a static fixed point, rather it exists on the whole domain of ψ, i.e. the circular manifold.

6.5.3 Taylor Expansion About the Coherent State

Our goal now is to quantify the global attraction of the coherent state by a linear stability analysis. To do so we Taylor expand the rate equation for χ_i (6.32) about the coherent state (6.35) which we denote by $\{\chi_i = 0\}$, and is also a fixed point of (6.32). Introducing the shifted variables about the coherent state $\bar{\chi}_i = \chi_i - 0$, and keeping only linear terms in the expansion yields

$$\dot{\bar{\chi}}_i = \sum_{k=2}^{L}\left[\frac{\partial}{\partial\chi_k}H_F(\psi, \{\chi_j\}) + \frac{\partial}{\partial\chi_k}H_Q(\psi, \{\chi_j\})\right]_{\{\chi_j=0\}}\bar{\chi}_k \tag{6.36}$$

where

$$H_F(\psi, \{\chi_j\}) = F(\theta_i(\psi, \{\chi_j\})) - F(\theta_1(\psi, \{\chi_j\})) \tag{6.37}$$

$$H_Q(\psi, \{\chi_i\}) = -\frac{q}{zg(\theta_i)}\left[\sin\chi_i - \sum_{j=2}^{L}\sin(\chi_j - \chi_i)\right] - \frac{q}{zg(\theta_1)}\sum_{j=2}^{L}\sin\chi_j \tag{6.38}$$

and the square bracket term is evaluated at the coherent state $\{\chi_j = 0\}$.

We evaluate each term in the square bracket separately. For H_F, we first do the differentiation using the chain rule with the definition of the variable transformation (6.30):

$$\begin{aligned}\frac{\partial}{\partial\chi_k}\Big(F(\theta_i)-F(\theta_1)\Big) &= \frac{\partial\theta_i}{\partial\chi_k}\frac{\partial}{\partial\theta_i}F(\theta_i)-\frac{\partial\theta_1}{\partial\chi_k}\frac{\partial}{\partial\theta_1}F(\theta_1)\\ &= \left(\delta_{ik}-\frac{1}{L}\right)\frac{\partial}{\partial\theta_i}F(\theta_i)+\frac{1}{L}\frac{\partial}{\partial\theta_1}F(\theta_1)\ . \end{aligned} \tag{6.39}$$

Evaluating this at the coherent state we have

$$\frac{\partial}{\partial\chi_k}H_F(\psi,\{\chi_j\})\bigg|_{\{\chi_j=0\}} = \delta_{ik}\frac{\partial}{\partial\theta}F(\theta)\bigg|_{\theta=\psi}\ . \tag{6.40}$$

For the H_Q term (6.38), we find taking the derivative

$$\begin{aligned}\frac{\partial}{\partial\chi_k}H_Q =& -\frac{q}{zg(\theta_i)}\left[\delta_{ik}\cos\chi_i-\cos(\chi_k-\chi_i)+\sum_{j=2}^{L}\cos(\chi_j-\chi_i)\delta_{ik}\right]\\ &-\frac{q}{zg(\theta_1)}\cos\chi_k\end{aligned} \tag{6.41}$$

where we do not write terms with derivatives of $g(\theta)$ as they become zero in the coherent state due to the coupling sinusoidal terms vanishing. Evaluating at the coherent state yields

$$\frac{\partial}{\partial\chi_k}H_Q(\psi,\{\chi_i\})\bigg|_{\theta=\psi} = -\frac{Lq}{zg(\psi)}\delta_{ik}\ . \tag{6.42}$$

Now substituting the evaluated derivatives (6.40) and (6.42) back into the Taylor expansion (6.36) gives

$$\begin{aligned}\dot{\bar{\chi}}_i &= \sum_{k=2}^{L}\left(\frac{\partial}{\partial\theta}F(\theta)\bigg|_{\theta=\psi}-\frac{Lq}{zg(\psi)}\right)\delta_{ik}\bar{\chi}_k\\ &= \left(\frac{\partial}{\partial\theta}F(\theta)\bigg|_{\theta=\psi}-\frac{Lq}{zg(\psi)}\right)\bar{\chi}_i\ .\end{aligned} \tag{6.43}$$

We now make the simplification of taking $z = L-1 \approx L$ when we have a

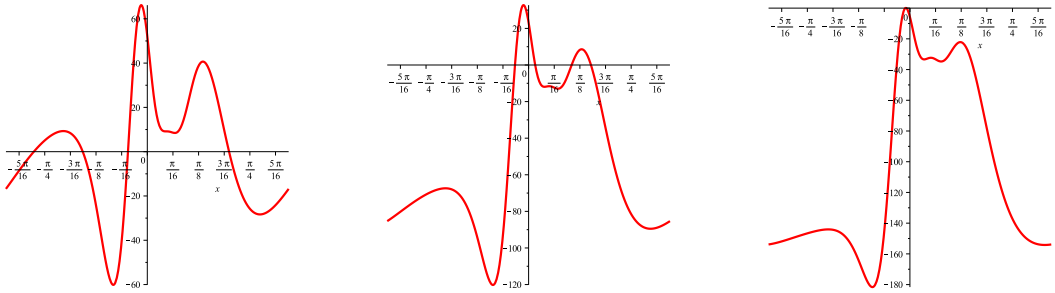

(a) $q = 0$ (b) $q = 100$ (c) $q = 200$

Figure 6.1: The ELF $\lambda(\psi)$ for different values of migration coupling q. The CM model parameters are $r_0 = \sqrt{0.5}$, $p_1 = 0$ and $p_2 = 0$.

suitably large enough number of oscillators. For example, for $L = 8$ oscillators, $L/(L-1) = 1.14$ is well approximated to 1. Implementing this gives us our final expression for the linearised rate equations near the coherent state for z oscillators

$$\dot{\bar{\chi}}_i = \left(\frac{\partial}{\partial \theta} F(\theta) \Big|_{\theta=\psi} - \frac{q}{g(\psi)} \right) \bar{\chi}_i \tag{6.44}$$

with the other variable being the average phase ψ, which as previously mentioned is the effective 1D system variable in the coherent state.

6.5.4 Eigenvalue Landscape Function

We see from the linearised equations (6.44) that when in the local neighbourhood of the coherent state, the attraction or repulsion of an oscillator to the coherent state is dictated by the term in parenthesis. We interpret it as the eigenvalue of the linear stability analysis. In the coherent state, all the oscillators j have the same phase $\theta_j = \theta$, yet the system can still take any value of the average phase ψ on the circular manifold. Therefore the eigenvalue is a function of the average angle ψ, which we call the eigenvalue landscape function (ELF):

$$\lambda(\psi) = \frac{\partial}{\partial \theta} F(\theta) \Big|_{\theta=\psi} - \frac{q}{g(\psi)} \, . \tag{6.45}$$

In figure 6.1 we show the ELF for different values of q. We see that as the coupling strength q increases, while the shape of the ELF may change, the main

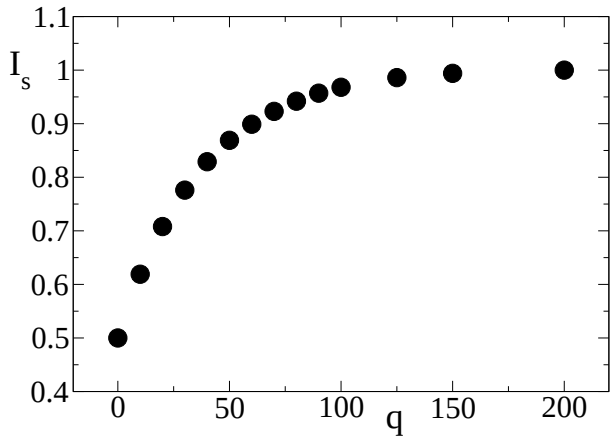

Figure 6.2: The relation between the global synchronisation I_s and the scaled migration rate q. The CM model parameters are $r_0 = \sqrt{0.5}$, $p_1 = 0$ and $p_2 = 0$.

effect is to lower it in relation to the attraction/repulsion line at $\lambda = 0$. Therefore for a large enough q each point of the landscape will be a restoring force to the coherent state, as the ELF always has a negative value. To quantify the overall synchronisation in the system we compute I_s, an averaged measure of the global attraction of the coherent state over the whole circular manifold. It is given by

$$I_s = \frac{I_a}{I_a + I_r} \tag{6.46}$$

where I_a is the integral given the total bounded area below $\lambda = 0$ and I_r is the the area above $\psi = 0$. In figure 6.2 we plot the relationship between I_s and the scaled coupling q, calculating the required integrals numerically using the mathematical software Maple(TM). In contrast to the Kuramoto model, we have for our system that the fully incoherent state, more specifically one with no coupling $q = 0$, that the measure of I_s is 0.5 rather than 0. However, as q increases and becomes sufficiently large we see the synchronisation saturating to the coherent state at $I_s = 1$.

In order to find how well this ELF method captures the synchronisation behaviour of the metapopulation we now look to compare it with some empirical measurements from simulations of the defining stochastic dynamics.

6.6 Measuring Synchronisation in Simulations

To study the spatially extended CM model with migration, we simulate the full stochastic dynamics using the Gillespie algorithm. As discussed in section 2.11, it is not possible to use random sequential updating for the multi-patch system because, unlike in the lattice spin model of section 3.6.1, the number of interacting constituents is not fixed for each patch and so the sampling would be wrong. For this reason, the number of patches we simulate becomes a limiting factor, as it becomes time-expensive to implement the full Gillespie algorithm.

For each of the simulation results presented in the figures in the remainder of this chapter, the equilibrium CM model parameters are $K = 5000$, $b = K^2$, $r_0 = \sqrt{0.5}$, $p_1 = 0$ and $p_2 = 0$, unless otherwise stated.

6.6.1 The Kuramoto Order Parameter

In the simulations we can calculate the angular positions of the oscillators which we denote by ϕ_i . Unlike for the CM model in section 5.5.1, ϕ_i are true spatial coordinates $\phi_i \in [-\pi, \pi]$ and not aggregated displacements. To use the Kuramoto order parameter s for synchronisation defined in (6.17), we swap ϕ for θ and expanding the complex exponential, yielding

$$s = \frac{1}{N} \sum_j [\cos(\phi_j - \psi) + i \sin(\phi_j - \psi)] \; . \tag{6.47}$$

Now calculating the modulus $|s|^2 = ss^*$ gives

$$\begin{aligned} |s|^2 &= \frac{1}{N^2} \sum_{j,k} [\cos(\phi_j - \psi)\cos(\phi_k - \psi) + i \sin(\phi_j - \psi)\sin(\phi_k - \psi)] \\ &= \frac{1}{N^2} \sum_{j,k} \cos(\phi_j - \phi_k) \\ &= \frac{1}{N^2} \left(\sum_j \cos\phi_j \sum_k \cos\phi_k + \sum_j \sin\phi_j \sum_k \sin\phi_k \right) \; , \end{aligned} \tag{6.48}$$

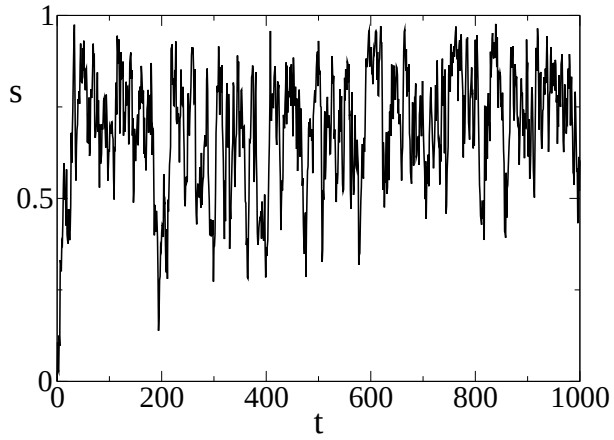

Figure 6.3: The modulus of the Kuramoto order parameter s against time for a system of $L = 4$ patches with no migration, $q = 0$.

which upon taking the real, positive square root yields the expression for the modulus $|s| \equiv s$,

$$s = \frac{1}{N}\sqrt{\left(\sum_j \cos\phi_j\right)^2 + \left(\sum_j \sin\phi_j\right)^2}\,. \tag{6.49}$$

This expression allows us to measure s directly from simulation, and to study how it depends on the coupling strength q. However we find it to not be a very good measure of synchronisation for our system. In figure 6.3 we show a typical time evolution of s for a system of $L = 4$ oscillators. We see that we do not get a well defined, constant measure of s, a problem that persists as L and q are increased. This could be a result of the frequency dependence of the potential in our system, not present in the Kuramoto model. The oscillators all diffuse in the same 1D potential and so we expect a background level of synchronisation, as they predominantly inhabit a broad potential well. Averaging over many realisations will very likely alleviate this problem and s will become a meaningful, accurate measure of synchronisation, but as mentioned already computing time is already at a premium, making an averaging procedure too time-expensive.

6.6.2 Displacement Method

We devise an alternative method for measuring the synchronisation of the system by simulation of the stochastic dynamics. We develop the method intuitively for two oscillators and then generalise the method to an arbitrary system of L oscillators.

Two Oscillators

If we consider a system of two oscillators, the distance ϕ between them in terms of their angular position on the circular manifold

$$\phi = \begin{cases} |\phi_2 - \phi_1| & \text{if } |\phi_2 - \phi_1| < \pi \\ 2\pi - |\phi_2 - \phi_1| & \text{otherwise} \end{cases} \tag{6.50}$$

tells us directly how similar the two phases are. We define a small constant ϵ to define a distance over which one can infer whether the phases are synchronised. We assign two counters $T_Y(t)$ and $T_N(t)$, which tally the total amount of time the oscillators have been in or out of sync. For each Monte Carlo sweep t of the system, we update the counters like

$$\begin{aligned} T_Y(t+1) &= T_Y(t) + 1 \quad \text{if } \phi < \epsilon \\ T_N(t+1) &= T_N(t) + 1 \quad \text{if } \phi > \epsilon \end{aligned} \ . \tag{6.51}$$

We then calculate a long-time frequential average T to find the typical state of synchronicity in the system,

$$T(t) = \frac{T_Y(t)}{t} \ . \tag{6.52}$$

As we will show, this grows rapidly at short times before saturating to a constant T_∞, which we take as our order parameter defining the synchronisation of the system.

L Oscillators

In trying to generalise this method to more than two oscillators, an immediate difficulty is in interpreting a measure of distance. The distance between ϕ_1 and ϕ_2 tells us nothing about the distance of either to ϕ_3. Our solution to this is to

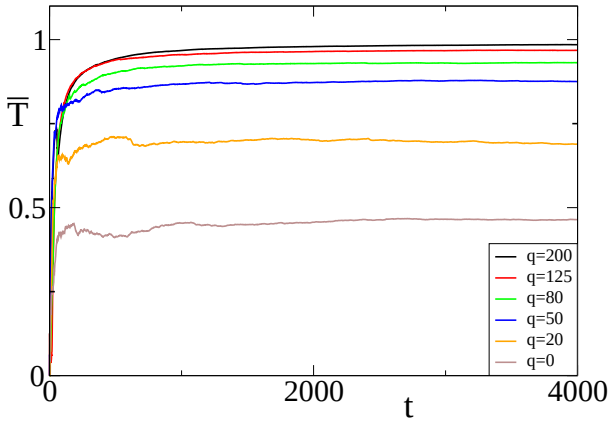

Figure 6.4: The time evolution of the ensemble time average $\bar{T}(t)$ for a system of $L = 4$ oscillators, with $\epsilon = 0.5$. It reaches different saturation constants $\bar{T}_\infty$ for different values of q.

define the distance $\Delta\phi_i$ for each oscillator to the average phase ψ:

$$\Delta\phi_i = \begin{cases} |\psi - \phi_i| & \text{if } |\psi - \phi_i| < \pi \\ 2\pi - |\psi - \phi_i| & \text{otherwise} \end{cases} . \tag{6.53}$$

Then, analogously to (6.51), to evaluate the synchronisation of the system at each Monte Carlo sweep t we have counters for each oscillator to see how similar their phase is to the average phase, using a small parameter ϵ:

$$\begin{aligned} T_Y^i(t+1) &= T_Y^i(t) + 1 \quad \text{if } \Delta\phi_i < \epsilon \\ T_N^i(t+1) &= T_N^i(t) + 1 \quad \text{if } \Delta\phi_i > \epsilon \end{aligned} . \tag{6.54}$$

We again define our long time average quantity (6.52), but now we require one for each oscillator,

$$T^i(t) = \frac{T_Y^i(t)}{T_Y^i(t) + T_N^i(t)} . \tag{6.55}$$

However, what we really want is a single quantity telling us a global measure of synchronisation in the system. The simplest and most obvious one we construct is the patch-ensemble average $\bar{T}$ of the time averages T^i,

$$\bar{T}(t) = \frac{1}{L} \sum_j T^j(t) . \tag{6.56}$$

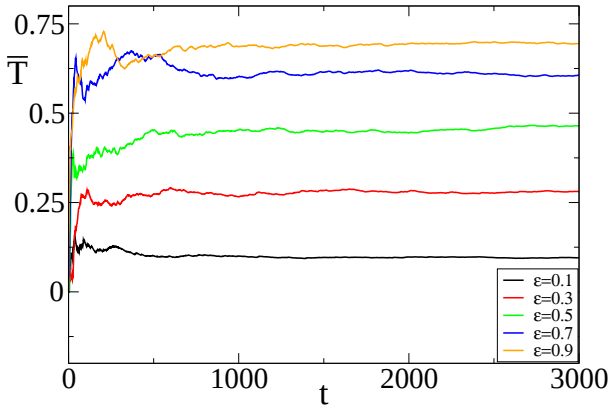

Figure 6.5: Comparison of the average $\bar{T}$ for different values of the synchronisation parameter ϵ for a system of size $L = 4$ with $q = 0$.

In figure 6.4 are measurements of $\bar{T}$ from Monte Carlo simulation of the defining birth, death and migration stochastic processes of the multi-patch CM model. We observe rapid growth at early times before a saturation to some constant value $\bar{T}_\infty$, which we define as our global synchronisation order parameter. This not only gives us a simple scalar measure of the synchronicity of the system, but also direct insight into how the coupling of the system through the migration constant q enhances the phase alignment of the system.

Setting the ϵ Parameter

In the displacement method measurement we introduce one arbitrary parameter ϵ which is defined via (6.54). It is clear that if $\epsilon \approx 2\pi$, the oscillators would be found to be fully synchronised all the time, while if $\epsilon \approx 0$ then, simply due to the inherent noise for each oscillator the method would barely register any instances of synchronicity. While being able to intuitively select a reasonable value for $0 \leq \epsilon \leq 2\pi$, we can be guided by trying to tune it to our analytical work using the ELF (6.45). Here, we know that in the zero migration, fully decoupled case of $q = 0$, our measurements of the background synchronicity of the system is $I_s = 0.5$. Therefore to tune our simulation results to the ELF analysis, we can choose an ϵ which gives a similar background measure.

In figure 6.5 we show the time evolution of $\bar{T}$ for a range of different values of ϵ. We see that choosing $\epsilon = 0.5$ gives a good fit to the $q = 0$ synchronisation measure of $I_s = 0.5$. It is not clear to us if their is a physical significance

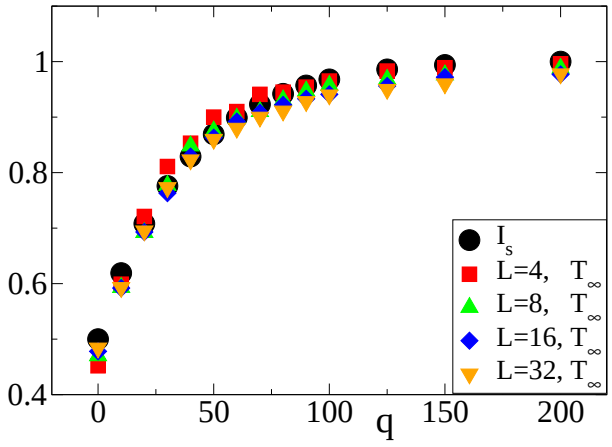

Figure 6.6: Comparison of the global measurements of synchronisation from the ELF measure I_s and the empirical measure T_∞ for a range of system size L with $\epsilon = 0.5$.

of this particular value of the ϵ parameter. Two possibly important factors to be considered are the size of the potential landscape typically explored by the oscillators, defined by the width of a well, and the strength of the thermal noise which gives a measure of their typical diffusion. It could be that when one considers how these two factors, a length scale emerges describing the domain of an oscillator in the well, and that it is analogous to $\epsilon = 0.5$. We do not conduct any such study here however, and instead proceed to analyse data for this tuned parameter value.

6.6.3 Comparison of Measurements

We now compare T_∞, the empirical measurement of synchronisation direct from simulation, with I_s, found by integration of the ELF. We do so by plotting them for a range of system sizes L against the scaled migration rate $q = Q/z$ where $z = L - 1$. The results are shown in figure 6.6, where we find excellent agreement between the two measurements across a broad range of system sizes.

The agreement of the two measurements in describing the relationship between the synchronisation and the coupling strength q is remarkable, not only in the similarity of individual measurements but more generally in identifying accurately the range of q over which the system evolves from the incoherent state to the fully synchronised state at $I_s = \bar{T}_\infty = 1$. The agreement is even more remarkable when

one considers the very different bases of of each measurement. From simulation, T_∞ is a dynamical measure of the full stochastic dynamics, which has been averaged in the long time limit. On the other hand, I_s is calculated from a linearised treatment of the rate equations, which itself has been dimensionally reduced from $L-1$ variables to 1 variable, the average phase ψ.

However while the ELF and displacement method measurements agree well qualitatively, we acknowledge that the quantitative agreement only holds for the tuned parameter value $\epsilon = 0.5$. We now present one final method of measurement of synchronisation by simulation, which does not require any parameter to be optimised. This will provide further insight into how well the linearised ELF method captures the synchronisation in the full stochastic dynamics due to the coupling strength q.

6.6.4 Step Method

Recalling the typical way quasicycles arise for a single patch population in the CM model in chapter 5, we observed that an oscillator would sit in a potential well on the circular manifold for a time, before being carried over a barrier by the demographic noise. When the noise becomes dethermalised there is a non-zero angular velocity which leads to a bias in which barrier the oscillator exits the well by, resulting in quasicycles.

In figure 5.8, we saw that this waiting time for the noise to carry the system over the barrier, results in a *step motion* in the time evolution of the aggregate phase ϕ. After a period of time in the potential well the system would rapidly pass over the barrier and return to the well. We now exploit this typical behaviour to measure the synchronisation between the systems. We return to the use of the aggregate angle definition employed for the CM model, as defined in sections 4.5.2 and 5.5.1, where ϕ is the total angular displacement in the positive anticlockwise direction.

For each patch i the step motion of the phase ϕ_i will occur. Therefore we also expect a step motion in the difference between two oscillators $\phi_j - \phi_i$, as they both occupy the same region of the well for the vast majority of the time, but then when one jumps, a 2π interval opens between them. Defining the displacements

$$d_i = \phi_L - \phi_i \tag{6.57}$$

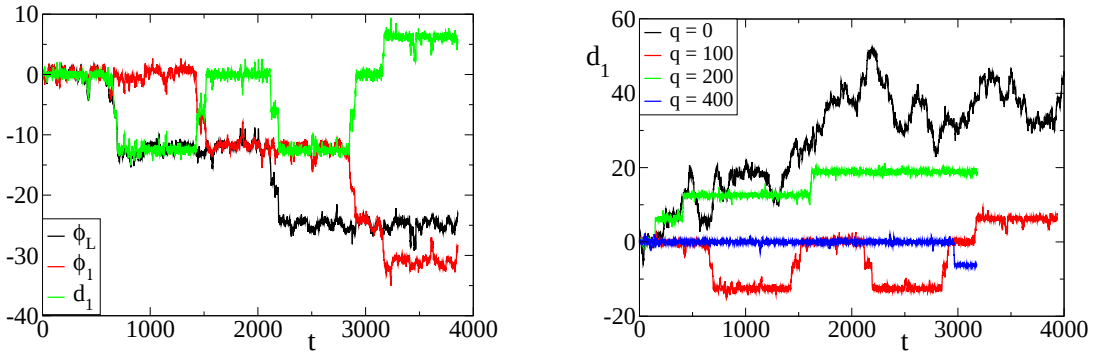

(a) (b)

Figure 6.7: (a) The step motion of the displacements d_1 as well as that of the oscillators ϕ_1 and ϕ_L for a system with $L = 4$ patches and $q = 100$. (b) The step motion of the displacement d_1 for different coupling strengths q in a $L = 4$ size system.

we confirm this picture directly in figure 6.7(a) from simulations of the stochastic dynamics. In the incoherent state $q = 0$, there is no synchronisation and we expect each ϕ_i will evolve randomly. However as q increases the times at which the steps occur in the displacements d_i will become more correlated, occurring together in smaller and smaller time windows, as once one oscillator moves over the barrier, the others are more likely to follow. In the coherent state, we expect the steps to occur almost simultaneously. Practically this means in the length of a Monte Carlo sweep in the simulations, we will no longer see the steps in the displacements d_i. We confirm this picture in figure 6.7(b).

More particularly, in increasing the coupling strength q to go between the incoherent and coherent states, the synchronisation increases and the time between steps will become longer for the displacements d_i. The length of this step interval we can measure from simulation. To do so, we begin each simulation with each patch population having the same initial condition. In order to observe as many steps as possible, we induce a current to flow by setting the current parameters of the CM model to be $p_1 = 20$, $p_2 = 0$ for each patch. This means that when uncoupled, each patch has the same non-zero angular velocity, inducing a biased diffusion which leads to more complete orbits of the circular manifold.

Due to the initial condition, the initial displacements are $d_i = 0$. We store these values in the variables D_i. For each Monte Carlo sweep t, the new $d_i(t)$ are evaluated. To find out if an oscillator has moved up or down a step we compare

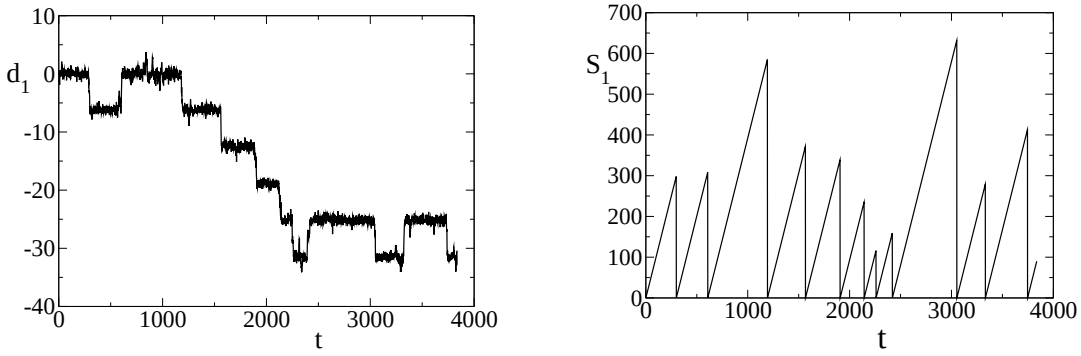

(a) (b)

Figure 6.8: (a) Step motion of a displacement d_1, with a step height of approximately 6.0. (b) The equivalent step interval counter S_1 with step height parameter $\Delta = 6.0$. There is close agreement in the measurement of the step interval lengths of the displacement shown in (a). The system parameters are $q = 100$ and $L = 4$ with $p_1 = 20$ and $p_2 = 0$.

it to D_i. If

$$|d_i(t) - D_i| > \Delta \tag{6.58}$$

where Δ is a positive parameter representing the height of a step, then we know it has. Then, we reset the value of D_i to $D_i = d_i(t)$. If not, the oscillator has not undergone a rapid full cycle of the manifold by passing over a barrier and remains on the same step. We use the counters S_i to record the length of a step interval for each oscillator. Starting the counter from zero, at each sweep the counter is updated as

$$S_i = \begin{cases} S_i + 1 & \text{if } |d_i(t) - D_i| < \Delta \\ 0 & \text{otherwise} \end{cases} . \tag{6.59}$$

To take a meaningful global measure from these counters in order to compare the synchronicity at different coupling strengths, we compute the average step interval S. We do this in two steps, first computing the running average step interval $\bar{S}_i$ for each oscillator during the simulation and then finding the patch-ensemble average

$$S = \frac{1}{z} \sum_j \bar{S}_j \, . \tag{6.60}$$

In order to implement this method we must set the value of the step height Δ. We know previously from the single patch dynamics of the CM model that the size of a

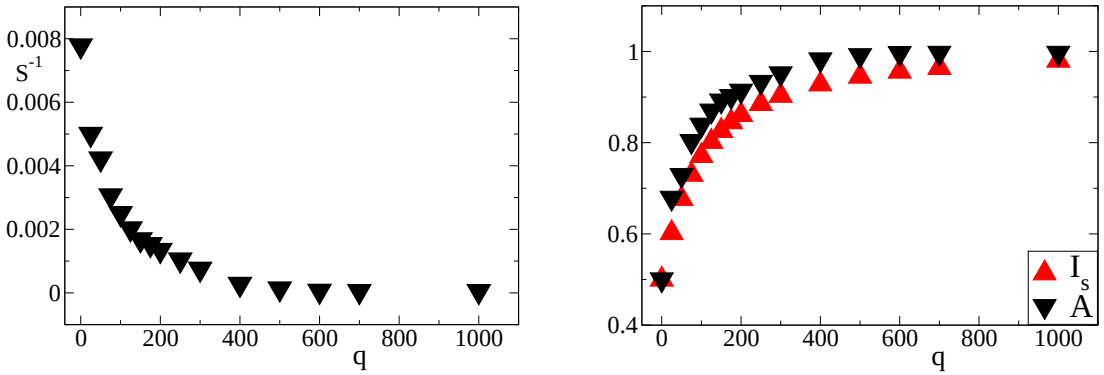

(a) (b)

Figure 6.9: (a) The inverse average step interval S^{-1} versus q with $L = 4$ and $\Delta = 6.0$. As predicted, we see a decay to 0 as q increases. (b) The ELF measure of synchronisation I_s for the same parameters $p_1 = 20$ and $p_2 = 0$ as in (a) alongside the transformed data A for the step method, with fitting parameter $a = 0.5039$.

step is approximately 2π as the oscillator crosses over a barrier, completes a rapid cycle of the manifold and returns to the well. Therefore we set $\Delta = 6.0 \approx 2\pi$. From inspection of figure 6.8(a) we see that this is a good estimate of the step height in a displacement d_1. We confirm this is a good value of Δ in figure 6.8(b) where the equivalent counter S_1 is displayed, which accurately identifies the times at which the steps occur, accounting for the background thermal noise that occurs in the well during a step interval in figure 6.8(a). Setting the value of Δ in this way is a self-consistent part of implementing the step method correctly, not an arbitrary assignment or tuned fit with other measurement methods.

In measuring the synchronisation using the step method, for $q = 0$ we expect a small value of S. The value of S will increase with increasing q, becoming infinitely large once q is sufficiently large for the system to inhabit the coherent state indefinitely. Therefore we expect an inverse relationship between S^{-1} and q, with the inverse step interval length decaying to zero as the coupling strength increases. This predicted behaviour is borne out in figure 6.9(a). The simulations were run for a total of 20000 Monte Carlo sweeps, during which no step motion was observed in the final two data points figure 6.9(a). We would expect if the simulations were run for longer that the quantitative values of the data would change, but the qualitative trend would persist.

In order to compare this directly with the ELF method we transform the data

displayed in figure 6.9(a) by

$$A = 1 - aS^{-1} \tag{6.61}$$

meaning that A will increase with q and saturate to 1 for some sufficiently large q. The fitting parameter a is set so that the $q = 0$ data point coincides with that of the ELF measurement of $I_s = 0.5$, giving $a = 0.5039$. This data is displayed in figure 6.9(b) alongside that obtained for the equivalent I_s data. We see a very close qualitative agreement in the two measurements over the same domain of q.

6.7 Discussion and Conclusion

In this chapter we have investigated the emergence of synchronisation in the quasicycles of a multi-patch population. We studied how the synchronisation of the system relates to the coupling strength q due to the migration of species between patches. To conduct this study we derived a governing set of of coupled Langevin equations to describe the synchronisation bought about by the sub-deterministic migration process. We adopted the conceptual framework of the Kuramoto model, describing a system of coupled oscillators in a state of partial synchronisation for a non-zero q, which reaches the fully synchronised, coherent state—where the phase of each oscillator is the same—above some sufficiently large q. Unlike in the Kuramoto model, we saw no evidence of a transition from incoherence to partial synchronisation at some critical value of the coupling strength q_c. Rather, the partial synchronisation seems to appear in the system when the coupling is switched on. We posit that the transition to partial synchronisation occurs exactly at $q_c = 0$ or in a small range of q that we have not probed, a possible question for future study.

We developed our own analytical method of quantifying the synchronisation between phases by conducting a linear stability analysis of the coherent state, deriving an effective one-dimensional reduction to the average phase ψ to describe the attraction or repulsion experienced by an oscillator to the coherent state. This is encapsulated in the eigenvalue landscape function, or ELF, (6.45). We compute a global average measure of the attraction of the coherent state I_s by integrating the ELF over the domain of the circular manifold. This serves as an order parameter to describe the level of synchronisation in the quasicycles of the metapopulation.

To test the validity of the linear ELF method in describing the synchronisation in the full stochastic dynamics of the system, we developed two methods of measuring the synchronisation from Monte Carlo simulations. The first was related to the ELF method measuring the distance of each oscillator from the average phase ψ. We calculated the long time average T_∞, which measures the relative time the oscillators spend within a defined synchronisation distance ϵ. We found very good quantitative agreement between T_∞ with the ELF measure I_s for the tuned parameter value $\epsilon = 0.5$. The second empirical measurement was based on the step motion of the aggregate phase of each oscillator, measuring the displacements between pairs of oscillators. The inverse average step interval S^{-1} decays to zero as the coupling strength q increases. We found that the decay has a strong qualitative agreement over the same domain of q with the empirical measure T_∞ and the numerical measure I_s to the fully synchronised coherent state $T_\infty = I_s = 1$. Furthermore the single parameter Δ is set self-consistently in the simulation making it an independent empirical definition and measure of the synchronisation in the system, making it more preferable to the T_∞ order parameter, where the arbitrary distance measuring synchronicity ϵ has to be defined.

At the outset of the study of the governing Langevin equations of the coupled system (6.15), we transformed to an alternative set of Langevin equations where the demographic noise has an additive form, not multiplicative. While then proceeding to probe the deterministic behaviour of these equations, the multiplicative noise factor $g(\theta)$ remains, and is present in each term that appears in the final expression for the ELF (6.45). Given the good qualitative agreement derived from the ELF method with the empirical measures from simulations of the full stochastic dynamics, we see that to describe analytically the observed synchronisation, an understanding of the multiplicative form of the demographic noise is vital. This understanding is facilitated by taking an individual based modelling approach. In introducing the migration process in the multi-patch CM model, we carefully evaluated how the migration enters at the deterministic level and into both the drift and diffusion terms. A more *ad hoc* approach of adding migration terms to the system dynamics would make differentiating between the consequences of the inherent demographic noise for each patch and the migration between patches difficult. As discussed in the introduction to this chapter these

are important features in spatial metapopulation dynamics, and so it is desirable to recognise and control each of them when studying their effect.

Looking to the future, there is still much to be that could be studied in this spatially extended model. As stated at the outset, in order to focus on synchronisation we set up the model in the simplest way possible, with each patch having the same parameters in the birth and death rates. In principle each patch could have its own rates, carrying capacity and migration rates. This is a preferred method for studying spatially heterogeneity in populations, which lead to spatially dependent fitnesses which are important in microbial populations [57].

More straightforwardly and incrementally, it would be interesting to study the synchronisation effects of this model when each patch is identical except for the current parameters p_1 and p_2. In the language of the Kuramoto model this would mean that each patch had a different natural frequency, and it would be interesting to find what the resulting frequency of the effective 1D oscillator would be in the fully synchronised system. In doing so, the question posed by Khasin *e*t al [118] could be addressed for this system, considering in the limit of fast migration whether we expect to see the metapopulation behaving as one large patch population with the equivalent dynamics of a single patch population.

Chapter 7

Conclusion

In this thesis we have shown that demographic noise can have profound consequences on the dynamics of non-equilibrium systems. Through analytical and numerical study of individual-based, microscopic models we have observed three striking examples of emergent macroscopic behaviour in finite model systems.

In chapter 3 we studied the role that noise can play in the ordering dynamics of systems with two symmetric absorbing states. We found that there is a dynamical transition between two universal modes of domain coarsening at some non-zero critical value of the noise strength. In the low noise regime, the system exhibits coarsening dynamics emblematic of the sub-critical Ising model, due to surface tension at domain interfaces. However when the noise strength becomes sufficiently strong the multiplicative form of the noise becomes relevant and the surface tension vanishes from the system. In this high noise regime, we observe global ordering characteristic of the voter model which is driven by interfacial fluctuations.

In chapter 4 we investigated whether it was possible to observe macroscopic probability currents in finite populations, and if so, whether they could give rise to cycling behaviour in the species densities. For two-species populations which deterministically evolve to reside at a stable fixed point, we derived the general conditions for which the system reaches a non-equilibrium steady state. We found that while dethermalisation of the noise induced a steady-state current to flow, this was not sufficient to allow global quasicycles to be observed. In chapter 5 we demonstrated that this stochastic mechanism could induce cycling behaviour if it

was coupled with a deterministic component of the dynamics which constrained the system to a closed, circular manifold. The athermal nature of the noise then leads to a biased diffusion about the manifold, resulting in quasicycles.

Finally, in chapter 6 we studied the synchronisation of several quasicycles in a spatially extended version of the circular manifold model of chapter 5, in which the multi-patch populations are coupled through migration. We devised two empirical measurements by Monte Carlo simulation to quantify the synchronisation of the system and to qualitatively observe its relation to the coupling strength. We successfully captured this behaviour analytically through a linearised stability analysis of the global synchronised state. This was predicated on the derivation and transformation of a set of Langevin equations describing the metapopulation dynamics, in which the multiplicative nature of the demographic noise is a key feature.

The models we constructed to facilitate our study of these very different global dynamical phenomena are necessarily specific to the system under consideration. Nevertheless, in the course of studying each of them some common themes emerged which may prove insightful in any future approach to formulating a more general framework for studying stochastic dynamical systems. A recurring feature in our analysis has been the separation of the models' dynamics into slow and fast processes.

In the microscopic spin model of chapter 3, the noise becomes a relevant parameter when its inverse amplitude h, which set the rate of diffusion in the spatially extended system, is sufficiently small that two timescales emerge in the phase ordering dynamics. Below some non-zero h_* the local, on-site dynamics becomes a fast process, taking each site to a locally absorbing state. This means that on the timescale of the slow diffusion process the dimension of the system is effectively reduced from N spins to 1 spin per lattice site.

In the circular manifold model in chapter 5, we exploit a slow manifold in the deterministic dynamics to constrain the two-dimensional (2D) stochastic dynamics to the neighbourhood of a 1D closed manifold, allowing us to approximate the diffusion due to the demographic noise as a 1D process. The subsequent analysis showed this to be a good approximation of the full 2D stochastic dynamics. These reductions due to the emergence of fast and slow processes in the dynamics allows us to to exploit the mathematical machinery

available in analysing 1D non-equilibrium systems which are governed by Langevin equations or their equivalent Fokker-Planck equations. In particular, mapping the non-equilibrium dynamics onto a thermal diffusion process has proven to be conceptually insightful and allows quantitative comparison with numerical simulation of the complete defining stochastic dynamics of the models.

We have seen in this thesis that the interplay between the demographic stochasticity and the deterministic dynamics can give rise to macroscopically observable effects unaccounted for in population level models of finite systems governed by ordinary differential equations. In the study of deterministic dynamical systems there exists a wide range of methods for exploiting the difference in timescales and relaxation of variables between fast and slow processes. For example, in applied mathematics, slow manifold theory is a well established technique in studying non-linear systems [100], while the separation of timescales is a central tenet in mode-coupling theory in the study of glassy systems [121]. We speculate—echoing a similar notion expressed recently by Constable, McKane and Rogers in [99]—that if by coupling an individual based modelling approach with a broader toolkit of analytical techniques to exploit the dynamical separation of stochastic processes, a more general framework could emerge for studying how fluctuations due to the discrete nature of finite systems give rise to phenomena unpredicted by deterministic models.

The development of such a framework along with universal principles and general analytical tools in the study of complex systems is very much in demand. There is a growing consensus in the scientific community on the need for an interdisciplinary approach to be taken in tackling important problems in 21$^{\text{st}}$ century science. The expansion of the relatively new fields of quantitative biology and biological physics have shown where the transfer of knowledge can be invaluable, for example in the study of protein aggregation [122], cell biology [123], antibiotic resistance [124] and evolutionary biology [125]. Often this comes in the form of greater quantitative insight, which allows for simplifications of models and guides researchers in probing the vital aspects of the systems under consideration. Stochastic modelling of individual based models, such as that performed in this thesis, can play a vital role in bridging the gap between real systems in the natural and social sciences and the analytical power of statistical physics.

Bibliography

[1] Weaver, W. (1948) Science and complexity. *Am. Sci.*, **36**, pp. 536–544.

[2] Watson, J. D. and Crick, F. H. C. (1953) Molecular structure of nucleic acids. *Nature*, **171**, 737.

[3] Higgs, P. W. (1964) Broken symmetries and the masses of gauge bosons. *Phys. Rev. Lett.*, **13**, 508–509.

[4] ATLAS Collaboration. (2012) Observation of a new particle in the search for the standard model Higgs boson with the ATLAS detector at the LHC. *Phys. Lett. B*, **716**, 1 – 29.

[5] Jaeger, H. M. and Liu, A. J. (2007) *Condensed-Matter and Materials Physics: the science of the world around us*, chap. Far-From-Equilibrium Physics: An Overview. National Academies Press, Washington, DC.

[6] Bar-Yam, Y. (1997) *Dynamics of Complex Systems (Studies in Nonlinearity)*. Westview Press, First Edition.

[7] van Kampen, N. G. (2007) *Stochastic Process in Physics and Chemistry, Third Edition*. Amsterdam, Elsevier.

[8] Castellano, C., Fortunato, S., and Loreto, V. (2009) Statistical physics of social dynamics. *Rev. Mod. Phys.*, **81**, 591–646.

[9] Yakovenko, V. (2009) Econophysics, statistical mechanics approach to. Meyers, R. A. (ed.), *Encyclopedia of Complexity and Systems Science*, pp. 2800–2826, Springer New York.

[10] Feigenbaum, J. (2003) Financial physics. *Rep. Prog. Phys.*, **66**, 1611.

[11] Wolfgang, P. and Baschnagel, J. (1999) *Stochastic Processes: From Physics to Finance*. Springer-Verlag.

[12] Huang, K. (1987) *Statistical Mechanics, Second Edition*. Wiley.

[13] Ritort, F. and Felix, S. (2008) *Nonequilibrium Fluctuations in Small Systems: From Physics to Biology*, pp. 31–123. John Wiley & Sons, Inc.

[14] Mandl, F. (1988) *Statistical Physics, Second Edition*. Wiley.

[15] Kubo, R. (1966) The fluctuation-dissipation theorem. *Rep. Prog. Phys.*, **29**, 255.

[16] Crooks, G. E. (2000) Path-ensemble averages in systems driven far from equilibrium. *Phys. Rev. E*, **61**, 2361–2366.

[17] Jarzynski, C. (1997) Nonequilibrium equality for free energy differences. *Phys. Rev. Lett.*, **78**, 2690–2693.

[18] Kurchan, J. (2007) Non-equilibrium work relations. *J. Stat. Mech.*, **2007**, P07005.

[19] Seifert, U. (2012) Stochastic thermodynamics, fluctuation theorems, and molecular machines. *Rep. Prog. Phys.*, **75**, 126001.

[20] Kurchan, J. (1998) Fluctuation theorem for stochastic dynamics. *J. Phys. A: Math. Gen.*, **31**, 3719.

[21] Chou, T., Mallick, K., and Zia, R. K. P. (2011) Non-equilibrium statistical mechanics: from a paradigmatic model to biological transport. *Rep. Prog. Phys.*, **74**, 116601.

[22] Rondoni, L. and Meja-Monasterio, C. (2007) Fluctuations in nonequilibrium statistical mechanics: models, mathematical theory, physical mechanisms. *Nonlinearity*, **20**, R1.

[23] Murray, J. D. (2002) *Mathematical Biology: I. An Introduction, Third Edition*. Springer.

[24] Hartl, D. L. and Clark, A. G. (2007) *Principles of Population Genetics, Fourth Edition*. Sinauer.

[25] Black, A. J. and McKane, A. J. (2012) Stochastic formulation of ecological models and their applications. *Trends Ecol. Evol.*, **27**, 337 – 345.

[26] Gardiner, C. (2009) *Stochastic Methods: A Handbook for the Natural and Social Sciences, Fourth Edition*. Springer, Berlin, Heidelberg.

[27] McKane, A. J. and Newman, T. J. (2004) Stochastic models in population biology and their deterministic analogs. *Phys. Rev. E*, **70**, 041902.

[28] Newman, M. E. J. and Barkema, G. T. (1999) *Monte Carlo Methods in Statistical Physics*. Oxford University Press, USA.

[29] Gillespie, D. T. (1976) A general method for numerically simulating the stochastic time evolution of coupled chemical reactions. *J. Comput. Phys.*, **22**, 403 – 434.

[30] Henkel, M., Hinrichsen, H., and Lübeck, S. (2008) *Non-Equilibrium Phase Transitions*. Springer.

[31] Hinrichsen, H. (2000) Non-equilibrium critical phenomena and phase transitions into absorbing states. *Adv. Phys.*, **49**, 815–958.

[32] Al Hammal, O., Chate, H., Dornic, I., and Munoz, M. (2005) Langevin description of critical phenomena with two symmetric absorbing states. *Phys. Rev. Lett.*, **94**, 230601.

[33] Droz, M., Ferreira, A. L., and Lipowski, A. (2003) Splitting the voter Potts model critical point. *Phys. Rev. E*, **67**, 056108.

[34] Dornic, I., Chaté, H., Chave, J., and Hinrichsen, H. (2001) Critical coarsening without surface tension: The universality class of the voter model. *Phys. Rev. Lett*, **87**, 045701.

[35] Allen, S. M. and Cahn, J. W. (1979) Microscopic theory for antiphase boundary motion and its application to antiphase domain coarsening. *Acta Metall. Mater.*, **27**, 1085–1095.

[36] Jones, R. A. L. (2002) *Soft Condensed Matter*. Oxford University Press.

[37] Evans, R. M. L. (2010) Lecture series: Soft matter and complex fluids. *Physics by the Sea*.

[38] Clifford, P. and Sudbury, A. (1973) Model for spatial conflict. *Biometrika*, **60**, 581–588.

[39] Bray, A. J. (1994) Theory of phase-ordering kinetics. *Adv. Phys.*, **43**, 357–459.

[40] Melbourne, B. A. and Hastings, A. (2008) Extinction risk depends strongly on factors contributing to stochasticity. *Nature*, **454**, 100.

[41] Purvis, A., Gittleman, J. L., Cowlishaw, G., and Mace, G. M. (2000) Predicting extinction risk in declining species. *Proc. R. Soc. B*, **267**, 1947–1952.

[42] Lotka, A. J. (1920) Analytical note on certain rhythmic relations in organic systems. *Proc. Natl. Acad. Sci. USA*, **6**, 410–415.

[43] Volterra, V. (1931) Leçons sur la théorie mathématique de la lutte pour la vie. *Gauthier-Villars, Paris.*.

[44] McKane, A. J. and Newman, T. J. (2005) Predator-prey cycles from resonant amplification of demographic stochasticity. *Phys Rev Lett*, **94**, 218102.

[45] McKane, A. J., Nagy, J. D., Newman, T. J., and Stefanini, M. O. (2007) Amplified biochemical oscillations in cellular systems. *J. Stat. Phys.*, **128**, 165–191.

[46] Alonso, D., McKane, A. J., and Pascual, M. (2007) Stochastic amplification in epidemics. *J. R. Soc. Interface*, **4**, 575.

[47] Acebrón, J. A., Bonilla, L. L., Pérez Vicente, C. J., Ritort, F., and Spigler, R. (2005) The Kuramoto model: A simple paradigm for synchronization phenomena. *Rev. Mod. Phys.*, **77**, 137–185.

[48] Mirello, R. E. and Strogatz, S. H. (1990) Synchronisation of pulse-coupled oscillators. *SIAM J. Appl. Math.*, **50, 6**, 16645.

[49] Strogatz, S. H. (2003) *SYNC: The Emerging Science of Spontaneous Order*. Hyperion.

[50] Lai, Y. M., Newby, J., and Bressloff, P. C. (2011) Effects of demographic noise on the synchronization of a metapopulation in a fluctuating environment. *Phys. Rev. Lett.*, **107**, 118102.

[51] Hanski, I. (1998) Metapopulation dynamics. *Nature (London)*, **396**, 41.

[52] Abta, R., Schiffer, M., and Shnerb, N. M. (2007) Amplitude-dependent frequency, desynchronization, and stabilization in noisy metapopulation dynamics. *Phys. Rev. Lett.*, **98**, 098104.

[53] Abta, R., Schiffer, M., and Shnerb, N. M. (2008) Stabilisation of metapopulation cycles: Towards a classification scheme. *Theor. Popul. Biol.*, **74**, 273–282.

[54] Risken, H. (1996) *The Fokker-Planck Equation: Methods of Solutions and Applications, Second Edition*. Springer Series in Synergetics, Springer.

[55] Brush, S. G. (1967) History of the Lenz-Ising Model. *Rev. Mod. Phys.*, **39**, 883–893.

[56] Briggs, C. J. and Hoopes, M. F. (2004) Stabilizing effects in spatial parasitoid–host and predator–prey models: a review. *Theor. Popul. Biol.*, **65**, 299–315.

[57] Hermsen, R. and Hwa, T. (2010) Sources and sinks: A stochastic model of evolution in heterogeneous environments. *Phys. Rev. Lett.*, **105**, 248104.

[58] Pawula, R. F. (1967) Approximation of the linear Boltzmann equation by the Fokker-Planck equation. *Phys. Rev.*, **162**, 186–188.

[59] Grima, R., Thomas, P., and Straube, A. V. (2011) How accurate are the nonlinear chemical Fokker-Planck and chemical Langevin equations? *J. Chem. Phys.*, **135**, 084103.

[60] Melbinger, A., Cremer, J., and Frey, E. (2010) Evolutionary game theory in growing populations. *Phys. Rev. Lett.*, **105**, 178101.

[61] Bortz, A., Kalos, M., and Lebowitz, J. (1975) A new algorithm for Monte Carlo simulation of Ising spin systems. *J. Comp. Phys.*, **17**, 10 – 18.

[62] Blythe, R. A. and McKane, A. J. (2007) Stochastic models of evolution in genetics, ecology and linguistics. *J. Stat. Mech.*, **2007**, P07018.

[63] Ziff, R. M., Gulari, E., and Barshad, Y. (1986) Kinetic phase transitions in an irreversible surface-reaction model. *Phys. Rev. Lett.*, **56**, 2553.

[64] Bär, M., Falcke, M., Levine, H., and Tsimring, L. (2000) Discrete stochastic modeling of calcium channel dynamics. *Phys. Rev. Lett.*, **84**, 5664.

[65] Ódor, G. (2008) *Universality in Nonequilibrium Lattice Systems: Theoretical Foundations*. World Scientific.

[66] Dickman, R. and Tretyakov, A. Y. (1995) Hyperscaling in the domany-kinzel cellular automaton. *Phys. Rev. E*, **52**, 3218–3220.

[67] Muñoz, M. A., Grinstein, G., and Tu, Y. (1997) Survival probability and field theory in systems with absorbing states. *Phys. Rev. E*, **56**, 5101–5105.

[68] Dornic, I., Chaté, H., and Munoz, M. A. (2005) Integration of Langevin equations with multiplicative noise and the viability of field theories for absorbing phase transitions. *Phys. Rev. Lett.*, **94**, 100601.

[69] Hohenberg, P. C. and Halperin, B. I. (1977) Theory of dynamic critical phenomena. *Rev. Mod. Phys.*, **49**, 435–479.

[70] Frachebourg, L. and Krapivsky, P. L. (1996) Exact results for kinetics of catalytic reactions. *Phys. Rev. E*, **53**, R3009–R3012.

[71] Cox, J. T. (1989) Coalescing random-walks and voter model consensus times on the torus in zd. *Ann. Probab.*, **17**, 1333–1366.

[72] Holley, R. A. and Liggett, T. M. (1975) Ergodic theorems for weakly interacting infinite systems and the voter model. *Ann. Probab.*, **3**, 643.

[73] Krapivsky, P. L. (1992) Kinetics of monomer-monomer surface catalytic reactions. *Phys. Rev. A*, **45**, 1067–1072.

[74] Drouffe, J. M. and Godrèche, C. (1999) Phase ordering and persistence in a class of stochastic processes interpolating between the Ising and voter models. *J. Phys. A: Math. Gen.*, **32**, 249–261.

[75] Hwang, W., Kwon, S., Park, H., and Park, H. (1998) Critical phenomena of nonequilibrium dynamical systems with two absorbing states. *Phys. Rev. E*, **57**, 6438–6450.

[76] Dall'Asta, L. and Galla, T. (2008) Algebraic coarsening in voter models with intermediate states. *J. Phys. A*, **41**, 435003.

[77] Vazquez, F. and Lopez, C. (2008) Systems with two symmetric absorbing states: Relating the microscopic dynamics with the macroscopic behavior. *Phys. Rev. E*, **78**, 061127.

[78] Dall'Asta, L. and Castellano, C. (2007) Effective surface-tension in the noise-reduced voter model. *Europhys. Lett.*, **77**, 60005.

[79] Russell, D. I. (2009) *The Physics of Consensus: The Construction and Analysis of Non-Linear Versions of the Utterance Selection Model of Language Change*. Master's thesis, School of Physics and Astronomy, University of Edinburgh.

[80] Gordon, E., Campbell, L., Hay, J., Maclagan, M., Sudbury, A., and Trudgill, P. (2004) *New Zealand English: Its Origins and Evolution (Studies in English Language)*. Cambridge University Press.

[81] Baxter, G. J., Blythe, R. A., Croft, W., and McKane, A. J. (2006) Utterance selection model of language change. *Phys. Rev. E*, **73**, 046118.

[82] Hudson-Kam, C. and Newport, E. (2005) Regularizing unpredictable variation: The roles of adult and child learners in language formation and change. *Lang. Learn. Devel.*, **1**, 151–195.

[83] Baxter, G. J., Blythe, R. A., Croft., W., and McKane, A. J. (2009) Modeling language change: An evaluation of Trudgill's theory of the emergence of the New Zealand English language dialect. *Lang. Var. Change*, **21**, 257.

[84] Nowak, M. A. (2006) *Evolutionary Dynamics: Exploring the Equations of Life*. Harvard University Press.

[85] Castellano, C., Muñoz, M. A., and Pastor-Satorras, R. (2009) Nonlinear q-voter model. *Phys. Rev. E*, **80**, 041129.

[86] Press, W. H., Flannery, B. P., Teukolsky, S. A., and Vetterling, W. T. (1992) *Numerical Recipes in FORTRAN 77: The Art of Scientific Computing (v. 1), Second Edition*. Cambridge University Press.

[87] Möhle, M. (1998) A convergence theorem for markov chains arising in population genetics and the coalescent with selfing. *Adv. Appl. Probab.*, **30**, 493.

[88] Barrett-Freeman, C., Evans, M. R., Marenduzzo, D., and Tailleur, J. (2010) The role of noise and advection in absorbing state phase transitions. *Europhys. Lett.*, **90**, 16003.

[89] Tanner, J. T. (1975) The stability and the intrinsic growth rates of prey and predator populations. *Ecology*, **56**, pp. 855–867.

[90] Gasull, A., Kooij, R. E., and Torregrosa, J. (1997) Limit cycles in the Holling-Tanner model. *Publ. Math.*, **41**, 149.

[91] Nisbet, R. and Gurney, S. (1976) A simple mechanism for population cycles. *Nature*, **263**, 319–320.

[92] Tomé, T. and de Oliveira, M. J. (2009) Role of noise in population dynamics cycles. *Phys. Rev. E*, **79**, 061128.

[93] Black, A. J. and McKane, A. J. (2010) Stochastic amplification in an epidemic model with seasonal forcing. *J. Theor. Biol.*, **267**, 85 – 94.

[94] Parker, M. and Kamenev, A. (2009) Extinction in the Lotka-Volterra model. *Phys. Rev. E*, **80**, 021129.

[95] Parker, M. and Kamenev, A. (2010) Mean extinction time in predator-prey model. *J. Stat. Phys.*, **141**, 201–216.

[96] Stenseth, N. C. (1999) Population cycles in voles and lemmings: Density dependence and phase dependence in a stochastic world. *Oikos*, **87**, pp. 427–461.

[97] Stenseth, N. C., Chan, K., Framstad, E., and Tong, H. (1998) Phase- and density-dependent population dynamics in norwegian lemmings: interaction between deterministic and stochastic processes. *Proc. R. Soc. B*, **265**, 1957–1968.

[98] Roichmani, Y., Sun, B., Stolarski, A., and Grier, D. (2008) Influence of nonconservative optical forces on the dynamics of optically trapped colloidal spheres: The fountain of probability. *Phys. Rev. Lett.*, **101**, 128301.

[99] Constable, G. W. A., McKane, A. J., and Rogers, T. (2013) Stochastic dynamics on slow manifolds. *J Phys A: Math. Theor.*, **46**, 295002.

[100] Carr, J. (1981) *Applications of Centre Manifold Theory*. Springer-Verlag.

[101] Strogatz, S. H. (2001) *Nonlinear Dynamics And Chaos: With Applications To Physics, Biology, Chemistry, And Engineering (Studies in Nonlinearity), First Edition*. Studies in Nonlinearity, Westview Press.

[102] Kwon, C., Ao, P., and Thouless, D. (2005) Structure of stochastic dynamics near fixed points. *Proc. Natl. Acad. Sci. USA*, **102**, 13029–13033.

[103] Kwon, C., Noh, J. D., and Park, H. (2011) Nonequilibrium fluctuations for linear diffusion dynamics. *Phys. Rev. E*, **83**, 061145.

[104] Kwon, C. and Ao, P. (2011) Nonequilibrium steady state of a stochastic system driven by a nonlinear drift force. *Phys. Rev. E*, **84**, 061106.

[105] Uhlenbeck, G. E. and Ornstein, L. S. (1930) On the theory of the brownian motion. *Phys. Rev.*, **36**, 823–841.

[106] Zauderer, E. (2006) *Partial Differential Equations of Applied Mathematics, Third Edition*. Wiley-Blackwell.

[107] Altland, A. and Simons, B. (2010) *Condensed Matter Field Theory, Second Edition*. Cambridge.

[108] Riley, K. F., Hobson, M. P., and Bence., S. J. (2002) *Mathematical Methods for Physics and Engineering, Second Edition*. Cambridge University Press.

[109] Tomé, T., Rodrigues, A. L., Arashiro, E., and de Oliveira, M. J. (2009) The stochastic nature of predator-prey cycles. *Comput. Phys. Commun.*, **180**, 536 – 539.

[110] Parsons, T. L. and Quince, C. (2007) Fixation in haploid populations exhibiting density dependence II: The quasi-neutral case. *Theor. Popul. Biol.*, **72**, 468–479.

[111] Thomas, P., Grima, R., and Straube, A. (2012) Rigorous elimination of fast stochastic variables from the linear noise approximation using projection operators. *Phys. Rev. E*, **86**, 041110.

[112] Gardiner, C. W. (1984) Adiabatic elimination in stochastic systems. i. formulation of methods and application to few-variable systems. *Phys. Rev. A*, **29**, 2814–2822.

[113] Parsons, T. L. and Quince, C. (2007) Fixation in haploid populations exhibiting density dependence I: The non-neutral case. *Theor. Popul. Biol.*, **72**, 121–135.

[114] Kramers, H. (1940) Brownian motion in a field of force and the diffusion model of chemical reactions. *Physica*, **7**, 284 – 304.

[115] Boland, R. P., Galla, T., and McKane, A. J. (2008) How limit cycles and quasi-cycles are related in system with intrinsic noise. *J. Stat. Mech. -Theory Exp*, p. P09001.

[116] Boland, R. P., Galla, T., and McKane, A. J. (2009) Limit cycles, complex floquet multipliers, and intrinsic noise. *Phys. Rev. E*, **79**, 051131.

[117] Kerr, B., Neuhauser, C., Bohannan, B. J. M., and Dean, A. M. (2006) Local migration promotes competitive restraint in a hostpathogen: tragedy of the commons. *Nature (London)*, **442**, 75.

[118] Khasin, M., Khain, E., and Sander, L. M. (2012) Fast migration and emergent population dynamics. *Phys. Rev. Lett.*, **109**, 248102.

[119] Kuramoto, Y. (1975) International symposium on mathematical problems in theoretical physics, edited by H. Araki. *Lecture Notes in Physics No. 30 (Springer, New York), p. 420*.

[120] Kuramoto, Y. (1984) *Chemical Oscillations, Waves and Turbulence*. Springer, New York.

[121] Das, S. P. (2004) Mode-coupling theory and the glass transition in supercooled liquids. *Rev. Mod. Phys.*, **76**, 785–851.

[122] Morris, R. J., Eden, K., Yarwood, R., Jourdain, L., Allen, R., and MacPhee, C. E. (2013) Mechanistic and environmental control of the prevalence and lifetime of amyloid oligomers. *Nat. Commun.*, **4**, 1891.

[123] Wolgemuth, C. W. (2011) Does cell biology need physicists? *Physics*, **4**, 4.

[124] Greulich, P., Waclaw, B., and Allen, R. J. (2012) Mutational pathway determines whether drug gradients accelerate evolution of drug-resistant cells. *Phys. Rev. Lett.*, **109**, 088101.

[125] Sella, G. and Hirsh, A. E. (2005) The application of statistical physics to evolutionary biology. *Proc. Natl. Acad. Sci. USA*, **102**, 9541–9546.

Publications

Russell, D. I. and Blythe, R. A. (2011) Noise-induced dynamical transition in systems with symmetric absorbing states. *Phys. Rev. Lett.*, **106**, 165702.

Russell, D. I. and Blythe, R. A. (2013) Macroscopically observable probability currents in finite populations. *J. Stat. Mech.*, **2013**, P06008.